Shahrukh Khan

Control and Development of a Wearable Semi-Active Tremor Suppression Device

Master's thesis in Engineering Cybernetics
Supervisor: Jan Tommy Gravdahl
January 2019

Master's thesis

NTNU
Norwegian University of
Science and Technology

Shahrukh Khan

Control and Development of a Wearable Semi-Active Tremor Suppression Device

Master's thesis in Engineering Cybernetics
Supervisor: Jan Tommy Gravdahl
January 2019

Norwegian University of Science and Technology
Faculty of Information Technology and Electrical Engineering
Department of Engineering Cybernetics

NTNU
Norwegian University of
Science and Technology

NTNU
Norges teknisk-naturvitenskapelige
universitet

Fakultet for informasjonsteknologi,
matematikk og elektroteknikk
Institutt for teknisk kybernetikk

MSc thesis assignment

Name of the candidate: Shahrukh Khan
Subject: Engineering Cybernetics
Title: Control and Development of a Wearable Semi-Active Tremor
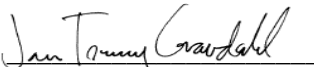   Suppression Device

Background

This thesis work aims for the use of a robotic manipulator to emulate a prototype semi-active tremor suppression device.

Tasks:

- Review different scales used to assess tremors
- Based on [1,2], design a method and a setup to test a semi-active tremor suppression device by emulating it with the UR5 robotic manipulator located at the Dept. of Engineering Cybernetics
- Based on [1,2,3], implement a dynamic vibration absorber (DVA) as an admittance controller on the UR5 robotic manipulator.
- Investigate if it is possible to test the set-up on patients
- Design an experimental procedure to test the method and the set-ups ability to suppress tremors.

To be handed in by: 27/1-2019
Co-supervisor: Mathias Hauan Arbo

Jan Tommy Gravdahl
Professor, supervisor

[1] Ida Estenstad. "Design and Validation of a Wearable Device for Upper Limb Tremor Suppression", MSc thesis. Department of Mechanical & Industrial Engineering, NTNU 2018.
[2] Bjarte Mehus Sunde. "Estimation of multiple frequencies in pathological hand tremor for a semi-active 2DOF dynamic vibration absorber designed for tremor suppression", MSc thesis. Department of Engineering Cybernetics, NTNU, 2018.
[3] Mads Johan Laastad. "Robotic rehabilitation of upper-limb after stroke", MSc thesis. Department of Engineering Cybernetics, NTNU, 2017.

To my parents, my sister, family and friends. For all your love and everlasting support.

Summary

Tremors are one of the most prevalent movement disorders in the world. They cause involuntary rhythmic shaking of parts of the body, such as the hands. The most common types of tremors are essential tremor (ET) and tremors caused by Parkinson's disease (PD). The tremors often impede daily activities, and many people experience the shaking as embarrassing. Treatment today consist of medications and neurosurgery, however they are often not perceived as adequate enough by patients.

This thesis is a part of an ongoing student project on the development of a wearable device for tremor suppression. The goal of the project is to create an aid that can be used as a supplement by people who suffer from tremors. As a part of the development process, this thesis aims to implement a previously developed tremor suppression concept on a robot manipulator. The concept, called a dynamic vibration absorber (DVA), was tested as a passive device in preceding master theses. In this thesis the concept is extended into a semi-active device. To be able to test the concept more efficiently, a robotic manipulator was utilised.

The work done in this thesis consists of a literature review on tremor assessment; testing and validation of an earlier implementation of a compliance controller for the robotic manipulator; system design of the tremor suppression system; design, implementation, test and validation of a complete control system for a robotic tremor suppression system, including implementation of an admittance controller on the robotic manipulator; implementing and establishing real-time communication between an Arduino Uno and the robotic manipulator to expand the system from a passive to a semi-active system; and a design of an experimental procedure to test the method and the setup's ability to suppress tremors and investigate the effect of a semi-active system opposed to a passive one.

The work yields a successful implementation of the system, but the setup is still in a working phase, and must be improved. A new and improved design of the hardware interface is suggested as future work, in addition to a suggestion to develop a hybrid controller for compliance and admittance.

Sammendrag

Skjelvinger er en av de bevegelsesforstyrrelsene med høyest prevalens. De er definert som ufrivillig, rytmisk skjelving av kroppsdeler, som for eksempel i hender. De mest typiske formene for skjelvinger er essensiell tremor (ET) og skjelvinger forårsaket av Parkinsons syndrom (PD). Skjelvingene er ofte hemmende for dagligdags aktivitet, og mange opplever skjelvingene som sjenerende. I dag blir skjelvinger behandlet med medikamenter og nevrokirurgi, dessverre oppleves denne behandlingsformen ofte som inadekvat av pasientene.

Denne masteroppgaven er en del av et pågående studentprosjekt som utvikler et bærbart hjelpemiddel for å forhindre skjelvinger i hender. Målet med prosjektet er å lage et produkt som kan fungere som et supplement for personer som lider av skjelvinger. Som en del av utviklingsprosessen, søker denne masteroppgaven etter å implementere et tidligere utviklet skjelvedempende konsept på en robot manipulator. Konseptet, kalt dynamisk vibrasjons absorbere (DVA), ble testet som en passiv enhet i tidligere masteroppgaver. Denne masteroppgaven har som mål å videreutvikle konseptet til en semi-aktiv enhet. En robot manipulator har blitt tatt i bruk for å teste enheten og konseptet mer effektivt.

Arbeidet som er gjennomført i denne oppgaven består av et literatursøk på evaluering av skjelvinger; testing og validering av en tidligere implementasjon av en "compliance"-kontroller for robotsystemet; systemdesign av dempesystemet; design, implementasjon, testing og validering av et komplett kontrollsystem for et robotisk dempesystem for skjelvinger, som inkluderer implementasjon av en "admittance"-kontroller på robot manipulatoren; implementering og opprettelse av kommunikasjon i sanntid mellom en Arduino Uno og robotsystemet for å utvide systemet fra et passivt til et semi-aktivt system; og design av et ekseperimentell prosedyre for å teste metoden og oppsettes evne til å dempe skjelvinger og videre utforske effekten av et semi-aktivt system i motsetning til et passivt system.

Arbeidet viser til en vellyket implementasjon av systemet, men oppsettet har fortsatt et forbedringspotensial. Et nytt og forbedret hardware interface design er foreslått som et punkt under fremtidig arbeid, i tillegg til blant annet å utvikle en hybrid kontroller for compliance og admittance.

Preface

This thesis was carried out at the Department of Engineering Cybernetics (ITK), at the Norwegian University of Science and Technology (NTNU), in Trondheim during the fall of 2018. It was supervised by Prof. Jan Tommy Gravdahl and co-supervised by Mathias Hauan Arbo.

The thesis is the culmination of a 5 year masters program in the field of engineering cybernetics. Working with this thesis has both been challenging and frustrating, but at the same time fun and rewarding. Being able to work with such a diverse assignment, combining so many fields within the field of cybernetics has been enjoyable and shown me how much I have learned the last five years.

The idea of the thesis was established during the interdisciplinary course, Experts in Teamwork (EiT). After the course was completed, the team kept working with the idea, with the hope and goal of establishing a tech-company and develop a wearable device for tremor suppression. During our research we met with many people suffering from tremor diseases, e.g. members of The Norwegian Parkinson Foundation. Knowing that our work might help and ease these peoples everyday life was the greatest motivation in this project. All current development of the wearable device has been done through several master theses.

During the work some challenges and limitations have presented themselves, and altered the course of the thesis. Originally, the development done in this thesis was meant to be conducted on real patients. A remit assessment was applied for to the Regional Committees for Medical and Health Research Ethics (REC/REK). They concluded that the project needed REK approval through a larger project application. A reassessment was done, and due to shortage of time, a risk assessment of the robotic system, and the development being in the initial phases, my supervisor and I assessed that a virtual patient should be used instead.

This paragraph lists all the contributions to the work of the thesis. The F/T sensor utilised in this thesis is made available by SINTEF trough a collaboration with ITK. NTNU has provided access to the robot manipulator system, desktop computers and virtual patient equipment. They have also provided student access to various software, e.g. MATLAB. The code is mainly based on work by Mads Johan Laastad [1], who utilises UR drivers, called *ur_modern_driver*, developed by Thomas Timm Andersen [2]. The BMWFLC code is written and developed by Bjarte Sunde [3].

The remaining hardware, like the Arduino and accelerometers are self-acquired, funded by prize money won by Inalto through pitching competitions and Spark NTNU's TrønderEnergibidraget (TEB).

Acknowledgements

Table of Contents

List of Tables

List of Figures

Abbreviations

EiT	=	Experts in Teamwork
MTP	=	Department of Mechanical and Industrial Engineering
ITK	=	Department of Engineering Cybernetics
REK/REC	=	Regional Committees for Medical and Health Research Ethics
ET	=	Essential Tremor
PD	=	Parkinson's Disease
DBS	=	Deep Brain Stimulation
ADL	=	Activities of Daily Living
FTM	=	Fahn-Tolosa-Marin Tremor Rating Scale
TETRAS	=	The Essential Tremor Rating Assessment Scale
CGI-S	=	Clinical Global Impression Scale
ACT	=	Active Cancellation of Tremor
STFT	=	Short-time Fourier Transform
PSD	=	Power Spectrum Density
DVA	=	Dynamic Vibration Absorber
DH	=	Denavit-Hartenberg
DOF	=	Degree(s) of Freedom
F/T	=	Force/Torque
MCU	=	Microcontroller Unit
FLC	=	Fourier Linear Combiner
WFLC	=	Weighted FLC
BMFLC	=	Band-limited Multiple FLC
E-BMFLC	=	Enhanced BMFLC
BMWFLC	=	Band-limited Multiple WFLC

Chapter 1

Introduction

This master thesis is conducted in the fall of 2018. It is a part of a project begun during the course Experts in Teamwork (EiT) in 2017, with the aim to develop a wearable device for tremor suppression. There have been two theses written on this project thus far: one at The Department of Mechanical and Industrial Engineering (MTP), with focus on the development process of a wearable device for upper limb tremor suppression; and one at The Department of Engineering Cybernetics (ITK), with the focus on tracking and estimation of tremor frequencies. This project is thought to be the next step from previous theses towards a final product.

The thesis presents initial studies on the development and implementation of a mechanical tremor suppression concept through an UR5 robotic manipulator. It further extends a formerly passive system to a semi-active system by the feedback of filtered accelerometer/gyroscope data.

1.1 Background and Motivation

Hands are essential tools in human life. They enable us in many of our daily activities, like drinking and eating or writing and typing; anything from pushing, pulling, grasping or touching. They provide us with a powerful grip, but at the same time they are precision tools allowing us to manipulate small and fragile objects.

However, there is a vast number of people suffering from tremors. Tremors are, as defined in [4], involuntary, rhythmic oscillations of one or more body parts. Hence, tremors in the upper extremities of one's body may inhibit or impede certain daily activities to various degrees.

Essential Tremor (ET) and Parkinson's Disease (PD) are the two diagnoses with the highest prevalence of tremor in the upper limbs [5, 6]. In Norway, it is estimated that about 8000 people suffer from PD [7]. Worldwide, the number is more than 10 million [8, 9].

For ET, the prevalence is between $0.4 - 6\%$ of the world population [10]. As the world population is ageing and increasing, the patient group is expected to increase.

People are affected in different ways by different types of tremor in different stages of life. A survey conducted by The International Essential Tremor Foundation [11], among 3000 of their members, shows that as many as 80% of the respondents had a hard time writing, while between 66% and 68% of the respondents found it difficult to either eat, drink or hold items. Studies also show that many people suffering from tremors experience the shaking as embarrassing and restraining [12], and social anxiety is reported among people with ET [13].

Today, tremors are treated with either medication or neurosurgery. In addition, there exists a variety of assistive technology that may aid a person in specified daily tasks. Unfortunately, side effects are common with medication and many patients abandon their treatment because of this [14, 15, 16]. On the matter of neurosurgery, the most common method is Deep Brain Stimulation (DBS). It is a neurological procedure that involves implanting a medical device in the brain [17]. The method has shown to be effective in treating tremors caused by PD, but patients in Norway are only considered for the operation when symptoms cannot be treated sufficiently through medication [18]. DBS may also lead to severe side effects [19, 20].

This issue was first addressed by the team during the course (EiT) at NTNU in 2017. After a successful project, the team did not wish to give up the project and proceeded to establish a start-up that would continue to work on the project. The long-term goal is to develop a product that can reduce tremors, in a non-embarrassing way, and enable people to accomplish daily tasks by themselves without the need for help.

1.2 Thesis Structure

The background and motivation presented in this chapter describes the problem that forms the basis of the following work. **Chapter 2** presents the previous work done on the project, focusing on the work in the preceding master theses. In **Chapter 3**, basic theory on tremor, and relevant mathematical and technological concepts are established. A literature review on tremor assessment is performed in **Chapter 4**. In **Chapter 5** the system components and the system overview is presented. **Chapter 6** presents the work done related to the system design and implementation. In **Chapter 7** the conducted experiment is presented, while **Chapter 8** and **Chapter 9** presents the conclusion and future work, respectively.

1.3 Contribution

Several contributions are directly related to the task description presented in the master thesis assignment.

- **Review of current tremor assessment scales**. A literature review of current tremor assessment methods are used to analyse how to validate a tremor suppression device.

- **System design**. A system design has been made by choosing and compiling various components for a semi-active robotic tremor suppression system.

- **Validation of preceding implementation**. Test setup and experiment conducted by Laastad [21] has been replicated to verify a force controller implementation on a UR5 robotic manipulator.

- **Design, implementation, and validation of a control system for robotic tremor suppression**. A control system was designed, based on a set of specifications made from an analysis of the desired system behaviour. Said control system was further implemented on a robotic manipulator, including implementation of an admittance controller. Each component of the control system was tested and validated.

- **Implementation of communication between an Arduino Uno and the robotic manipulator in Linux C++**. Communication between an Arduino Uno and the robotic manipulator was established to feedback the peak frequencies calculated by the BMWFLC algorithm.

- **Design and implementation of experimental procedure**. An experimental procedure was designed to test the complete system.

The thesis has, to a great extent, revolved around the design and the implementation of the system. This includes identifying, analysing and solving numerous implementation challenges, some of which are described in the thesis. Other notable contributions include performing a risk assessment of the intended application and interaction between the UR5 robot manipulator and humans. A remit assessment was applied to REK, who concluded that a larger project application is needed in the case of patient testing.

Chapter 2

Previous Work

As stated in the introduction, the project on the development of a tremor suppression device began during the course EiT in the spring of 2017. During the course, a user group was defined along with a product demand specification; a choice of actuator to suppress the tremors was made; and several designs were proposed. Finally, a device that demonstrated the concept was developed. Even though the initial technological concept has later been dismissed, the course laid a foundation for further development of a solution.

In the spring of 2018 Ida Estenstad [22] and Bjarte Mehus Sunde [23] wrote their respective master theses on the development of a tremor suppressing device. Some parts were written in collaboration, while the rest were specific for their respective fields. Figure 2.1a and 2.1b illustrate the total system design of both Estenstad and Sunde's theses. Here, the sensors return real-time position value, x_k, to the filter. The filter uses these values to return the two fundamental frequencies, $\omega_{n_1}, \omega_{n_2}$ of the signal. From the frequencies, the stiffness, k_{a_1} and k_{a_2}, of the mass-spring-damper systems are calculated for optimising the Dual DVA parameters. The sensor and filter part of the system design were the main focus of Sunde's thesis, while the other half of the design was the main focus of Estenstad's thesis.
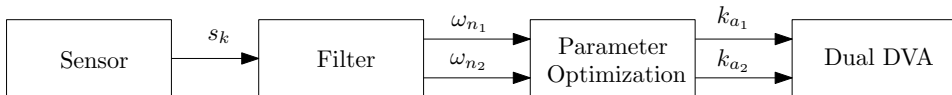
(a) General Tremor System Design [Author], inspired by [22, 23]
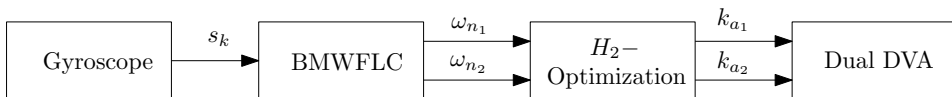
(b) Final Tremor System Design [Author], inspired by [22, 23]

Figure 2.1: System Design of Previous Theses [Author], Inspired by [23, 22]

2.1   Real-Time Frequency Estimation Filter

In his master thesis, Sunde developed and validated a real-time frequency estimation filter for tracking of multiple frequencies in pathological hand tremor. The filter is shown in figure 2.2, while its process is shown in the flowchart in figure B.1 in appendix B.
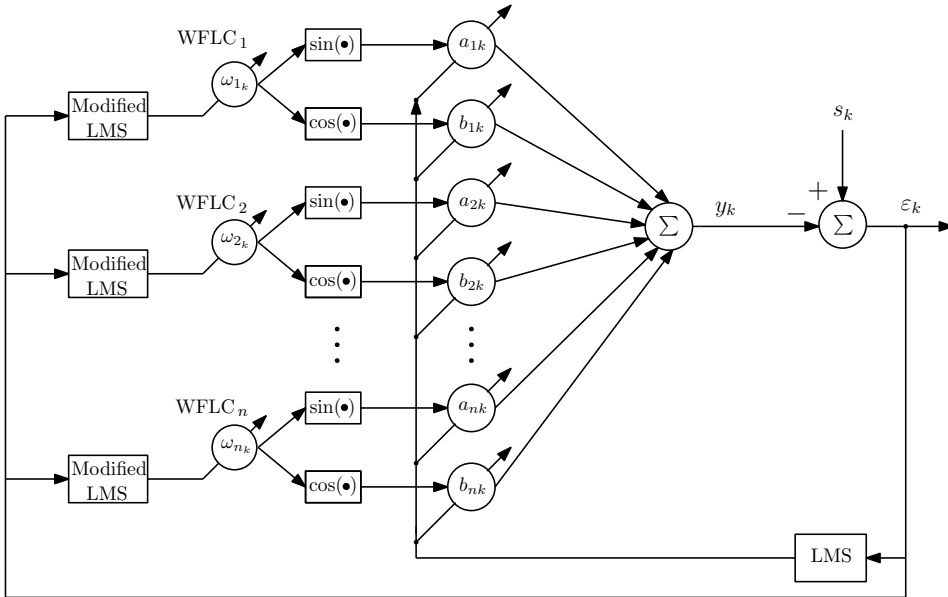
Figure 2.2: BMWFLC [Author], inspired by [23]

This filter is called the *Band-limited Multiple Weighted Fourier Linear Combiner* (BMWFLC) and is based on other filters for tremor frequency estimation; namely the Fourier Linear Combiner (FLC) [24], the Weighted Fourier Linear Combiner (WFLC) [25], the Band-limited Multiple Fourier Linear Combiner (BMFLC) [26] and the Enhanced Band-limited Multiple Fourier Linear Combiner (E-BMFLC) [27]. The main difference between the filter developed by Sunde and the other filters is that the BMWFLC is able to track multiple frequencies.

The core equations, and other important definitions of the BMWFLC are stated together with the filter algorithms in appendix A.

2.2   Dual Dynamic Vibration Absorbers

Estenstad, on the other hand, investigated various mechanical concepts for tremor suppression in her thesis. An analysis of the existing solutions and technology was conducted, and a concept similar to Gebai et al. [28] was developed. A *Dual Dynamic Vibration Absorber* (figure 2.3) was suggested, but unlike the passive system by Gebai et al., Estenstad suggest a semi-active one. This concept is further explained in chapter 3.3.1.
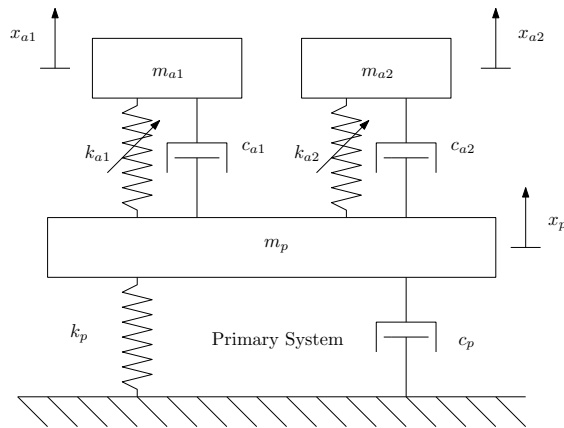
Figure 2.3: Dual DVA [Author], Inspired by [22, 23]

A single DVA system was tested and validated through a constructed test rig. The test rig is illustrated and depicted in figure 2.4a and figure 2.4b. A total of nine different setups were used to validate the concept. Estenstad elaborated on the Dual DVA concept. Her thesis presents suggestions regarding design, parameter optimisation technique, and regulation of the damper's stiffness tuning.

Estenstad found indications that tuning a DVA to the two frequencies of highest power will dampen the tremors more effectively, than by only focusing on the frequency with the highest power not all the power of the tremors is suppressed. Hence, the choice of Dual DVA was made. The design of the DVA was chosen to be a parallel DVA, because of the simplicity and space saving characteristics, even though a serial DVA shows slightly better performance. In addition, according to Estenstad a damper should be added to the design.
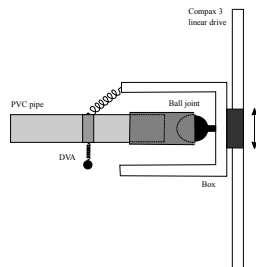
(a) Test setup illustration [22]
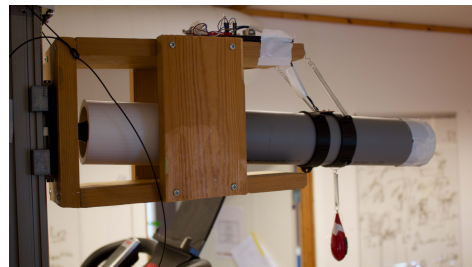
(b) Picture of test rig [22]

Figure 2.4: Test rig by [22]

The theory behind the vibration dampening and DVA is further explained in section 3.3.1.

2.3   Results - Previous Work

The test rig was used to validate both the DVA concept and the BMWFLC algorithm. The percentage reduction with respect to Power Spectral Density (PSD) are presented in table 2.1. The signal and PSD plots for an example test, are shown in figure 2.5 and figure 2.6.

The results presented show unaccounted for effects, however, these results are not of an optimal setup. The DVA system is a single DVA system; it is passive and will not adapt the spring stiffness to the fundamental frequencies from the BMWFLC like a semi-active system will; in addition, the system has only been made for 1 Degree of Freedom (DOF), and the resolution and the window size of the microcontroller utilised in the test was not good enough to track the 2nd harmonic of the signal. Despite these limitations, the results are promising and motivate taking these concepts of mechanical tremor suppression and frequency tracking to further development.
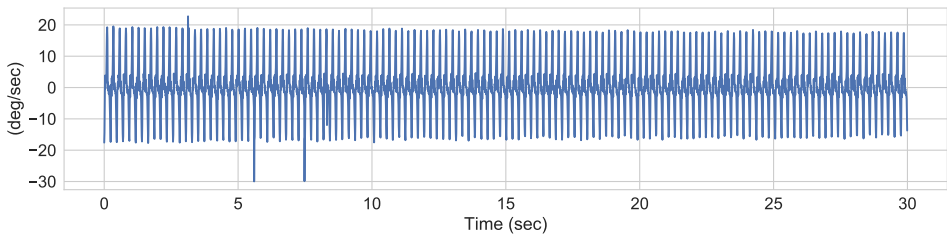
(a) 30 sec recording from test rig [23]
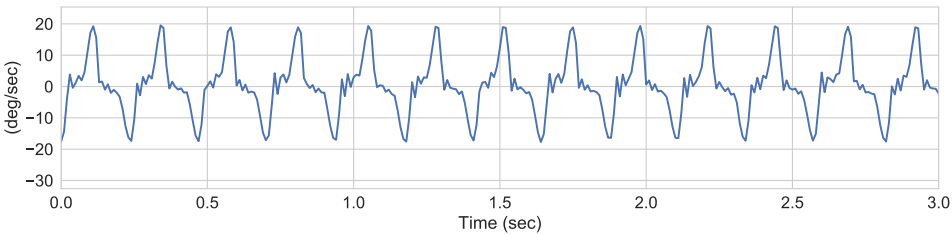
(b) 30 sec recording, zoomed view [23]

Figure 2.5: Recorded Signal from Test Rig [23, 22]
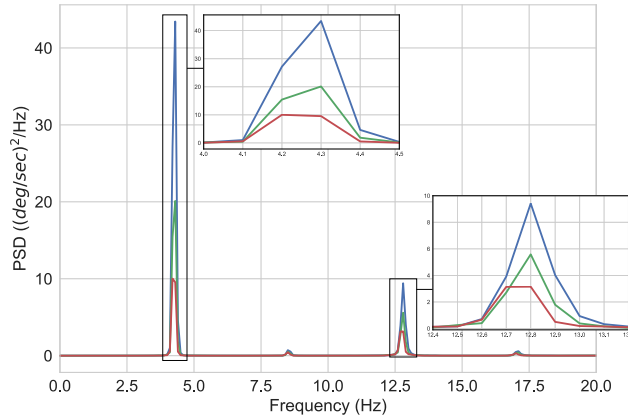
Figure 2.6: Linear PSD of simulated tremor on test rig. Plots with nothing, weight and DVA attached; blue, green and red line respectively [23]

	PSD	PSD w/DVA	PSD w/mass	% reduction w/DVA	% reduction w/mass
Test 1	66.69	38.01	34.93	43.00 %	47.62 %
Test 2	230.8	55.65	107.3	75.89 %	53.51 %
Test 3	189.3	146.3	168.4	22.72 %	11.04 %
Test 4	571.1	106.2	327.3	81.40 %	42.69 %
Test 5	274.7	109.9	135.6	59.99 %	50.64 %
Test 6	78.41	61.96	73.09	20.98 %	6.78 %
Test 7	116.5	7.864	39.91	93.25 %	65.74 %
Test 8	74.52	22.08	50.64	70.37 %	32.05 %
Test 9	170.1	108.1	100.3	36.45 %	41.03 %

Table 2.1: PSD results and percentage reduction when adding DVA and mass [22]

Chapter 3

Basic Theory

The basic theory of the most important aspects of the project is established in this chapter. The chapter begins with an overview of tremors from a medical point of view, then moves on to the theory behind vibration damping. Further, methods of time-frequency analysis will be presented.

3.1 Tremors

Tremors are rhythmic oscillatory movements of one or more body parts about a fixed plane in space [4, 29, 30, 31]. These rhythmic oscillatory movements occur more specifically in reciprocally innervated, antagonistic muscle pairs, usually in the upper extremities and head/neck area [31]. Tremors themselves are not a disease, rather, they are symptoms of many other diseases; and finding the cause of tremors is important because both the prognosis and the treatment varies [29, 31, 32, 33]. Table 3.1 lists various syndromes that cause tremors and their frequencies. Evidently, the range of the tremors depends on the diagnosis.

However, not all tremors are symptoms of diseases. Everyone can experience tremors, e.g. when doing precision work with their hands, or when feeling nervous. These kind of tremors are called *physiological tremors* and are considered normal, and not of inconvenience for people [30, 34].

The tremors associated with diseases, that noticeably impair normal functioning and are visible for the naked eye are called *pathological tremors* [35, 36]. These are further classified as either *rest tremors* or *action tremors*. Rest tremors are prevalent when the affected limbs are at rest, supported against gravity [29, 30, 31, 32, 37]; and the tremors usually stop or are reduced when the limb is in motion. Action tremors work in the opposite way of rest tremors, the tremors are prevalent when the affected limbs are in motion, and reduced when the limbs are at rest [29, 30, 31, 32, 37]. Action tremors can be further divided into *postural* and *kinetic* tremors. Postural tremors are prevalent when a limb is maintain-

ing a posture against gravity, and kinetic tremors are prevalent when the affected limb is performing a voluntary motion.

Tremor Syndrome	Frequency [Hz]
Enhanced physiological tremor	10-14
Essential tremor syndrome	4-12
Primary orthostatic tremor	14-18
Task spesific tremor	4-8
Holmes tremor	3-5
Tremor of Parkinson disease	3-7
Cerebellar tremor	5-7
Palatal tremor	2-6
Dystonic tremor	5-7
Alcoholic tremor	3-4
Toxic and drug induced tremor	5-10
Psychogenic tremor	Variable

Table 3.1: Various tremor syndromes and their corresponding frequencies [38]

3.1.1   Essential Tremor

Essential Tremor (ET) is the most common movement disorder in adults [29, 30, 31, 32, 33, 39, 40]. It is an action tremor, where kinetic tremor is more common than posture. Stress, tiredness and nervousness are all typical triggers of the tremors, in addition to intentional movements. The tremors usually affect the arms/hands or the head and are typically bilateral [29, 30, 31, 33, 39, 40, 41]. The movement of the tremors in the wrist is characterised by a flexion-extension movement [42].

The exact prevalence of ET is uncertain, since there does not exist any diagnostic criteria in terms of pathological or biochemical markers to make a confident diagnosis [34, 39]. Yet, several diagnostic criteria through tests have been proposed (see section 4.1). It is however, estimated that between 0.4 and 6% of the world population suffers from ET [30], but according to [43, 44] up to 90% of ET patients does not seek medical attention. Thus, these numbers are expected to be higher. The progression of the disease is slow, and as with most tremor syndromes the prevalence increases with age [31, 36]. It is estimated that as many as 6 - 9% of the population over the age of 60 experience tremor due to ET [38]. The inheritance of ET is transmitted in a autosomal dominant fashion, but the penetrance within families is variable [29, 30, 31, 32, 39, 40, 41]. Use of betablockers is a treatment that helps many ET-patients [45, 46], also alcohol has shown to reduce tremors in ET significantly [45, 46].

The tremor frequency of ET range between 4 and 12 Hz (table 3.1), but the highest prevalence is in the range of 7 - 10 Hz [38]. It has been shown that the frequency decreases by 0.06 - 0.08 Hz each year, and that it correlates with an increase in amplitude [47].

3.1.2 Parkinson's disease

Parkinson's Disease (PD) is the second most common neurodegenerative disease after Alzheimer's Disease, and the main cause of parkinsonism [48, 49, 50, 51]. The cause of PD is due to a disruption of dopamine [31, 41, 48, 52], which is a neurotransmitter, a hormon that is used as a mean of communication between the substantia nigra and the basal ganglia in the brain [48, 52]. Due to the biochemical imbalance that arises, PD is manifested by six features: tremor, rigidity, bradykinesia, loss of postural reflexes, flexed posture and freeze [6, 38, 48, 49, 53]. The tremor of PD is a resting tremor in limbs, commonly constituted in the extremities and initially unilateral. As the disease progresses it commonly evolves to an asymmetric bilateral tremor [32, 38, 53]. The tremors are also characterised by a pronation-supination movement [41, 54]. Levodopa therapy and dopamine agonists are commonly used treatments of PD symptoms, however, they are only used to slow down the disease, prolong life expectancy and better quality of life. No cure to PD is presently available [30, 31, 41, 48, 49, 53, 54].

The prevalence of PD is estimated to be about 1% of the world population between the age of 50 and 70 [35, 38, 49, 54]. The prevalence is expected to increase as the life expectancy is increasing [48, 49], and it is expected to double by the year 2030 [35].

The tremor frequency of PD is estimated to be in the range of 3 to 7 Hz [38], but many studies operate with the range 4 - 6 Hz as well [31, 41, 54, 55].

3.1.3 Comparison

A summary of the previous sections and a comparison of the two most prevalent diseases associated with tremor, ET and PD, is done in table 3.2.

	Essential Tremor	Parkinson's Disease
Common Limbs Affected	Hands, Head & Voice	Upper & Lower Extremities and Chin
Accompanying Symptoms	None	Rigidity, Bradykinesia and Postural Instability
Frequency	Range from 4 - 12 Hz, but mainly 7 - 10 Hz	3 - 6 Hz
Tremor Classification	Action Tremor, Kinetic more than Posture, may have a slight resting component if severe	Resting, may have a slight action component if severe
Symmetry	Bilateral, can be mildly asymmetrical	unilateral initially, then bilateral and asymmetrical in advanced stage
Course	Progressive	Progressive
Response to alcohol	Significant	None
Effect of caffeine, stress and other stimulants	Increases	Increases
Inheritance	Autosomal Dominant with variable penetrance	Sporadic or related to genetics of Parkinson's disease

Table 3.2: Comparison of ET and PD [38]

3.2 Fourier Analysis

3.2.1 Fourier Series

A *Fourier series* is a representation of any arbitrary periodic function through an infinite sum of weighted sinusoids [56, 57, 58]. This series can be expressed in three different ways: *amplitude-phase*, *exponential*, and *trigonometric*. Only the latter will be discussed further. Let $f(t)$ be any periodic signal with period T_0. Then $f(t)$ can be written as a trigonometric Fourier series of the form

$$f(t) = a_0 + \sum_{n=1}^{\infty} [a_n \cos(2\pi n f_0 t) + b_n \sin(2\pi n f_0 t)] \tag{3.1}$$

with

$$a_0 = \frac{2}{T_0} \int_{t_0}^{t_0+T_0} f(t)dt, \tag{3.2}$$

$$a_n = \frac{1}{2T_0} \int_{t_0}^{t_0+T_0} f(t) \cos(n f_0 t)dt, \tag{3.3}$$

and

$$b_n = \frac{1}{2T_0} \int_{t_0}^{t_0+T_0} f(t) \sin(n f_0 t)dt, \tag{3.4}$$

From which it can be seen that a_0 is the time averaging component of the signal $f(t)$, and a_n and b_n is the amplitude component of its cosinusoid and sinusoid, respectively. In Eq.3.1, Fourier proved that the signal $f(t)$ can be represented by a sum of scaled sines and cosines at multiples of the *fundamental frequency* f_0, which is defined as $f_0 = 1/T_0$. These multiples, or scaled sines and cosines, are called *harmonics*, and a sinusoid or cosinusoid at frequency $n f_0$ is called the nth harmonic [57, 58].
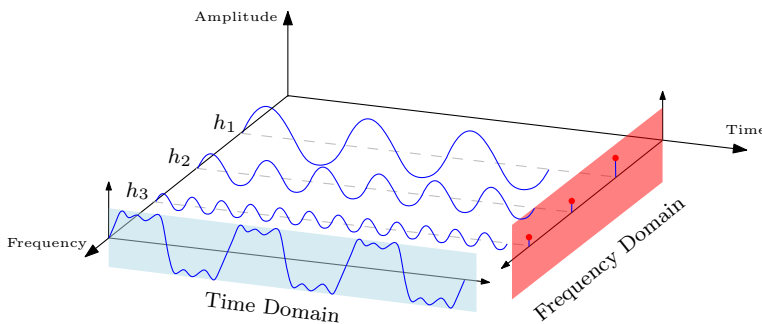
Figure 3.1: Visual example of a time function of a square wave, its first three harmonics and its representation in the frequency domain [Author], based on figure in [23]

3.2.2 Short-Time Fourier Transform

Using the Fourier series (or the Fourier Transform for non-periodic signals) one can represent the time-series in the frequency domain. However, the spectral content is not always stationary, so a method to represent a signal's frequency over time is found in the Short-Time Fourier Transform (STFT). With the STFT it is possible to analyse a signal that has a frequency content that is changing over time. It is defined as

$$F(\tau, \omega) = \int_{-\infty}^{\infty} f(t)w(t - \tau)e^{-j\omega t}dt, \tag{3.5}$$

Basically, with the STFT one defines a window, the overlap between windows and a window function (the form of the window). The original signal is then multiplied with the window to generate smaller, filtered segments of the original signal. For each segment, the frequency content is found and the result is usually represented as a spectra of time and frequency.

3.3 Vibrations and Vibration damping

Already from the first year, engineering students are introduced to the world of vibrations. Vibrations are a common phenomenon, and they occur in everything from numerous functions in the human body to most mechanical and structural systems. They are commonly introduced in subjects concerning differential equations, e.g. in linear algebra or physics courses, mostly known in the form of *oscillations* of mass-spring-damper systems or pendulums.

A vibrating system in general consists of three elements. A means of storing potential energy, commonly through an elastic/stiffness property (e.g. a spring); a means of storing kinetic energy, commonly through an inertia property (e.g. a mass); and a means of depleting energy from the system, commonly through a damping property of (e.g. a damper) [59, 60, 61].

There are several ways to classify vibrations. Vibrations can be seen as *free* or *forced*. Free vibrations are vibrations where the system is in motion due to its own properties, whereas forced vibrations are the vibrations subjected onto a system by an external force. They may be *deterministic* (periodic), where the value of the excitation is known at any given time; or completely *random*. If energy dissipates from the vibration, due to e.g. friction or other resistance, the vibration is *damped*, else the vibration is an undamped vibration. The final distinction between vibrations is whether or not they are *linear* or *nonlinear*, which has to do with the three elements of vibration and if they behave linearly or not [59, 61].

In its simplest form a vibrating system can be described by its equation of motion (EoM):

$$m\ddot{x} + c\dot{x} + kx = F(t). \tag{3.6}$$

$\omega_0 = \sqrt{\frac{k}{m}}$	Natural Frequency
$c_c = 2m\omega_0$	Critical damping Coefficient
$\zeta = \frac{c}{c_c}$	Damping Ratio/Factor
$\omega_d = \omega_n \sqrt{1 - \zeta^2}$	Damped Natural Frequency

Table 3.3: Fundamental Terms of Vibration Theory (Information gathered from [62, 59, 60, 63])

This is derived directly from Newton's 2nd law of motion. The generalized position is represented by x, and the dots represent differentiation with respect to time t; hence $\dot{x}$ and $\ddot{x}$ is velocity and acceleration, respectively. The mass is given by m, c represents the damping, while k represents stiffness. For more complex systems, other methods like Lagrange's EoM are more suited to find the differential equation of the system.

The solution of Eq. 3.6 consists of two parts, the solution to the homogeneous equation ($F(t) = 0$), $x_h(t)$; and the solution to the particular equation, $x_p(t)$:

$$x(t) = x_h(t) + x_p(t). \tag{3.7}$$

Introducing the terms in table 3.3, and rearranging Eq. 3.6, the rewritten equation yields:

$$\ddot{x} + \frac{c}{m}\dot{x} + \frac{k}{m}x = \frac{1}{m}F(t) \tag{3.8}$$

$$\ddot{x} + 2\zeta\omega_0\dot{x} + \omega_0^2 x = \frac{1}{m}F(t) \tag{3.9}$$

For vibrations to occur and last, the system needs to be either a free ($\dot{x}$ term $= 0$), or a forced underdamped ($\zeta < 1$) system; else the system will eventually come to a stop. More often than not, vibrations are not desired; may it be in structures, buildings, engines, transportation systems, and so on. Stiffening, damping and isolation are several methods of avoiding vibrations. However, vibration damping is the most relevant method when it comes to suppression of vibrations [64, 59].

The vibration damping may be differentiated in three ways: passive, active or semi-active damping. A passive damper does not take into account any measurements from the primary system (see figure 3.2), other than what was used to tune it initially. It relies solely on its non-adjustable properties to dampen the vibrations. On the other hand, an active damper will use sensors to measure the signal from the primary system, and use some sort of actuator to produce an output, e.g. force, which will counter the vibrations. A semi-active solution will combine the passive and active solutions where the properties of a passive damper can be adjusted to measurements from the primary system using sensors and actuators. These methods are exemplified in figure 3.2, where the dampers are vibration absorbers [59, 23].
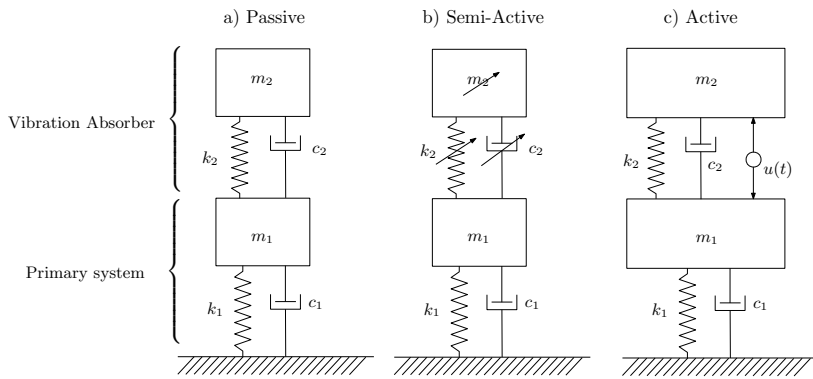
Figure 3.2: Vibration Absorber Types [Author], inspired by [23]

3.3.1 Dynamic Vibration Absorber

The dynamic vibration absorber (DVA) is a mechanical device, used to reduce or cancel vibration. Essentially it is a mass-spring-damper system that is connected to a primary system which is not desired to vibrate [59, 64, 65]. For simplicity, both the primary system and the DVA are modelled as a single DOF each, resulting in a two DOF system (See figure 3.3) with two natural frequencies.
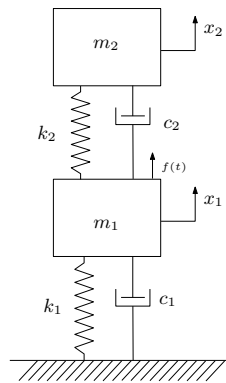
Figure 3.3: Free-Body Diagram of DVA [Author]

Typical areas of application of the DVA include reciprocating tools, for instance electric saws, sanders, or combustion engines. Without a vibration damper in these systems, the device might be impossible to hold or control due to the reciprocating forces. Other applications of DVA are civil engineering structures, such as high-rise structures or bridges, where wind and load may cause unwanted vibrations [59, 64, 65].

The behaviour of the DVA can be explained by looking at the equations of motion:

$$\begin{bmatrix} m_1 & 0 \\ 0 & m_2 \end{bmatrix} \begin{Bmatrix} \ddot{x}_1 \\ \ddot{x}_2 \end{Bmatrix} + \begin{bmatrix} c_1 + c_2 & -c_2 \\ -c_2 & c_2 \end{bmatrix} \begin{Bmatrix} \dot{x}_1 \\ \dot{x}_2 \end{Bmatrix} + \begin{bmatrix} k_1 + k_2 & -k_2 \\ -k_2 & k_2 \end{bmatrix} \begin{Bmatrix} x_1 \\ x_2 \end{Bmatrix} = \begin{Bmatrix} f(t) \\ 0 \end{Bmatrix} .$$
(3.10)

These equations are derived by considering the free-body diagram (figure 3.3. Further, the Laplace transformation gives the EoM as functions of frequency:

$$\begin{bmatrix} m_1 s^2 + (c_1 + c_2)s + (k_1 + k_2) & -c_2 s - k_2 \\ -c_2 s - k_2 & m_2 s^2 + c_2 s + k_2 \end{bmatrix} \begin{Bmatrix} x_1 \\ x_2 \end{Bmatrix} = \begin{Bmatrix} f(t) \\ 0 \end{Bmatrix}$$
(3.11)

$$\begin{Bmatrix} x_1 \\ x_2 \end{Bmatrix} = \frac{1}{\Delta(s)} \begin{bmatrix} m_2 s^2 + c_2 s + k_2 & c_2 s + k_2 \\ c_2 s + k_2 & m_1 s^2 + (c_1 + c_2)s + (k_1 + k_2) \end{bmatrix} \begin{Bmatrix} f(t) \\ 0 \end{Bmatrix}$$
(3.12)

Eq. 3.12 gives the displacement of the system masses, where $\Delta(s)$ is the determinant of the matrix in Eq. 3.11. Now, the DVA parameters (k_2 and c_2) needs to be tuned. The tuning depends on the nature of the excitation and whether the suppression device is to act in a narrow or wide frequency band..

Given a narrow bandwidth, which will be the focus of the thesis, the absorber is tuned to one particular frequency [59, 64]. Assuming an excitation of harmonic nature, the force and the related displacement can be expressed as:

$$f(t) = Fe^{j\omega t}$$
$$x_1(t) = X_1 e^{j\omega t}$$
$$x_2(t) = X_2 e^{j\omega t}$$

then Eq. 3.12 can be rearranged as:

$$\frac{X_1}{F} = \frac{k_2 + j\omega c_2 - \omega^2 m_2}{\Delta(j\omega)}$$
(3.13)

$$\frac{X_2}{X_1} = \frac{k_2 + j\omega c_2}{k_2 + j\omega c_2 - \omega^2 m_2}$$
(3.14)

Looking at Eq 3.13, if the excitation frequency ω is constant, then $c_2 = 0$ and $\sqrt{k_2/m_2} = \omega$ are the best choice of parameters.

3.4 Signal Processing

In this thesis, Power Spectral Density (PSD) is the main analysis tool used to evaluate the tremor signal data.

The tremor data to be analysed is a time series of accelerometer/gyroscope data that measures the angular velocity [deg/sec] of flexion-extension or pronation-supination movement of the wrist. Traditionally, accelerometers have been used for measuring tremors,

however, in the previous work done by Sunde and Estenstad, the choice to use gyroscope sensors was made due to the gyroscope's property of compensating for the orientation change caused by gravity.

An example of the data from the gyroscope can be seen in figure 2.5.

3.4.1   Power Spectral Density

The Power Spectral Density is defined as:

$$S_x(\omega) = \lim_{T \to \infty} \frac{1}{T} E\big[|\mathcal{F}\{\omega\}|^2\big], \tag{3.15}$$

where, $S_x(w)$ is the PSD, and $\mathcal{F}\{x\}$ is the Fourier transform of the time signal per unit time.

The PSD is the frequency response of a random or periodic signal, and is used to obtain the distribution of power across frequencies.

Since PSD is a density function, if the process $x(t)$ has the unit [m] (meters), then the PSD will have the unit [m^2/Hz]. This is because the frequency with unit [Hz] is the independent variable. For accelerometer data the PSD unit is often [g^2/Hz], where g is g-force (acceleration at free fall).

There are two types of PSD plots, linear and logarithmic. The linear scale provides the same level of detail for all frequency values, from which it is easy to distinguish the highest peaks of the signal. However, smaller peaks and the details of the signal are lost. The logarithmic scale "compresses" the signal, so that details of the higher harmonics (smaller peaks) are shown.

Welch-Barlett method of PSD estimation is the most common method of PSD analysis used on tremor signals [66, 67, 68]. A duration of 5-10s window is recommended for most tremor signals, with an overlap of 50% [66]; consenquently, a Hanning window of 10s with an overlap of 10% is used for all plots in this thesis. The plots are made with the *scipy.signal.welch* module from the open-source software SciPy.

Chapter 4

Preliminary Study

This chapter presents a literature study on the assessment of tremors. To be able to verify or reject the technology in a forthcoming experiment, it is important to know how tremors are evaluated.

4.1 Tremor Assessment Literature Study

When evaluating assistive devices there are several aspects to consider. Whether or not the effects of the assistive device are positive is one of them. The answer to that is in many cases subjective to the user, however, the effect needs to be verified. In this study, the goal is to be able to answer two main questions:

- What method should be utilised to analyse the collected data?
- What tests should be performed when testing on humans?

As stated in section 2, Sunde and Estenstad utilised PSD (see section 3.4.1) to evaluate the vibration's frequency estimation. These tools for spectral and time-frequency analysis are well established in the literature and commonly used in vibration or tremor analysis [66].

In the paper by Arnold et al. [69], the effectiveness of a controlled-energy-dissipation orthosis prototype, CEDO 1, for persons disabled by pathological intention tremors were assessed. The system is built up by an orthosis that mounts to a wheelchair or table for "table-top" activities. The investigation was conducted on five tremor-disabled and five able-bodied subjects. Their forearms were secured to the CEDO 1 and they were given pursuit tracking tasks on a computer to verify that the dampening load the CEDO 1 applied did selectively dissipate upper-extremity intention tremor. In addition, to determine the range of dampening loads needed, both linear and nonlinear damping trials were done.

The data from the trials were analysed in both time and frequency domains. In the time domain the $2D$ X and Y positions of the target and response markers were recorded as functions of time, in addition to the angles and angular velocities of the CEDO 1 brake

axes and commanded brake torques. In the frequency domain a MATLAB$^{\circledR}$ spectral analysis algorithm, based on the Welch method of power spectrum estimation was utilised; much like in [22, 23].

The results were assessed in terms of tremor power and tracking performance. Tremor power was computed by summing the tremor position spectrum, while the tracking performance was assessed based on a ratio of signal power, the sum of cross-power spectra; and the tremor power. Furthermore, subjective responses from test subjects were provided in addition to an analysis of the repeatabilitiy of the results based on multiple test sessions.

Yusop et al. [70] aim to evaluate an assistive device for hand tremor suppression during writing. The device acts as the pen and tremor suppressor by passively absorbing hand vibrations when writing. The device is mainly developed to suppress tremors vibrating perpendicular to the forearm, as it is in the general direction vibrations occur during writing. It consists simply of two springs functioning to absorb the vibrations, and a centre core functioning as the system mass. As the system is completely passive, the springs need to be chosen correctly.

The system is validated through a test conducted by one clinical diagnosed ET patient, and two healthy individuals. They were to perform two tasks during two different conditions: sitting with arm resting on the table, and standing when the arm is prevented from resting on the table. The tasks the subjects needed to perform were to trace the Archimedes Spiral and to trace the phrase "Hello World". The results were evaluated by time-frequency analysis by utilising PSD to compare the data, and they base the evaluation on the reduction of the signals.

Despite the fact that PSD is seemingly a good measure of tremor frequency a more clinical way of assessing tremors exists in the medical world. Several scales and screening instruments exist with the purpose of evaluating the tremor severity, and the disability and quality of life of the patients due to tremor.

The paper of Bain et al. [71] presents the assessment of a proposed clinical rating scale which measured the severity of tremor in total 28 patients, from which 20 suffered from ET and 8 from dystonia. The purpose of the study was to decide if a clinical rating scale could be used, reliably, to assess the severity of tremor in individuals with ET or dystonia. This evaluation was done for both inter and intra-rater reliability with four raters. A score between 0 and 10 was assigned based on the tremor severity in each of the patient's head, vocal, right upper limb, left upper limb, right lower limb and left lower limb. These scores were compared to upper limb accelerometry, an activity of daily living self-questionnaire and two written test: handwriting and drawing of an Archimedes Spiral.

Another clinical rating scale is proposed by Fahn et al. [72], namely the "Fahn-Tolosa-Marin Tremor Rating Scale" (FTM). The scale aims to evaluate the severity of several forms of tremor: rest, postural, action and intention. In addition, it aims to evaluate tremor during specific tasks like handwriting, contrary to scales like Sweet et al. [73], which evaluates body parts more generally.

The assessment is divided into three parts: A, B and C. Part A rates the severity of

tremors in the body for three situations: rest, maintaining a posture and performing an activity. Part B rates the action tremor of the upper extremities, by exposing the subjects to writing and pouring liquid tasks. Also here the Archimedes Spiral is used as one of the drawing tasks, in addition to straight lines. Part C assesses the functional disability, that is, it assesses the daily life activities like eating, hygienic care, dressing and working.

The scores are given on a scale between 0 and 4, but each part has its own definitions. Part A gives score based on amplitude, and has a subtotal score of 80 points. Part B has a subtotal of 36 points. The handwriting task is rated based on legibility, while the drawing task is based on the number of times the patients cross the lines they are supposed to draw between. The water pouring task is rated based on amount of water spilled. The scores of Part C are provided by the subjects themselves. The subtotal of Part C is 28 points. This makes the maximum possible score 144 points.

In addition to these three parts, a subjective overall severity assessment for both examiner and subject is allowed. Moreover a subjective comparison assessment, where the patients can state the severity of the tremors compared to last visit is allowed. The latter is incorporated to scale for evaluating the effectiveness of the treatment.

This clinical rating scale was not statistically evaluated for validity and reliability at the time it was proposed, however, as stated in [74], the Fahn-Tolosa-Marin scale was "the most widely used scale" until 2003. It was also assessed for inter and intra-rater reliability by Stacy et al. [75], with mixed results.

Both [71] and [72] are two of many scales that are assessed by a task force established by the Movement Disorder Society [76]. The task force seeks to review a set of rating scales for the assessment of tremors. In all, seven tremor severity scales, six activities of daily living (ADL) scales, four quality of life scales and five screening instruments were assessed. They were classified as either recommended, suggested or listed based on whether 3, 2, or 1 of the three criterion were met:

- Used in the assessment of tremor
- Used in published studies by people other than the developers
- Successful clinimetric testing

Clinimetric testing was considered successful if the scales were proven to be reliable, valid and sensitive to change.

Out of the seven severity scales five were classified recommended, including the FTM and the Bain and Findley Clinical Tremor Rating scale in [71]. The Essential Tremor Rating Assessment Scale (TETRAS) by the Tremor Research Group in Elble [74] was also one of the recommended severity scales. This scale is similar to the FTM, but it handle what it refers to as limited validation in ET and too low upper extremity tremor amplitude anchors for severe ET in the FTM. Like the FTM TETRAS requires little equipment, mainly pen and paper, to rate the tremors. The assessment can also be completed in about 10 minutes.

The scale has two sections, one performance section which resembles Part A of FTM, and one ADL section which resembles Part B of FTM. Each of the sections has a 5-points rating scale and they include 12 and 9 items/tasks for performance and ADL rating, respectively.

Although evaluation of assistive technology usually has more focus on signal processing and less focus on these types of rating scales, there are certain similarities in the assessment tasks. What the scales provide is a clinical measure that makes more sense to the common man.

Pathak et al. [77] have conducted a pilot study on a handheld assistive device, that works as a spoon that stabilises while eating. The device utilises Active Cancellation of Tremor (ACT) technology, which consists of the spoon, the controller/sensors, the motion generating platform and the power supply. The assessment of the device was done through three tasks on fifteen ET subjects, with the ACT device both turned on and off. The tasks the subjects were required to perform were holding, where the subject held the device midway between the table and their mouth; eating, where the subjects lifted the filled device to their lips; and transferring, where the subjects transferred the content of the spoon to a cup. The severity of the tremors was rated by the FTM, however, a subjective improvement scale was also utilised, namely the Clinical Global Impression Scale (CGI-S). The results yielded improved scores with the ACT device turned on in all three tasks. Time-frequency of the accelerometer data was also provided and analysed, in addition to statistical analysis of the FTM scores.

Based on this literature study, it is safe to say that there are many ways to assess tremors. However, some scales, like TETRAS, is specific for certain diagnosis; while other are more general. It is therefore important to understand what is to be evaluated and the extent of the evaluation when choosing in what way to assess a tremor. The flexibility of the rating scale also needs to be evaluated with regards to whether or not it is possible to remove tasks and still have a valid result. Nonetheless, some tasks seem well established for their purpose, such as drawing of the Archimedes Spiral as a written/drawing task.

   In conclusion, two ways to assess the effects seems prominent. Either by

1. Looking at the tremor signal before and after wearing the device.

2. Looking at the ability to perform certain tasks before and after wearing the device.

or a combination of them. However, the subjective opinion of the patient must not be forgotten, neither must the opinion of a trained professional. The FTM scale seems promising and is recommended for further use.

Chapter 5

System Overview

This chapter presents the hardware foundation and system architecture of the tremor suppression system. The various components and the complete system setup is described. In addition, laboratory safety is mentioned. To be able to test several setups more efficiently, the development is done on a robotic manipulator rather than a fixed prototype. However, design proposals for a prototype by Estenstad is presented in appendix C.

5.1 Universal Robots UR5

All hardware information in this chapter is acquired from [78], if not stated otherwise.

The development in this thesis is done on a Universal Robots UR5 robot provided by ITK at NTNU. The entire robotic system is made up by the 6-axis industrial manipulator, the Controller Box and the teach pendant, illustrated in figure 5.1.

The manipulator is applicable in most industries, especially due to its many built-in safety mechanisms. The UR5 is classified as a collaborative industrial robot, meaning it was made to work in environments consisting of humans, and still be safe. It complies to article 5.10.5 of the EN ISO 10218-1:2006 standard, which states that the robot can operate as a collaborative robot, without safety guards between the robot and the user/operator. The manipulator weighs 20.6 kg, has a reach of 850 mm and a maximum payload of 5 kg. A maximum of 150N is allowed for a collaborative operation.

The control hierarchy of the UR5 is presented in figure 5.2. There are three different methods to control the manipulator: through the user interface Polyscope, preprogrammed and embedded in the teach pendant; utilising Universal Robot's own script called URScript; or through a C-API for the manipulator. All three methods have a maximum joint servo updating rate limited by hardware to 125 Hz.

This thesis will utilise drivers based on URScript to program the UR5, for several rea-

Figure 5.1: Overview of the Universal Robots UR5 Robot system. It consists of three components: The robot manipulator, the controller box centred on the table, and the teach pendant attached to the controller box. Picture in courtesy of [79]
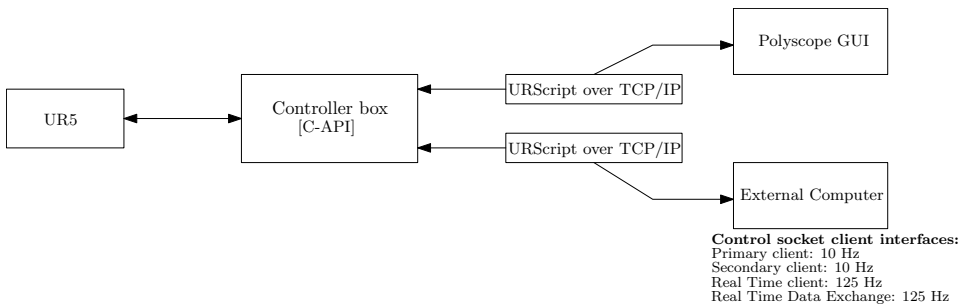
Figure 5.2: UR5 Control Hierarchy [Author], Inspired by [21]
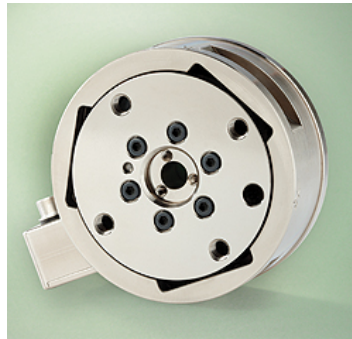
Figure 5.3: Gamma F/T sensor by ATI Industrial Automation [80]

sons. Firstly, the Polyscope interface on the teach pendant lacks the flexibility that is provided through programming. It is a simple GUI mainly developed for users without programming background, even though it can in provide fast implementation, debug and prototyping. The Polyscope can also be used to program the robot sequentially through a combination of URScript commands.

Secondly, the C-API, a C library provided by Universal robots, is not suitable either. The reason for that is the fact that the C-API does not support direct low-level joint torque control [21], which is probably a security measure to prevent override of the safety mechanism firmware. In addition, the library is not maintained and poorly documented [21].

The URScript on the other hand, is constantly being maintained and developed since it was developed specifically for controlling their manipulators. The robot is controlled by establishing a TCP/IP socket connection, and programmed using drivers which are written in modern programming languages like Python or C++.

5.2 Force/Torque Sensor

Hardware information in this chapter is acquired from [80], if not stated otherwise.

The force/torque (F/T) sensor used in this thesis is the ATI Industrial Automation Gamma F/T sensor. It was made available by ITK through a collaboration with SINTEF, who owns the sensor. The sensor, which is illustrated in figure 5.3, comes with a F/T Net Box which processes and further communicates the sensors readings to an external computer. The Net Box draws power and communicates trough a power over Ethernet switch, which enables users to establish a socket connection to the F/T sensor.

Through a network configuration interface it is possible to specify sensor settings e.g. the broadcasting frequency can be set between 1 and 7000 Hz, that is the sampling rate of the sensor. As the real-time interface for the UR5 is 125 Hz, and the F/T sensor is capable of running significantly faster, the manipulator can run at a higher frequency than

the tremors. Hence, according to Nyquist's sampling theorem, the minimal sampling frequency should be at least twice as fast as the quickest dynamic in the system [81, 82], we get that

$$f_{sampling} \geq 2 \times f_{max},$$
$$f_{sampling} \geq 2 \times f_{robot},$$
$$f_{sampling} = 2 \times 125Hz = 250Hz$$

The calibration settings are presented in table 5.1. It displays the embedded sensing range and resolution of the sensor.

The purpose of the force sensor in this thesis is to measure force to ensure a compliant manipulator. When the users are to execute different tasks, the manipulator must, at any time, be able to follow the hand.

Calibration	Sensing ranges				Resolution			
	F_x, F_y	F_z	T_x, T_y	T_z	F_x, F_y	F_z	T_x, T_y	T_z
SI-165-5	65 N	200 N	5 Nm	5 Nm	$\frac{1}{80}$ N	$\frac{1}{40}$ N	$\frac{10}{13333}$ Nm	$\frac{10}{13333}$ Nm

Table 5.1: Calibration details of the ATI Gamma F/T sensor [80]

5.3 Microcontroller

To implement the BMWFLC algorithm developed by Sunde (see section 2 and appendix A) a microcontroller and two sensors are used. The microcontroller is an Arduino Uno rev3 developer board, based on the ATmega328P Microcontroller Unit (MCU); and the sensors are of the Sparkfun LSM6DS3 type. The sensor board is an Inertial Measurement Unit (IMU) equipped with both accelerometer and gyroscope sensors. Traditionally, tremors have been measured using accelerometers, however, Sunde [23] argued for using gyroscope sensors instead. Hence, using the same setup as Sunde, only the gyroscope sensors on the board are activated. These sensors are used to measure the tremors on the wrist of the user, and possibly on the tremor suppression device, i.e. the UR5. In a final prototype device, only one sensor will be needed.

The Arduino Uno will process the data from the sensors with the BMWFLC algorithm and direct the processed data to an external computer.
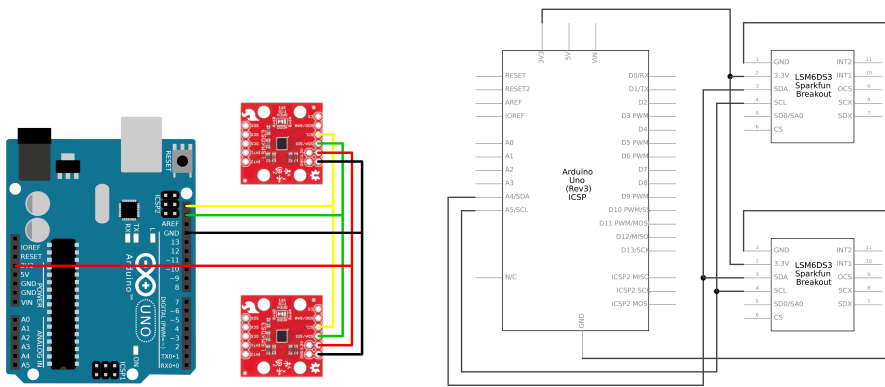
(a) Wiring Diagram of the Arduino Uno and two LSM6DS3 breakout boards [23]

(b) Connection between the Arduino and the two LSM6DS3 [23]

Figure 5.4: Schematics of the Microcontroller setup, used to implement the BMWFLC algorithm [23]

5.4 Hardware Interface

The interface between the robot manipulator and the user is depicted in figure 5.5. It is a simple velcro-band attached to a metal disk, which connects the F/T sensor to the band. The disk will provide a more even distribution of pressure to the sensor. The hardware interface was designed and made in collaboration with the technical staff at the mechanical workshop at ITK.
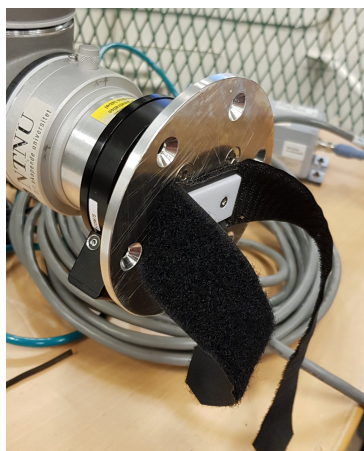
Figure 5.5: Hardware interface with F/T sensor attached to the UR5 end-effector [Author]
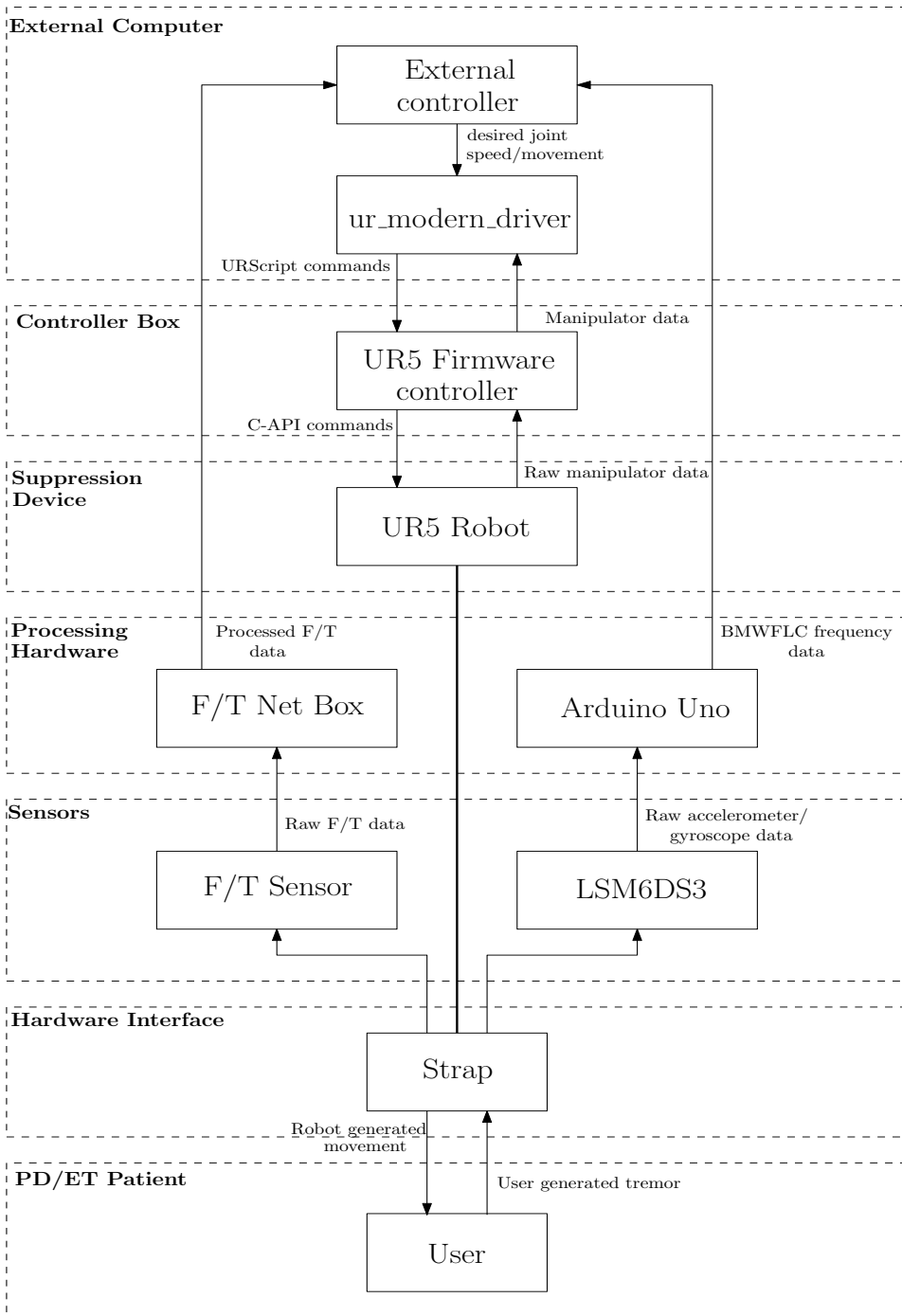
Figure 5.6: System architecture of the tremor suppression system [Author]

5.5 Complete System Setup

The complete system setup, combining the hardware and software components is illustrated in figure 5.6. Most of the architecture components can be changed out with other components, making the system highly modular. This will make the transition to prototyping of the actual wearable device smoother. The software is explained in greater depth in chapter 6.

5.5.1 Laboratory Safety

The hardware components of the complete system setup is depicted in figure 7.1c. When working in an environment like this, particularly with human interaction in mind, questions regarding safety arise. Consequently, a risk assessment has been performed to minimise damage to both humans and equipment. The assessment can be found in appendix G.

Chapter 6

System Design and Implementation

The behaviour of the UR5 as a tremor suppression device is realised through an external controller. This chapter presents the development and implementation of the control system design, strategy, calibration, tuning, and validation.

6.1 Specifications

Before implementation and analysis of the control system on the robot manipulator, it is important to establish the desired behaviour of the manipulator. The desired behaviour can be divided into two parts. Firstly, the patient strapped to the manipulator should be able to execute various tasks related to a chosen tremor assessment scale explored in chapter 4.1, hence the manipulator needs to be able to follow the movement of the patient's arm. Secondly, the manipulator needs to be able to dampen the tremors in the arm. In her thesis, Estenstad suggested to implement a form of semi-active DVA system. Consequently, a mass-spring-damper behaviour is desired, where the stiffness of the spring may be controlled.

In addition to these main concepts of behaviour, some additional specifications are necessary. These are as following

- Quick response

- Safe

- Smooth and precise

It is important that the manipulator follows the arm movements sufficiently fast. It should not be more difficult for the patient to execute tasks like writing or drinking due to inertia or delay in the manipulator. Hence, a quick response is necessary. It is equally, or more important, that the manipulator acts safely. The patient should not at any time feel unsafe while strapped to the robot. This is elaborated further in the risk assessment in appendix

G, however, no implementation should weaken the safety of the manipulator. At the same time unnecessary extra safety mechanisms that slow the system down should be avoided. Smooth and precise movements also have to do with safety. A manipulator moving in fits and starts will not be safe for the patients, additionally, the purpose of utilising the robot manipulator is lost. The manipulator should not apply any excessive force on the patient apart from what is necessary and required for the demonstration of the behaviour of the device.

When analysing the control system and the response of the manipulator, an evaluation of the manipulator's ability to adhere to these behavioural specifications should be performed.

6.2 Implementation Challenges

During implementation of the control system and tuning of the manipulator, several challenges occurred and should be addressed. Here, the two main challenges are identified and analysed, before a solution and its effect on the system is presented. Workspace limitations are not discussed, as the area of interaction in the experiment is limited well inside the boundaries of the manipulator workspace.

6.2.1 Unwanted Oscillations

Early testing of the force controller developed by Laastad [21] revealed unwanted shaking movement in the manipulator. It was suspected that this was due to an untuned controller, however, as this was addressed by Laastad as well, that hypothesis was discarded. Laastad implied that several sources generated these unwanted movements, including an unwanted feedback loop due to human arm inertia. However, this is more likely a reason for the unwanted movement to persist rather than the source of the movement. A more probable reason as a source may be noise and bias in the sensor.

Nevertheless, the movements can be identified as high-frequency oscillations. These are not dangerous for the patients, but may have an impact on the perception of safety by the patient and also feel uncomfortable.

The easiest way to counteract these oscillations is by low-pass filtering the sensor data. This can be done through an option in the F/T Net Box web interface. Several predefined cut-off frequencies are provided as option, ranging between 5Hz to 837Hz. Various frequencies were tested, and a cut-off frequency of 5Hz was clearly the frequency that provides best stability to the system.

There are both positive and negative sides to choosing a cut-off frequency of 5Hz. On one side, the delay caused by low-pass filtering 5Hz is ≈ 36ms, whereas a higher cut-off frequency would yield a lower delay. On the other side, the 5Hz provides a smooth and safe motion. Ultimately, the safety of the patient is more important, and a frequency of 5Hz is chosen.

6.2.2 Bias

Initial implementation also uncovered a bias in the sensor. It was speculated that this bias was a *mounting bias*, due to either the centre of mass of the hardware interface not aligning with the sensor origin, or because of the mounting screws. However, after corresponding with Mathias Hauan Aarbo, it was further speculated if this bias existed due to an *internal bias* in the sensor. The total bias in the sensor is presented in table 6.1. The risk of this bias creating any serious injuries is assessed to be small, however it is also assessed that the bias will generate unwanted movement, in the form of a constant drift. Hence, preventive measures should be taken.

Forces [N]			Torques [Nm]		
F_x	F_y	F_z	T_x	T_y	T_z
3.529	-0.391	5.886	0.154	-0.1008	-0.0637

Table 6.1: Bias in the F/T sensor [Author]

Using a software offset in the external controller the mounting bias can be removed. The F/T Net Box web-interface also has settings that compensates for bias within the sensor. However, this method masks both the bias and the gravity components of the equipment in initial tool frame. Any rotational movement in the end-effector will expose the equipment weight in the F/T sensor measurements.

When this was addressed by Laastad [21], both methods of removing bias were implemented as a double security measure. Due to the masking of the gravity components using the F/T Net Box bias remover, the external controller used a dead-band filter to compensate for the consequences of possible gravity compensation faults. In addition, an artificial gravity vector was introduced to separate the F/T mounting bias and the gravity components.

Since it was established that the bias exists due to, not only a mounting bias, but also an internal bias, a reconsideration of how the bias was going to be handled was done. Laastad used the initial raw data as an offset, essentially performing an estimation of the bias with the robot in its initial pose. However, when the dead-band filter was disengaged, some end-effector poses resulted in drift of the manipulator. An offline estimation was attempted, averaging the bias for two different poses of the end-effector and adding those values to an offset vector. Also this method resulted in drift for certain poses of the manipulator. Given that the bias in the force/torque sensors may be time-varying due to temperature variations in the metals in the F/T sensor, an estimation of the bias should be done before each use of the manipulator. An optimal solution would probably be an initialisation routine, where the raw data from multiple positions would be used to estimate the bias. Instead, the method of Laastad seemed sufficient, and was implemented along with other measures.

Firstly, the gravitational component was calculated as in Eq.6.1 and compensated for with

an artificial gravity vector, as done by Laastad,

$$F_{equipment} = m \times a \approx 0.150\text{kg} \times 9.81\frac{\text{m}}{\text{s}^2} = 1.472\text{N} \tag{6.1}$$

$$\tau_{equipment} = F \times l \approx 1.472\text{N} \times 0.005 = 0.000375\text{Nm}$$

Next the centre of mass was calculated and added to the DH-parameters. This was done according to eq.6.2.

$$\tau_{x,y} = F_z \times z_{com_{x,y}} \tag{6.2}$$

$$z_{com_{x,y}} = \frac{\tau_{x,y}}{F_z}$$

For x:

$$z_{com_x} = \frac{0.55}{6.641} \approx 0.083\text{cm}$$

For y:

$$z_{com_y} = \frac{0.56}{6.641} \approx 0.084\text{cm}$$

The force F_z is read directly from the F/T Net Box web interface when the end-effector was pointing downwards, parallel with a vertical line in the world frame. The end-effector is then rotated about the respective axes, x or y. Here, $\tau_{x,y}$ is read directly from the web interface from which the bias momentum is first subtracted. z_{com} is then averaged and added to the DH-parameter, to compensate for the position of the mass centre.

A "dead-band" filter was also incorporated to remove drift. The filter implemented by Laastad was a simple on/off filter, where the force or torque input would be divided by a number if it measured 1N and 0.5Nm respectively. Here, an upgraded filter using a type of a complement Gaussian filter is implemented:

$$F_{tresh} = (1 - e^{-\frac{F_{input}^2}{\sigma^2}})F_{input}. \tag{6.3}$$

Where σ is the window size, set to be $\sigma = 0.3$. This filter gives a more smooth transition while still removing drift.

Summarised, the measures taken to deal with bias in the sensor are gravity compensation, mass centre estimation, initial estimation by initial raw data offset and a dead-band filter. Most of the measures were also taken by Laastad, with exception of mass centre estimation. This thesis excludes the use of the F/T Net box bias reset, as it is considered unnecessary. The methods presented significantly reduce the effect of the bias, but if accurate force measurements are to be used in scientific trials where they are to represent the forces exerted by the patient, adaptive, online bias estimation techniques may be required as well as further calibration of the sensor itself.

6.3 Gravity Compensation Calibration and Validation

To compensate for the mounting bias, the F/T mounting bias and the gravity component was separated. An artificial gravity vector, *tool bias vector*, was implemented in the software and is experimentally verified here. The experiment is built up the same way as done in Laastad [21], by three individual verification tests for each rotation. The manipulator wrist is manually rotated two times in 90 degrees increments about each axis. There is no contact between the operator and the manipulator after each rotation, and each test has the same initial position and orientation. Figure 6.1 and 6.2 shows the response without, and with the bias vector implemented, respectively.

Figure 6.1: Gravity compensation test, without a compensating bias vector [Author]

Looking at figure 6.2, where the bias vector is implemented, the rotations are performed at the following times:

- X-axis: 2s $\to$ 5.7s and 11.4s $\to$ 14.9s

- Y-axis: 1.6s $\to$ 6s and 11.8s $\to$ 14.9s

- Z-axis: 3.6s $\to$ 7.7s and 11.5s and $\to$ 14.5s

The gravity compensation for the rotation about the X-axis is more or less exact, only a small deviation in the X-axis is observed after the first rotation, $F_{x,R_x,90°} \approx -0.25$, and in the Y-axis after the second, $F_{y,R_x,180°} \approx 0.15$. Rotation about both the Y- and Z-axes show some deviation from 0 after the first rotation, but both these deviations are
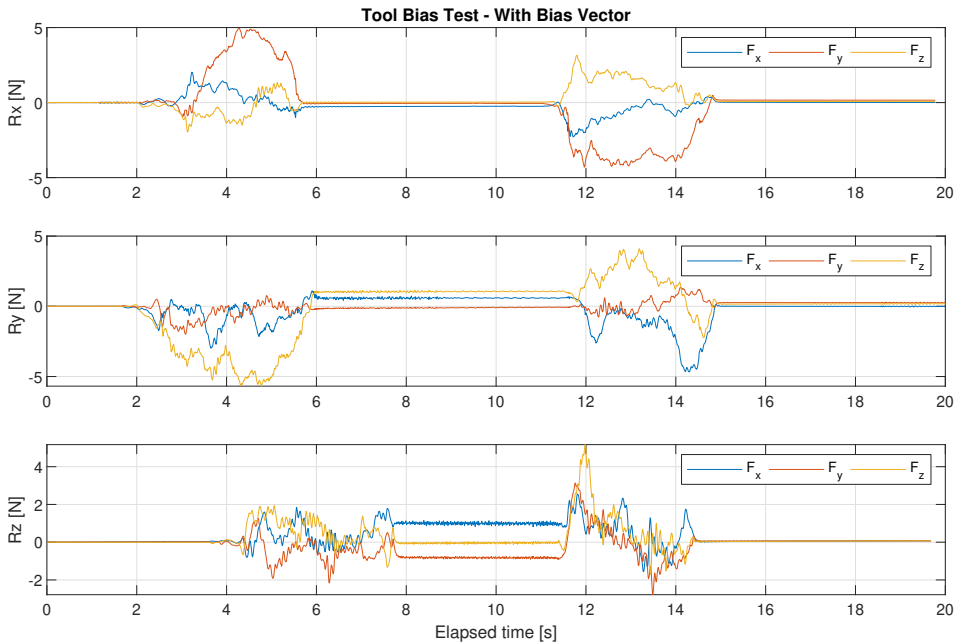
Figure 6.2: Gravity compensation test, with compensating bias vector [Author]

compensated after the second rotation. The deviations after the first rotations are as follows: $F_{x,R_y,90°} \approx 0.5$, $F_{z,R_y,90°} \approx 1$, $F_{x,R_z,90°} \approx 1$, and $F_{y,R_z,90°} \approx -1$. None of the deviations are larger than the estimated equipment weight force $F_{equipment} = 1.472$N, however, figure 6.1 shows that the largest deviation is larger then 2N.

The discrepancy is believed to stem from calibration problems associated with mounting and sensor bias. Laastad argued that this would pose a problem with a heavier interface design, our interface being approximately 0.1kg heavier than his. This would require an alternative to the simple dead-band filter. In practice, the complement Gaussian filter, Eq.6.3, suppresses the effect of the error.

Overall the gravity compensation is sufficient to carry out experiments. Further increasing the accuracy by on-line estimation of the sensor bias is considered future work.

6.4 Controller Design

This section presents the control strategy of a compliant manipulator with a mass-spring-damper behaviour. The controller may be divided into a low-level and high-level strategy, where the low-level controller ensure compliance of the manipulator. The DVA makes up the high-level strategy, which builds on the compliance mode.The controller hierarchy is illustrated in figure 6.3. Each level is elaborated further in the next sections.
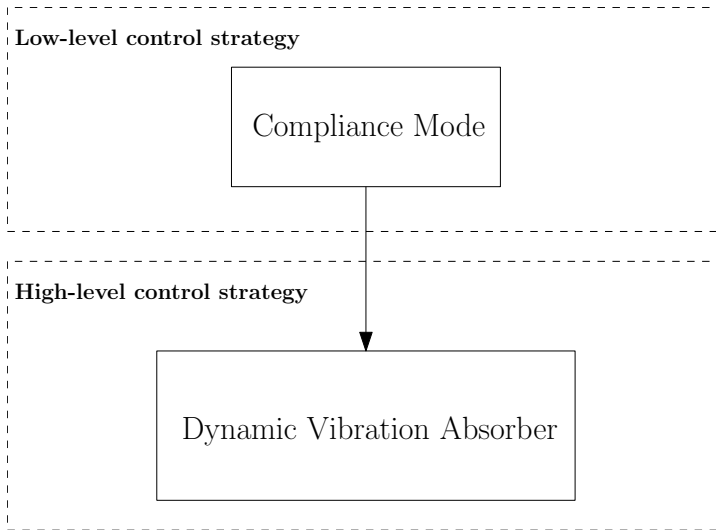
Figure 6.3: Controller Hierarchy [Author]

6.4.1 Low-level control strategy

The low-level system control scheme with an external force/torque controller is illustrated in figure 6.4; it is based on the work of Laastad [21]. It is comprised of both an external and an internal controller, where this section aims to develop the design of the external controller. The internal controller is lowest level of control, the direct servo control. These are largely proprietary, and descriptions of the lowest level controller in manipulators are not readily available. The internal controller is therefore regarded as a black box, meaning that all development should proceed with caution and in line with the risk assessment. The lowest control interface available for the external controller is a joint velocity interface. This is modified with safety limitations and motion buffers before being sent to the internal controller. It is assumed that it regulates the joint acceleration by manipulating the individual motor voltages. The joint accelerations are also modified with security measures before they are executed by the manipulator.
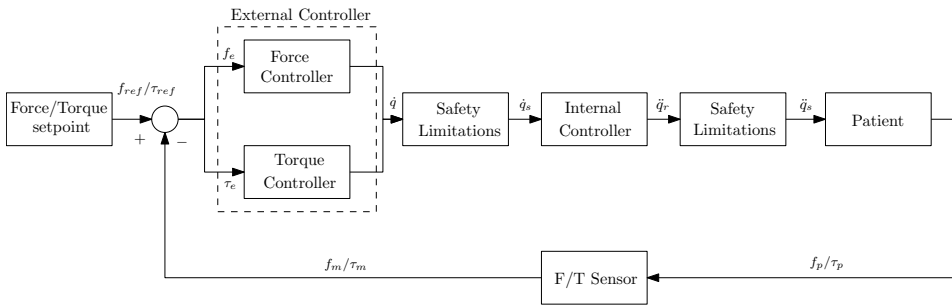
Figure 6.4: System control scheme with force/torque controller [Author], inspired by [21]

The safety limitations are summarised in the tables below. These are based on internal firmware limitations, and choices made to maximise safety in the external controller, respectively.

Manipulator Function	Description	Limitation
Joint position	Min. and Max. angular joint position	$\pm 360°$
Joint speed	Max. angular joint speed	$180°$
Force	Max. pushing force of the robot	150N
Momentum	Max. momentum of the robot arm	$25 \frac{\text{kg} \times \text{m}}{\text{s}}$
Power	Max. applied robot arm power	300W

Table 6.2: Firmware limiting safety mechanisms [Author], based on [21]

Manipulator Function	Description	Limitation
TCP force	Max. pushing force on robot TCP	50N
TCP torque	Max. rotating torque on the robot TCP	8Nm
Time	Max. controller run-time	200s
f_m/τ_m	Low-pass filter	5Hz
e_F	Dead-band filter force	± 1N
e_τ	Dead-band filter torque	± 0.5Nm

Table 6.3: External controller limiting safety mechanisms [Author], based on [21]

The compliance mode aims to follow any movement generated by the patient in six DOF. The F/T sensor measures the generated movement, compares it to the reference value, and passes the error to the external controller. In the system developed by Laastad, the force and torque controllers are separated since one set of gain parameters did not yield a desired behaviour for both transitional and rotational forces. Essentially, both controllers are the same with different gain parameters. This could have been solved with the gain parameters in a block-diagonal matrix, but for the sake of visualisation, they are separated

in figure 6.4. The resulting control values are added to a task space vector, which consist of of three linear velocity parameters, and three angular velocity parameters for the end-effector. Utilising Jacobian of the end-effector, the desired velocity control inputs are generated by inversion of the differential kinematics.

The controller itself needs to be chosen. Since the internal controller is unknown, it is unclear how the system will respond to an external controller. The worst case scenario is a conflict between the control signals of the respective controllers. The results of such a conflict is unpredictable. Because of the unknown outcome, in addition to non-linearities related to human-machine interaction, it is difficult to model the system, simulate and tune the parameters beforehand. Laastad suggested and conducted an incremental controller tuning process. The processes involves first implementing a P-controller, PI-controller, PD-controller and lastly a PID-controller for each force and torque. This is done to investigate the best solution with limitations imposed by the internal controller. The work of Laastad is validated by replicating his work in chapter 6.5.

6.4.2   High-level control strategy

Upon designing the high-level control strategy, new challenges emerged. These challenges are mainly related to the fact that a robot manipulator *must* have a compliant behaviour, while a wearable device does not. Initially, the thought was to build the DVA behaviour onto the compliance controller, the problem is that implementing a mass-spring-damper behaviour would need an initial position, an equilibrium point, about which the manipulator would oscillate. This means that the initially considered control strategy would only result in oscillations about the position the manipulator would be initialised in; any deviating movement from that point would only act as an external force that would introduce an inertia to the movement and when let go off would oscillate back to said point. Essentially, one would implement a system that would act like pulling a spring that is fixed to a wall.

To cope with this problem, the compliance and the DVA behaviour must be divided. To ensure compliance, it is assumed that a virtual wearable device is attached to the end-effector of the manipulator. This way, the equilibrium point can be attached to the end effector and the manipulator would be able to follow movement. When DVA is needed, the position the manipulator is in would initialise as equilibrium.

This, however, introduces a new problem; What is an intended movement and what is not? This problem is not solved in this thesis, but theoretically the solution is discussed.

A solution is to filter the F/T sensor data. The optimal filtering solution would be to band-pass filter the signal with the BMWFLC frequency as the cut-off frequency, as the BMWFLC is shown to separate intended and unintended movement. Hence, every movement with a frequency but the BMWFLC frequency would act as intended movement. For simplicity the system should be tested with a band-pass filter with frequencies within the range of the tremor, and let the residual frequencies be compliant movement. Another simple solution is a low pass filter with a cut-off frequency of e.g. 5Hz, if the manipulator displays safe movement with a F/T sensor cut-off frequency of 18Hz. Then all movement

with frequency below the cut-off frequency is assumed to be intended movement, while all movement above 5Hz is assumed to be tremors. This problem would of course not be a problem in a wearable device, hence it should only be implemented for the sake of testing on the manipulator. Theoretically, the solution of low-pass filtering is chosen in the development.

The resulting high-level control strategy is illustrated in figure 6.5. In addition to generating a force directly on the manipulator's end-effector, the patient will generate a movement. This movement, in form of acceleration is sensed by the IMU's accelerometer/gyroscope (LSM6DS3). The data is forwarded to an Arduino Uno where the BMWFLC algorithm processes the data and forwards the frequency with the most power to DVA. To be able to provide compliance, the DVA takes in all sensed F/T sensor data with frequencies over 5Hz in addition to the position and velocity of the manipulator end-effector. The F/T sensor data beneath 5Hz is sent to the F/T controller. The velocity from the DVA, $\dot{\tilde{x}}$, and the control output signal is then used to calculate a desired joint velocity, $\dot{q}_d$.
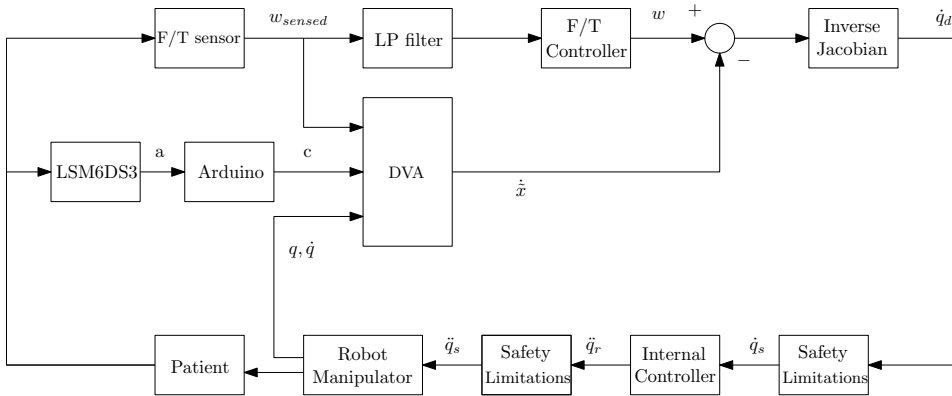

Figure 6.5: Complete control system with both low- and high-level strategies implemented [Author]

6.5 Force Control Validation and Tuning

This section aims to validate the controller parameters chosen by Laastad by replicating his experiment. The parameters will also be subjectively assessed, in terms of the specifications in chapter 6.1.

6.5.1 Testing setup

To validate and tune the controller the test setup used in Laastad is replicated. A simple cardboard box is placed on the table and the end effector is placed with the Z-axis pointing down, parallel with the vertical axis. For tuning of the force gains, the end effector is placed 1cm above the box. A reference of 2N pointing downwards is given for the duration of 5s. The setup for the torque gains are similar, however, the torque controller is given a reference of 1Nm about the Y-axis for the same duration.

It must be noted that the end-effector of the respective experiments are different, hence some discrepancy in the results are expected. The experimental testing, for instance, is not possible to recreate entirely in this thesis due to the design of the end-effector hardware interface. In Laastad's experiment an aluminium handle was made that pointed out of the end-effector. This handle was placed horizontally above the box, such that the Z-axis of the end-effector was parallel with the horizontal axis. The end-effector was then given a 1Nm torque about the Z-axis, so that the contact made between the handle and the box would generate torque measurements in the F/T sensor. As seen in figure 5.5, the hardware interface in this thesis does not have a handle, so a torque about the Z-axis in the same way, would not generate any measurements in the F/T sensor.

During the validation and tuning most of the safety features were turned off. A low-pass filtration with cut-off frequency in the F/T sensor was enabled. The cardboard box was used so that neither persons nor equipment would be damaged during experimental testing.
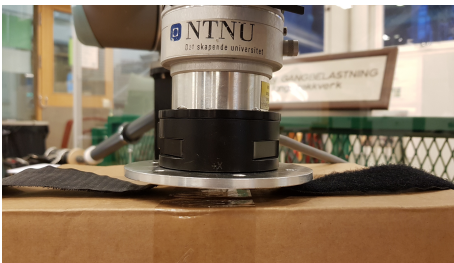
(a) Starting position for both force and torque gain estimation experiment.
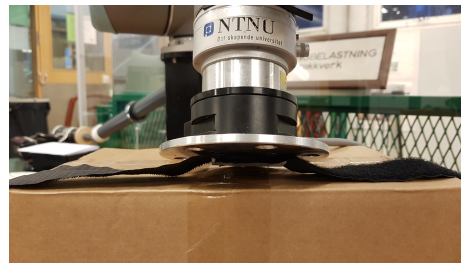
(b) The torque gain estimation is estimated by the end effector rotation about the Y-axis. Hence the edge of the end effector generating torque in the F/T sensor.

Figure 6.6: Force/Torque Controller Gain Estimation Test Setup [Author]

6.5.2   Force Controller

Proportional Gain Estimation

Numerous proportional gain parameters are tested for the force P-controller. The most relevant results are presented in figure 6.7.
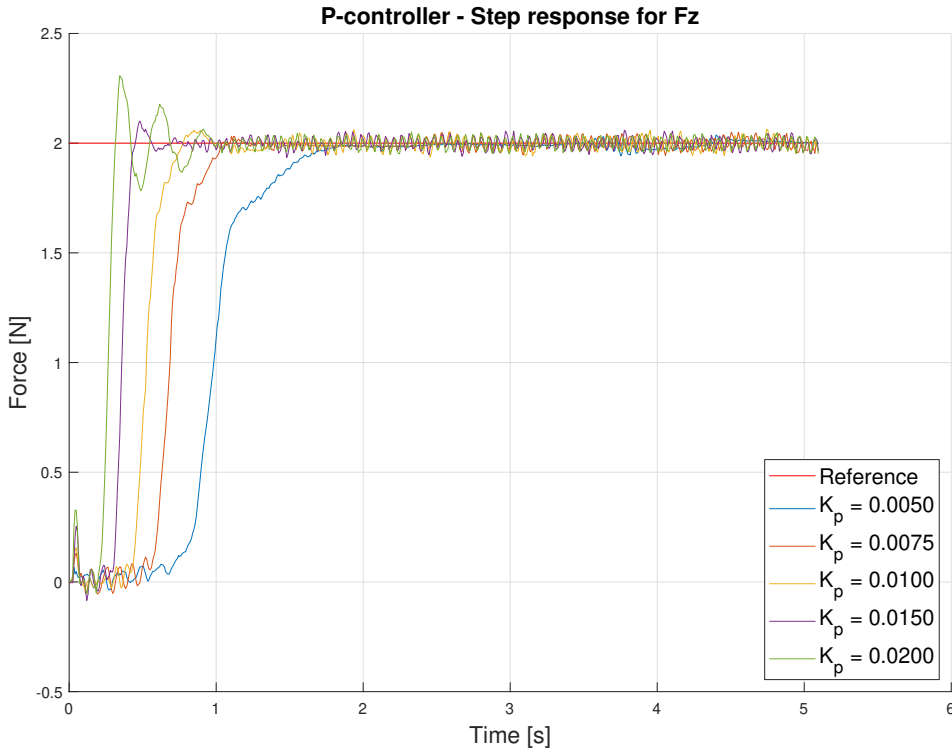
Figure 6.7: Experimental testing of the force P-controller [Author]

Comparison and performance analysis

These values are similar to those of Laastad. Although Laastad plotted other gain values, the tendencies are alike. Laastad chose a proportional gain value of $K_p = 0.005$ as it yields a stable response. In this work, a quick response is of higher importance. Hence a proportional gain value between $K_p = 0.0075$ and $K_p = 0.01$ is more fitting. Values above $K_p = 0.01$ returns a quicker response, unfortunately they also have small overshoots or oscillations. Signal noise around the reference value is observed for all proportional gain parameters.

Proportional-Integral Gain Estimation

All PI-controller gain estimations were tested with a proportional gain of $K_p = 0.008$. The most relevant parameter values are highlighted in figure 6.8.
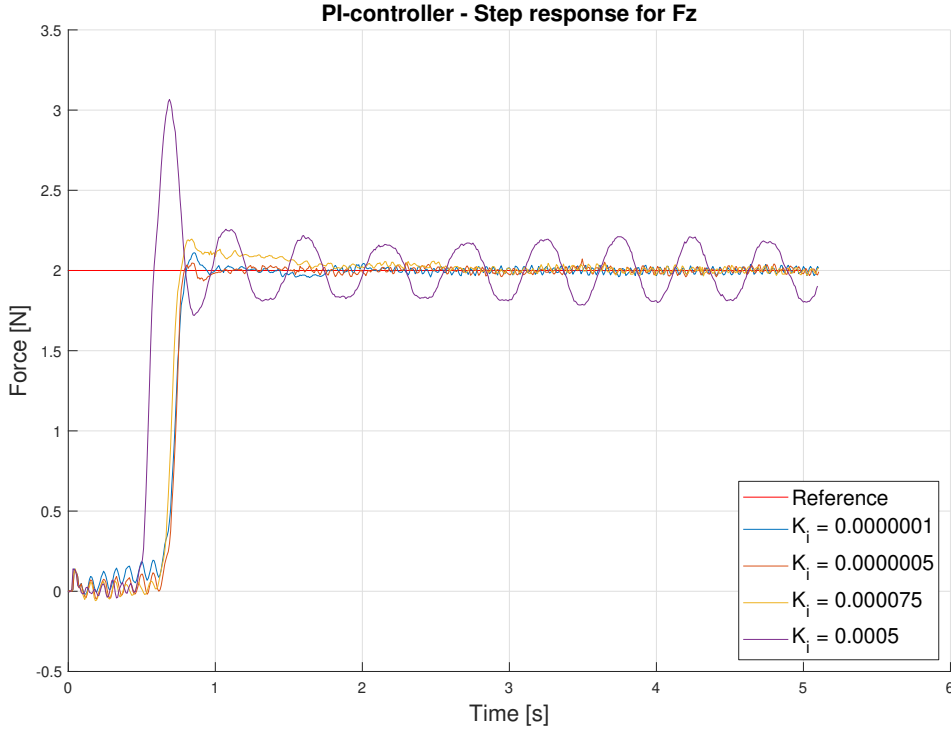
Figure 6.8: Experimental testing of the force PI-controller [Author]

Comparison and performance analysis

There are two notable differences between the response in this experiment and that of Laastad. These differences also occur for two reasons. First of, in his experiment, Laastad chose to use a proportional gain of $K_p = 0.005$. Secondly, Laastad plotted the responses of the integral values between $K_i = 0.001$ and $K_i = 0.0025$. These values are not plotted here. All the values plotted by Laastad, have a large overshoot of approximately 3.5N, but no steady-state error. Already at an integral gain value of $K_i = 0.000075$ a small overshoot can be detected. To demonstrate the response of a higher integral gain, the response of a gain value of $K_i = 0.005$ is included. Evidently, first a overshoot and then a standing wave is observed. A PI-controller with integral gain $K_i = 0.0000001$ is possible to implement, however as it is does not add any extra advantage over a P-controller, the P-controller seems safer to implement, as the behaviour of the internal controller is somewhat unknown.

Proportional-Derivative Gain Estimation

Like the PI-controller, all PD-controller gain estimation is done with a proportional gain value $K_p = 0.008$. The most relevant results are illustrated in figure 6.9.
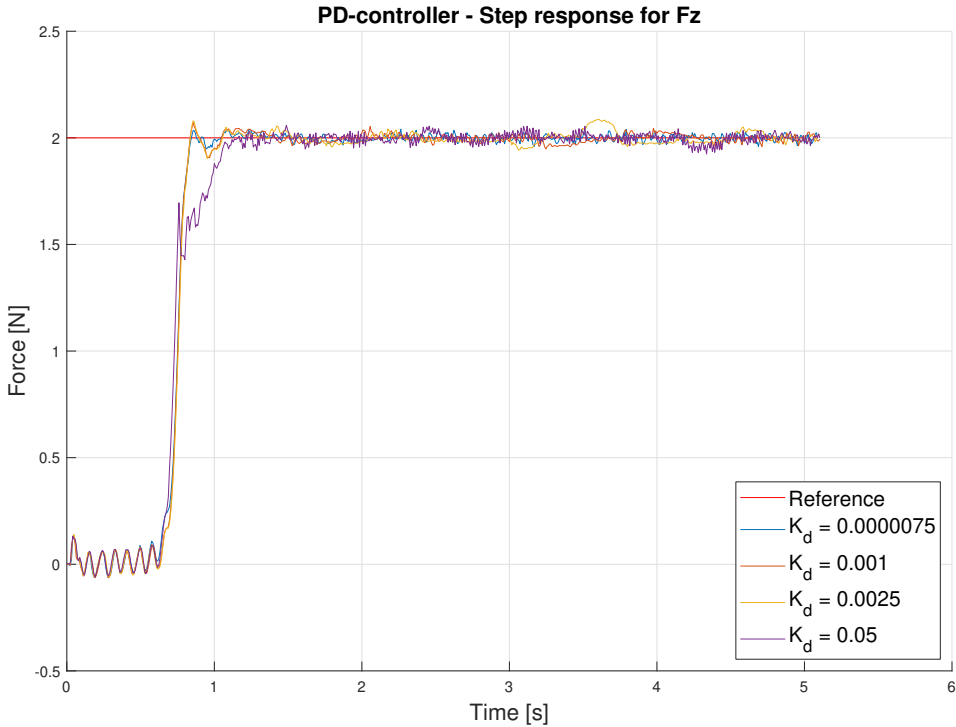
Figure 6.9: Experimental testing of the force PD-controller [Author]

Comparison and performance analysis

Noticeably, there are not big differences in the responses, although the derivative gain parameters span from $K_d = 0.0000075$ and $K_d = 0.05$. Generally, the derivative gain introduces a significant amount of noise, and a slower response. Larger gain values only slow the response. This tendency is also observed in Laastad's result. Nevertheless, no steady-state error is observed. Subjectively the PD-controller leads to a shaking behavior, that could be perceived as scary, and possibly be pose a danger for the patient. Like the PI-controller, the PD-controller is assessed to not possess any advantages over a P-controller.

Proportional-Integral-Derivative Gain Estimation

Numerous gain parameters are tested for the PID-controller. A selection of responses is highlighted in figure 6.10.
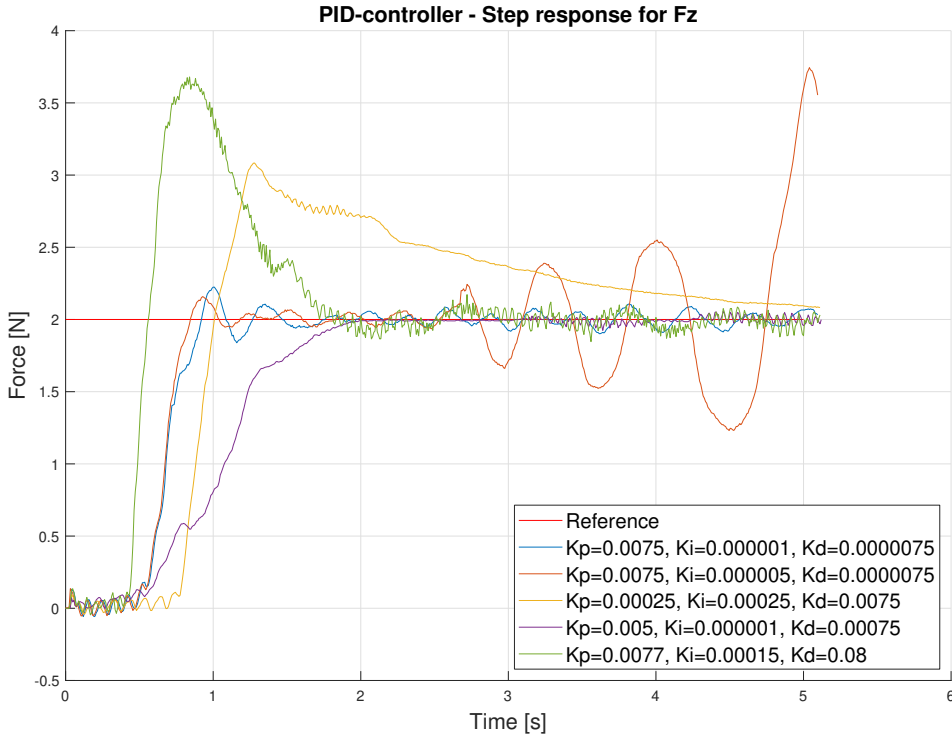
Figure 6.10: Experimental testing of the force PID-controller [Author]

Comparison and performance analysis

The PID-Controller is difficult to tune as evidently seen in the figure. Compared to Laastad's results the PID-controller responses are much alike. Small variation in any gain parameter resulted in either overshoot, steady-state error, or even instability of the response. The few stable responses were not able to reach the step in a timely matter. This suggests that the PID-controller is not suitable.

6.5.3 Torque Controller

Proportional Gain Estimation

The proportional gain was estimated with several values. In figure 6.11 the responses of
the values $K_p = 0.1$, $K_p = 0.3$, $K_p = 0.4$ and $K_p = 0.6$ are highlighted.

Figure 6.11: Experimental testing of the torque P-controller [Author]

Comparison and performance analysis

Like the force controller, the torque P-controller shows promising responses. The signal
seems more affected by noise than the force signal most apparent seen in the slowest signal,
where $K_p = 0.1$. Subjective assessments, both visual observations and manual movement
of the end-effector, were performed to evaluate the noise, however, no unwanted behaviour
was observed. The variations in the signal might have to do with the testing setup. Either
due to the hardware interface not having any natural point to rotate about to create force
measurements in the F/T sensor, or the cardboard box not being a good enough for this
test. In comparison, the responses in Laastad's test are both stable and quick. He chose a
proportional gain value between $K_p = 0.25$ and $K_p = 0.75$. These values appear feasible
here as well.

Proportional-Integral Gain Estimation

The torque PI-controller is tested with the proportional gain value $K_p = 0.45$ and several integral gain parameters. The most relevant responses are shown in figure 6.12.

Figure 6.12: Experimental testing of the torque PI-controller [Author]

Comparison and performance analysis

As with the P-controller, the responses of the torque PI-controller are not smooth. Likely due to the same noise reported previously. These findings are backed up by the responses seen in Laastad's tests. What is evident from the responses in figure 6.12, is the decrease in rise time. However, indications in the response for integral value $K_i = 0.00025$ show a small steady state error, which is made clear in the response of the integral value $K_i = 0.001$. This differs from the force PI-controller, which did not have a steady state error. What is difficult to see here, but more clearly shown in the result's of Laastad, is that the PI-controller also has a small overshoot, before the steady state error.

Proportional-Derivative Gain Estimation

The torque PD-controller is tested with a proportional gain of $K_p = 0.45$ and various derivative gains. The responses of the derivative gain parameters $K_d = 0.0005$, $K_d = 0.05$, $K_d = 1$, $K_d = 5$ and $K_d = 10$ are illustrated in figure 6.13.
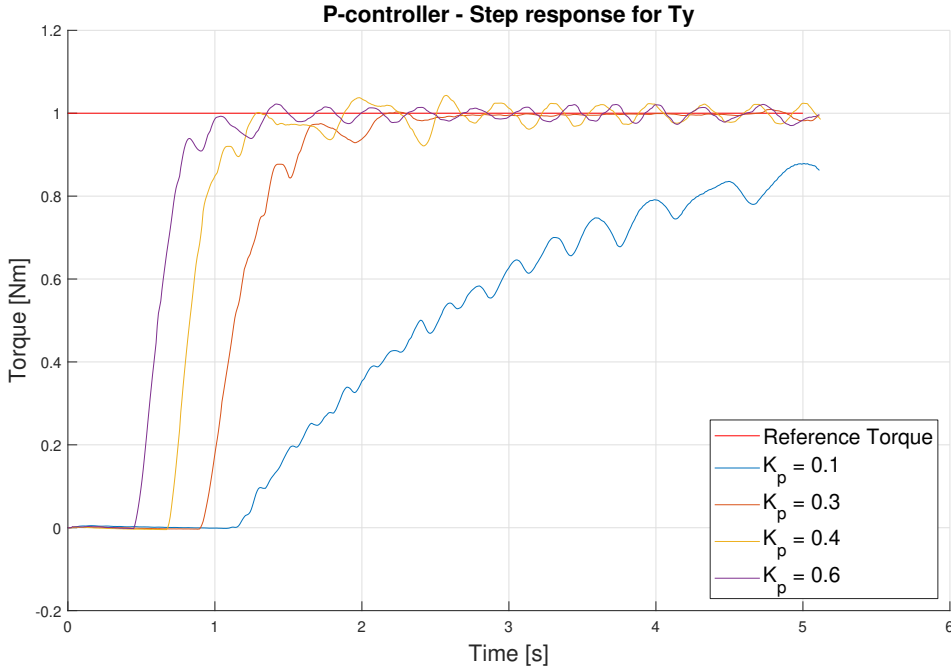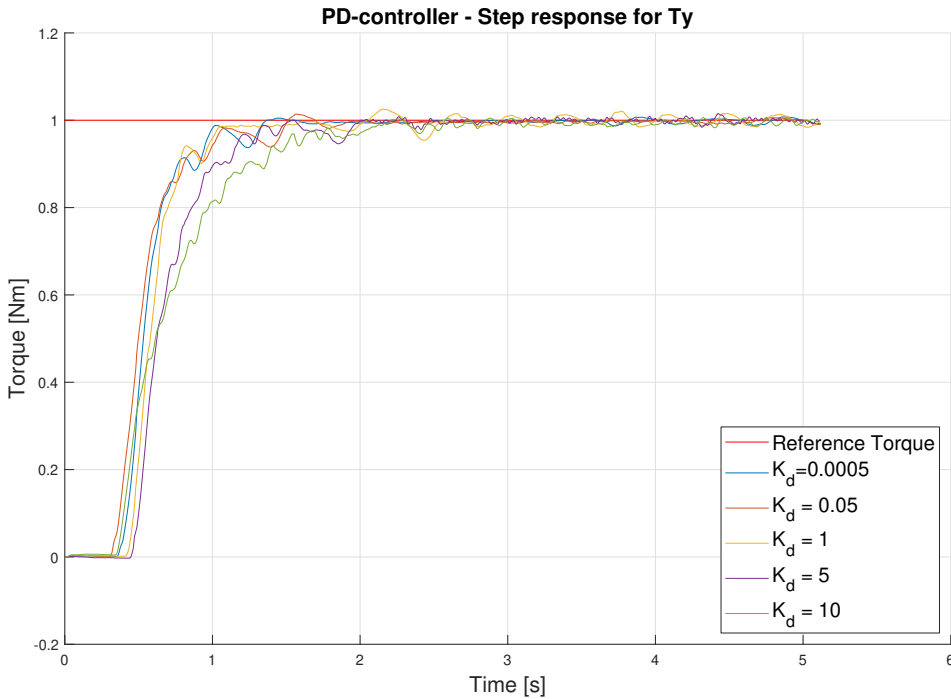

Figure 6.13: Experimental testing of the torque PD-controller [Author]

Comparison and performance analysis

The responses of the PD-controller does not differ much from the P-controller responses. As expected, small values of the derivative gain, like $K_d = 0.0005$ and $K_d = 0.05$ the rise time does not change visibly. However, with an increase in the derivative gain, the rise time increases as well. No steady state error is observed. The biggest challenge facing the force PD-controller was its sensitivity to noise. In the torque PD-controller this is more subtle, as the signal is not as noisy as the force PD-controller. However, for derivative gain value $K_d = 10$ this becomes more apparent, since the signal is not as smooth. This is also backed up by Laastad's results, where a derivative gain value of $K_d = 20$ is plotted. From which it is visible that a high frequency noise has manifested, and made the manipulator unstable. To verify these findings further a subjective assessment of the controller was made by manual rotation of the end effector. This resulted in an unpleasant shaking movement. For the smallest gain parameters, the PD-controller was indistinguishable from the P-controller.

Proportional-Integral-Derivative Gain Estimation

The torque PID-controller is tested with proportional gain $K_p = 0.45$ and several combinations of integral and derivative gain parameters. The most relevant responses are shown in figure 6.14.
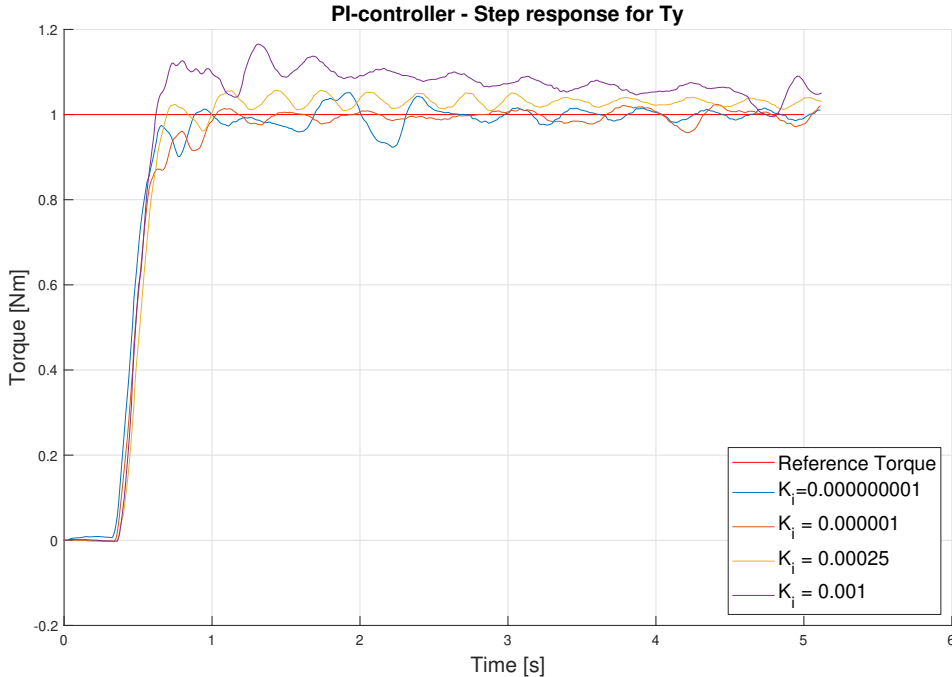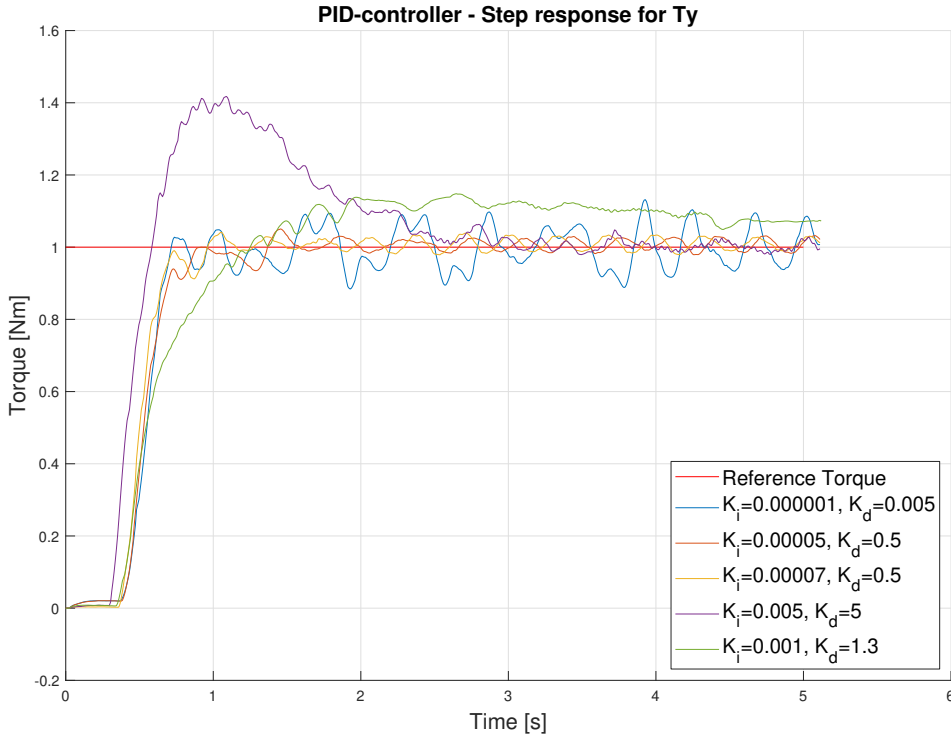

Figure 6.14: Experimental testing of the torque PID-controller [Author]

Comparison and performance analysis

The first noticeable response is that of $K_i = 0.005$ with $K_d = 5$. The gain parameters decrease the response's rise time to almost 0.5s, however the response has a dominating overshoot and is saturated with noise. It does however converge to the reference torque, meaning there is no steady state error. The signal with the smallest values, $K_i = 0.000001$ and $K_d = 0.005$ does not seem to be influenced by noise, however the signal seems unstable, or at its best converging too slowly to the reference torque. The two last responses do not seem to differ much from the torque PD-controller responses, hence either the PD or P-controller should be used instead.

6.5.4 Summary

The controller tuning process was performed for two reasons. The first reason was to find a suitable controller with gain values that resulted in a satisfying manipulator behaviour in terms of the specifications discussed in chapter 6.1. The other reason was to verify the findings in Laastad's thesis.

As Laastad points out, the experimental controller gain estimation process yields some interesting results about the dynamics between the internal and external controller. This is specially seen in the behaviour of both the P-controllers, where no steady state error is found. By implementing a P-controller on a velocity $\dot{q}_i$, the manipulator acts as if a PI-controller has been implemented on the position q_i.

The PI-controller, PD-controller and PID-controller for both force and torque yields equally good or in most cases worse results than the P-controller. The biggest problem with the PI-controllers was introducing overshoots and for the torque PI-controller an additional steady state error. The PD-controllers on the other hand, increased the rise time and amplified noise resulting in unwanted twitching movement in the manipulator. The PID-controllers did not improve the results. Rather the manipulator became more sensitive to small gain variations resulting in a more aggressive behaviour.

Even though the rotational axis was changed in the torque controller tests, and a different hardware interface was used, these results compares well to Laastad's.

Taking these results into account, the suggestion is to do as Laastad and implement a P-controller for both force and torque. However, due to different desired specifications the proportional gain values chosen are not the same. Here, the values of $K_p = 0.0075$ is chosen for the force P-controller, and $K_p = 0.5$ is chosen for the torque P-controller. This results in a slightly more aggressive manipulator, in terms of shorter rise time.

6.6 DVA implementation

The robot manipulator is used to simulate the DVA system, giving a mass-spring-damper behaviour to the end-effector. This can be done through numerous methods, but the most prominent ones are by implementing an impedance or an admittance controller.

The terms "impedance" and "admittance" are often used interchangeably, even to the extent where certain control systems referred to as admittance controllers by some are called impedance controllers by others. In this thesis, a clear distinction is made. Impedance controller is thought of in the same manner as defined by Hogan [83]:

> "Mechanical impedance at a port is a dynamic operator that determines an output force (torque) time function from an input velocity (angular velocity) time function at the same port."

Where the term port is used for a point at which energy may be exchanged with the environment. In other words, an impedance controller takes velocity as input and gives force as an output. Mechanical admittance on the other hand is defined as an dynamic operator that determines an output velocity from an input force [83]. Hence, an admittance controller is often seen as the inverse of an impedance controller. It is also often referred to as an impedance controller with inner motion control.

In this thesis, an admittance controller is implemented. The impedance controller requires joint torque setpoints. Without a joint torque interface, or full knowledge of the joint dynamics and servo controllers, admittance controller is the better option [84]. The controller is illustrated in figure 6.15 and 6.16.
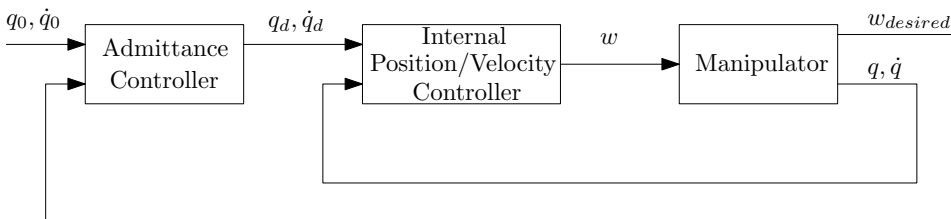
Figure 6.15: Overview of a generalised admittance controller [Author], based on [84]
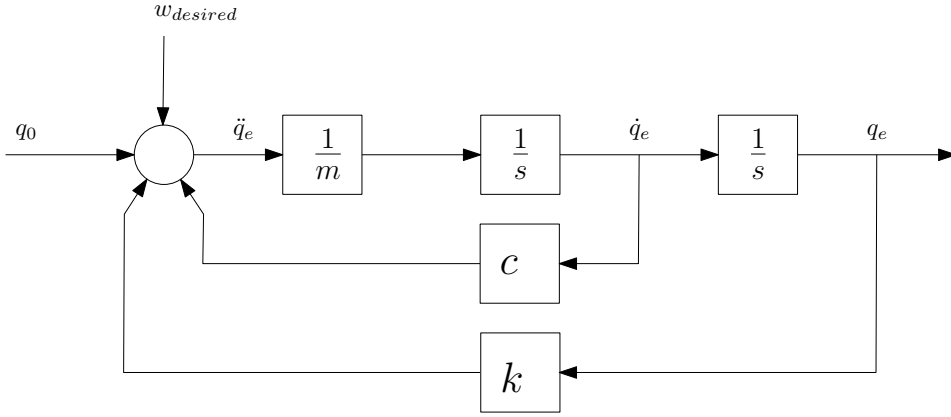
Figure 6.16: Mass-Spring-Damper behaviour of an generalised admittance controller in joint space [Author]

Which yields the following equation:

$$m(\ddot{q}_d - \ddot{q}_0) + c(\dot{q}_d - \dot{q}_0) + k(q_d - q_0) = \tau_{desired} \tag{6.4}$$

This thesis has implemented the admittance controller in Cartesian world frame, and not in angular joint frame. The desired position is also given in tool frame, not in base frame. Hence, some conversion is done through rotational matrices. The system equations is therefore given in following manner:

$$m(\ddot{x}_d - \ddot{x}_0) + c(\dot{x}_d - \dot{x}_0) + k(x_d - x_0) = \tau_{desired} \tag{6.5}$$

where $\ddot{x}_0 = \dot{x}_0 = 0$. Due to not having access to the joint acceleration in the controller interface, the acceleration is calculated by inverting Eq.6.5:

$$\ddot{x}_d = \frac{1}{m}(-c\dot{x}_d - k(x_d - x_0) + f) \tag{6.6}$$

then discretised and integrated to find the velocity for timestep t_i by

$$\dot{x}_{d,i+1} = \dot{x}_{d,i} + \ddot{x}_{d,i}\Delta_t \tag{6.7}$$

where Δ_t is the duration of the timestep. The desired joint speeds are then found by inverting the differential kinematics:

$$\dot{q}_{d,i} = J^{-1}\dot{x}_{d,i} \tag{6.8}$$

which are sent to the robot. This is also demonstrated in the code snippet below.

```
error_pos[0] = tfkin.O[0] - DESIREDXPOS;

error_pos_tool[0] = error_pos_tool[1] = error_pos_tool[2] =
    0;
```

```
vector_trans_base_tool(q, error_pos, error_pos_tool);

x_acc = (1.0/m)*(−c*vw[0] − k*error_pos_tool[0] +
    force_tresh[0] + references[0]);

vw[0] = vw[0] + x_acc*iteration_time;
```

Here, `tfkin.O[0]` is the actual Cartesian end-effector position in world frame. The `vector_trans_base_tool`, rotates the error vector from world frame to tool frame. And the `vw[0]` is the velocity vector, for which the inverse Jacobian is calculated, giving the manipulator a joint space angular coordinate. The code itself is elaborated in appendix E, and can be found as an attachment.

The mass-spring-damper coefficients, k and c are chosen according to the following equations, given a desired oscillation frequency f. The mass is chosen arbitrarily, which are unless stated otherwise, chosen to be $m = 1$.

$$k = f_d^2 m \tag{6.9}$$

$$c_c = 2\sqrt{km} \tag{6.10}$$

$$c = \zeta c_c \tag{6.11}$$

Where c_c and ζ is the same coefficients as stated in table 3.3.

6.6.1 Step Response

To verify that the manipulator has been programmed according to desired behaviour, two sets of experimental verification tests have been conducted. In this section a step response test is presented.

Axis	Frequency	Added reference for each iteration
X,Y and Z	3 [Hz]	0.007
X,Y and Z	7 [Hz]	0.01

Table 6.4: Step response reference signal for each iteration [Author]

The test setup is simple. The manipulator is positioned at an arbitrary position, in this case the manipulator is positioned with the end-effector pointing downwards well above the attached table, and no obstacles in its surroundings. A desired frequency for the manipulator oscillations is then chosen. For this test, a frequency of $f = 3$ and $f = 7$ is chosen. A reference signal is then added for each iteration for 250 iteration ≈ 2s, before the reference is reset to 0. The reference signal varies for each frequency and direction, the parameters are summarised in table 6.4.

This reference signal is not a classic step response input signal. Instead of applying a constant force for a given time period, the input signal gradually integrate the signal at a rate of 0.01N per timestep, resulting in a step from 2.5N to zero after approximately 2s.

The desired behaviour we would like to examine is the behaviour around the initial equilibrium position, x_0. If one could extract the intended motion from the patient, then x_0, $\dot{x}_0$ and $\ddot{x}_0$ would correspond with the patient's intended motion, and the DVA would act around that. That is why we look at the response when dropping down to the equilibrium position rather than when acted upon by a constant force.

The step response reference signal implementation can be summarised in the code snippet below.

```
// For Z-axis with f = 7
if (i <= 250){
    references[2] += 0.01;
}
else{
    references[2] = 0;
}
```

The step response result is presented in figure 6.17. Only the step response of the Z-axis is presented, as the other responses are similar. These can be found in appendix F.
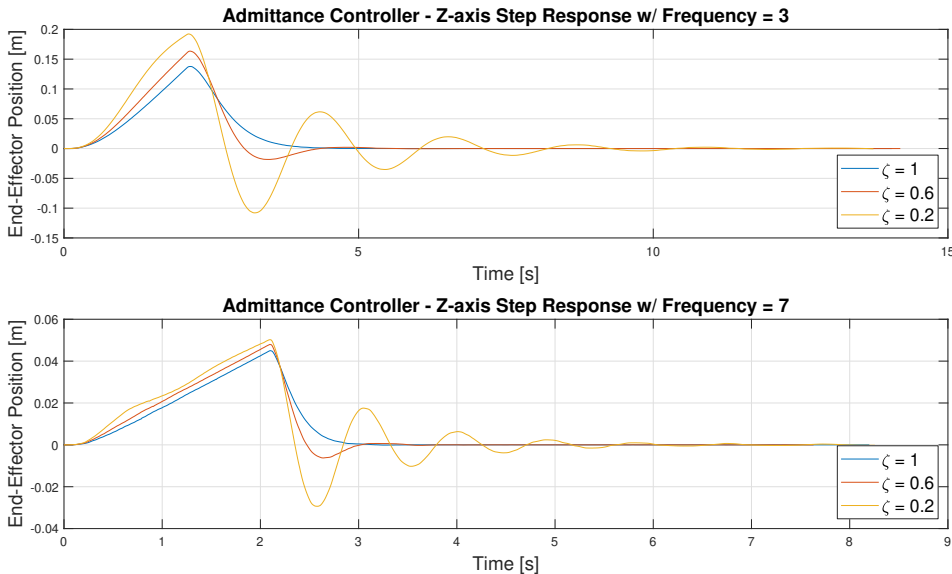
Figure 6.17: Step Response of Z-axis Admittance Controller [Author]

Nearly all responses in both plots begin with a linear displacement between 0 and 2 seconds. It is more clear from the plot where the desired frequency is set to 7 than from plot with desired frequency equal to 3. This is due to the stiffness of the virtual spring being a function of the desired frequency, see Eq.6.9 - Eq.6.11. The nonlinear start is likely due to the complement Gaussian filter that reduces the input force when it is too low. At the point of 2 seconds, the reference is reset to 0, and as a mass-spring-damper, the end-effector

seeks back to the equilibrium point.

The expected response is as following. For a critical damped signal, $\zeta = 1$, the response is expected to fall back to the equilibrium point without any overshoot, nor any steady-state error. For a mildly underdamped signal, $\zeta = 0.6$, a small overshoot is expected in the response. Lastly, for an heavily underdamped signal, $\zeta = 0.2$, oscillations are expected before the signal falls to rest at the equilibrium. This expected behaviour is achieved in both plots.

The difference between the two plots in figure 6.17, mainly concerns differences in amplitude and time. Even with a smaller force reference signal, the response of the plot with $f = 3$ has larger amplitude, and slower response. This also has to do with the stiffness of the virtual spring coefficient. A smaller stiffness needs less force to be displaced. For the same reason, it will take longer time to go back to the equilibrium point.

Conclusively, the step response of the robot manipulator with the implemented control system behaves as a mass-spring-damper.

6.6.2 Impulse Response

The second experimental verification test conducted is an impulse response test. The test setup is the same as for the step response test. Both $f = 3$ and $f = 7$ are tested here as well. The reference signal is now modified. The manipulator now waits 250 iterations ≈ 2 seconds before a reference signal is given for 5 iterations ≈ 0.04 seconds. This reference signal is for both frequencies and all axes, apart from the Z-axis with frequency $f = 3$, equal to 25N. The reference signal in the Z-direction with $f = 3$, a reference signal of 20N is given. This is done so that the manipulator does not slam into the attached table. The impulse response reference signal implementation can be summarised in the code snippet below.

```
// For Z-axis with f = 7
references[2] = 0;
    if (i >= 250 && i < 255){
        references[2] = 25;
    }
```

The Z-axis impulse response is presented in figure 6.18. The responses for the other axes can be found in appendix F.
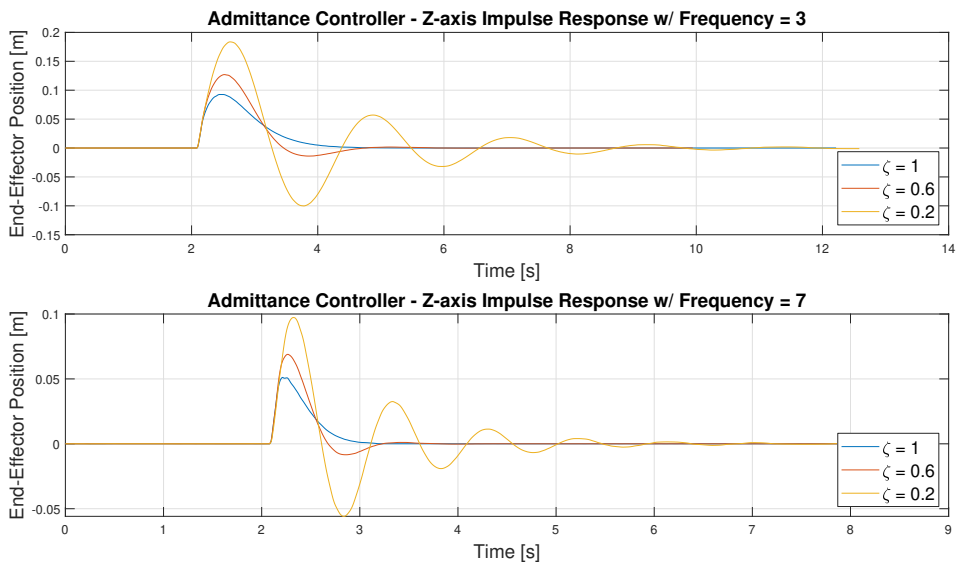
Figure 6.18: Impulse Response of Z-Axis Admittance Controller [Author]

The plot shows how the manipulator first waits ≈ 2 seconds for the impulse signal. Comparing the two plots, one can see that the form of the response is alike, however, the amplitude and response time is dissimilar. This, like for the step response, is likely due to the virtual spring stiffness being dissimilar. A plot of ideal impulse responses is presented in figure 6.19.
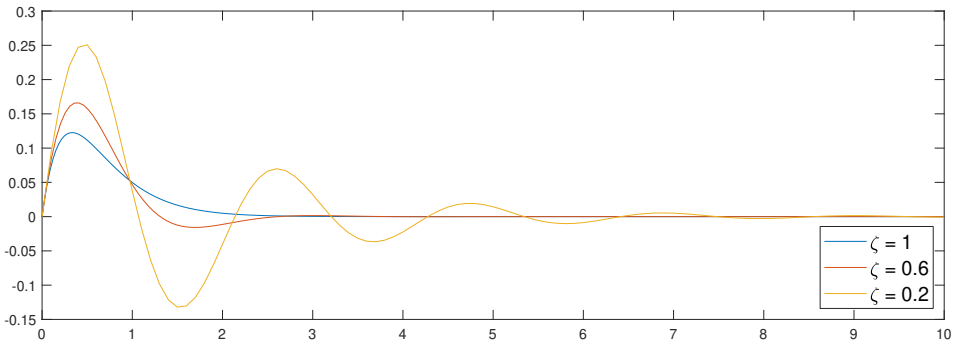
Figure 6.19: Ideal impulse response of mass-spring-damper system [Author]

The impulse response has been modelled with MATLAB's *impulse()* function. All the values are similar to those tested on the robot manipulator, and the desired frequency is set to $f = 3$. The only difference between the two plots and the respective responses is the amplitude. The most probable cause of that is the fact that the input signal to the MATLAB *impulse()* function is a Dirac pulse input, while the robot manipulator has a 20N input. Apart from this difference, the responses are alike, and conclusively, the admittance controller is implemented with the desired behaviour.

6.7 Frequency Feedback Implementation

To achieve a semi-active system, where the spring stiffness may be regulated, some sort of feedback is needed. As explained in the system overview in section 5, the BMWFLC filter for tracking and estimation of tremors is implemented on an Arduino Uno using an IMU as sensor. The IMU communicates with the Arduino Uno through I2C protocol. The data is presented as a serial data stream, however, the data needs to be communicated to the robot manipulator.

As the manipulator system communicates with the *ur_modern_driver* over TCP/IP through an external computer with Linux Ubuntu OS, communication between Linux and Arduino needs to be established in C++. In Linux, all connected devices are mounted to a given directory. To connect to these devices, the directory needs to be accessed. This is then implemented in the system, based on the code in [85]. Hence the Arduino is able to send data to the robot manipulator as string variables.

Both accelerometer data and peak frequency are sent to the external computer. The string variable containing these data is split up and converted to suitable types. The accelerometer data is used solely for logging each test or session. While the peak frequency is set as the desired frequency variable, continuously updating the spring stiffness variable.

Further, the behaviour of the mass-spring-damper with variable stiffness needs to be analysed. To do this, the step response test and the impulse test is conducted once more. The results of these responses for the Z-axis are illustrated in figure 6.20 and figure 6.21. The responses for axes X and Y may be found in appendix F.
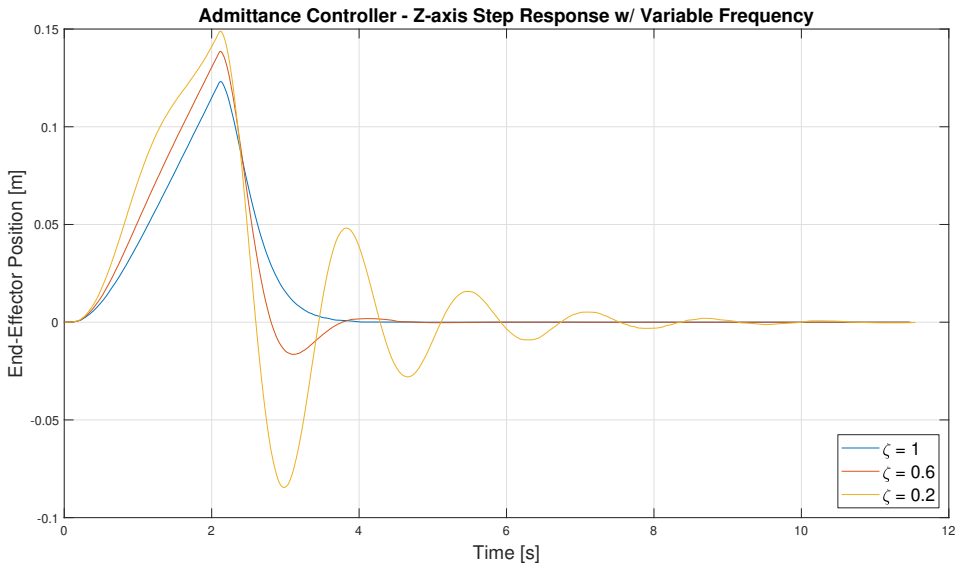

Figure 6.20: Step response of an admittance controller with variable stiffness [Author]
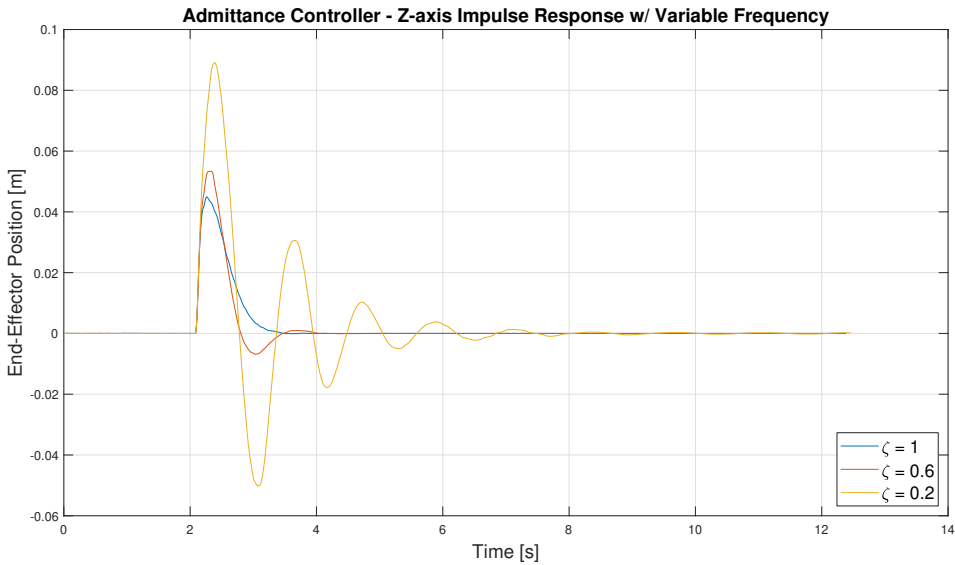
Figure 6.21: Impulse response of and admittance controller with variable stiffness [Author]

Examining the step responses first, it is clear that the shape of the signal still resembles a mass-spring-damper, and the desired behaviour is still present. For the test, the manipulator is given a reference of 0.01N for each iteration for 250 iterations, before the reference is reset to 0. The same reference value is given in every direction. This is, as stated in table 6.4, the same reference given to step response test with fixed frequency of $f = 7$. However, the response is closer to the response of the fixed frequency $f = 3$. Further examination of the frequency log file, shows that even though the frequency varies, the range of the variations is between $f = 3.9$ and $f = 4$.

As with the step response, both the shape and desired behaviour of the impulse response with variable frequency resembles a mass-spring-damper. The test setup is equal to the setup for fixed frequency impulse response test. The reference signal given in the Z-axis is 15N, while X and Y axes is given a reference signal of 20N. The reference signal is given at the same time and for the same amount of time as the fixed frequency impulse responses. Given the input, it is clear that the response is more aggressive than its fixed frequency counterpart. The behaviour of the response is closer to the response of fixed frequency $f = 7$. However, a closer look at the frequency log file of the test reveals that the range of frequency varies from $f = 3.9$ to $f = 7$.

The robot has a high displacement from the integrated force response, indicating that it accommodates a constant signal and has a low stiffness in the virtual spring under constant force. When the force resets, we have a slope back to zero (for the critically damped system) similar to the higher frequency response in the previous experiment. Indicating that the active strategy is trying to dampen the rapid change in force by increasing the

virtual spring stiffness.

The variation of frequency in the impulse response is possible to see in the response plot, especially in the response of $\zeta = 0.2$. Examining the response around every local maxima and minima of the signal, it becomes clear that the response is asymmetrical about the point. The response uses more time reaching the point, than leaving. That is, the rate of change is higher before the maxima and minima of the signal than after, like a nonlinear spring. This response coincides with the subjective assessment of the semi-active manipulator. During the subjective assessment, the manipulator was easy to pull away from the equilibrium point, but upon release it seemingly went quicker back to the equilibrium point.

At this point, it is assumed that the force input greatly impacts the behaviour of the manipulator. Further investigations on the behaviour of a manipulator with real-time tuneable stiffness should be made, however the rest of this thesis will focus on what impact this behaviour has on tremor suppression.

6.8   Summary

In this chapter, the specifications of the system was established, and implementation challenges were identified, for which solutions were found and tested. In addition, a system controller were designed, and each part was implemented, tested, verified and analysed.

The compliance controller and the admittance controller were never tested together in a completed system. However, given that the experimental tests will not be done on humans, this does not prevent the experiments going forward.

The overall system implemented in this thesis will in the actual wearable device be unnecessary. The device will mechanically have a mass-spring-damper behaviour and is attached to the user's hand, so compliance is a given. However, to be able to test the system on a robot manipulator, the controller is needed.

7

Experiment

The designed and implemented system shows desired behaviour, this chapter aims to explore the effect and impact of the system.

Initially, the experiment was thought to be performed on human patients, using an assessment scale from the literature study in chapter 4.1. However, before testing can be performed on human patients, experimental testing is required. The purpose of these experiments is to determine the effect of a semi-active system as opposed to a passive one.

7.1   Experimental setup

The experimental setup is shown in figure 7.1. To test the system, a virtual patient was built in cooperation with the mechanical workshop at ITK. It consists of a drill that is attached to a PVC pipe through a spring. These elements were secured to a piece of wood for stability. The pipe is kept in place at an angle through a metal loop, mainly to elevate the pipe, but also to limit the amplitude of the pipe movement. Whenever the drill was activated, the spring motion caused random movement in the pipe.

Three clamps were used in the setup, two of which were used to secure the virtual patient to the table. In figure 7.1c, it can be seen that the patient is not secured to the table attached to the manipulator structure, rather it is secured to the table with the external computer and the UR5 controller box. The reason for this is that initial tests revealed severe instability in the system when placing the virtual patient on the attached table. The structure on which the manipulator is secured and table is attached is in itself unstable. Manipulator shaking leads to shaking in the pillar which further leads to shaking in the table. Securing the patient to that table only leads to a closed loop of shaking making the system unstable.

The last clamp is used to apply steady pressure on the drill button, such that it has constant velocity throughout the test. The rest of the experimental setup includes the implemented

system described in chapters 5 and 6.
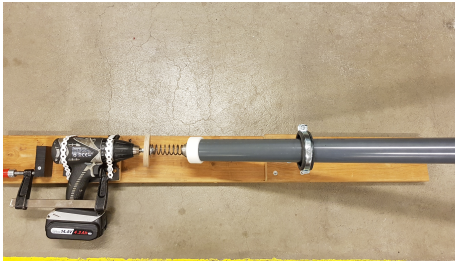
(a) Virtual Patient
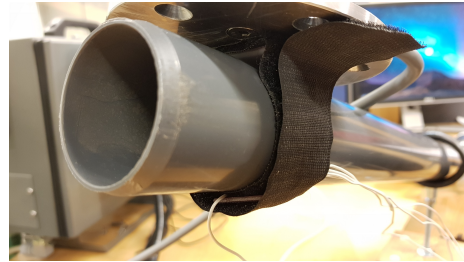
(b) Patient Attachment
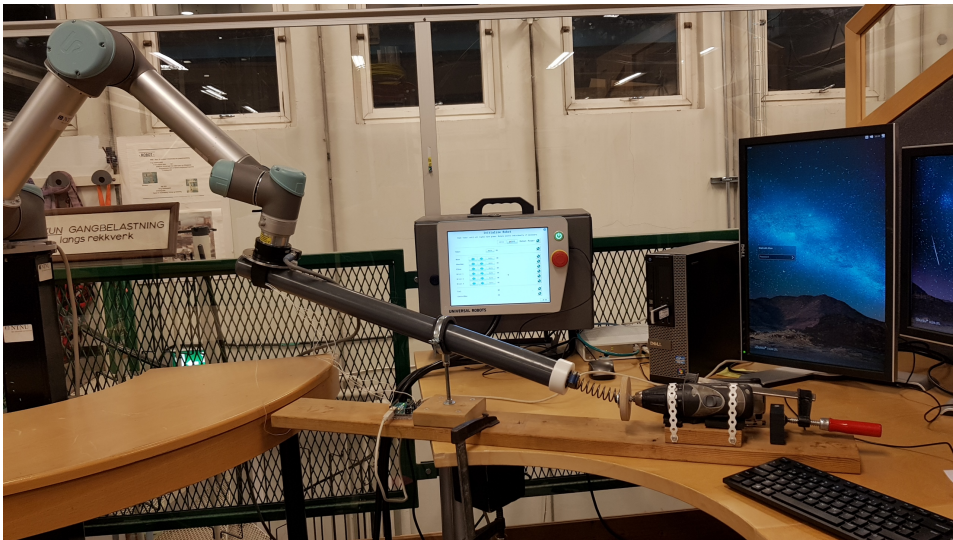
(c) Complete Experimental Lab Setup

Figure 7.1: Experimental Lab Setup [Author]

7.2 Method

The experiment starts by measuring the tremors in the virtual patient, without the manipulator attached. The setup of the accelerometer can be seen in figure 7.2a. The manipulator is then attached and a series of tests are conducted, where the stiffness and damping of the manipulator is changed from test to test. All tests measures the tremor in the Z-axis only, if not stated otherwise.

The tests are built up as follows. First, four different fixed frequencies are tested for a critical damped, $\zeta = 1$; mildly underdamped, $\zeta = 0.6$; and highly underdamped, $\zeta = 0.2$ system. Those frequencies are: $f = 15$, $f = 10$, $f = 6$ and $f = 3$. Then a feedback frequency from the BMWFLC algorithm is used to adapt the manipulator stiffness to the tremor frequency. This setup is then tested for the critical, mildly underdamped and highly underdamped case.

The experimental method can be summarised in the following bullet points.

- Measure tremor data of the virtual patient.

- Measure tremor data of the virtual patient and manipulator with multiple fixed frequencies and critical, mildly underdamped and highly underdamped dampening.

- Measure tremor data of the virtual patient and manipulator with feedback frequency and critical, mildly underdamped and highly underdamped dampening.

(a) Accelerometer placement when measuring without manipulator attached

(b) Accelerometer placement when measuring with manipulator attached

Figure 7.2: Tremor Measurment Setup [Author]

7.3   Results

The data presented in figure 7.3 is the tremor data from the virtual patient; where figure 7.3a is the estimated tremor signal, and 7.3b is the PSD plot of the estimated tremor. This data is the reference data to which the experimental tests will be compared to. However, this data will not be exactly the same in all the tests, as it is difficult to achieve the exact same velocity twice with the drill setup.

(a) Tremor Estimation of the virtual patient

(b) PSD plot of estimated virtual patient tremor
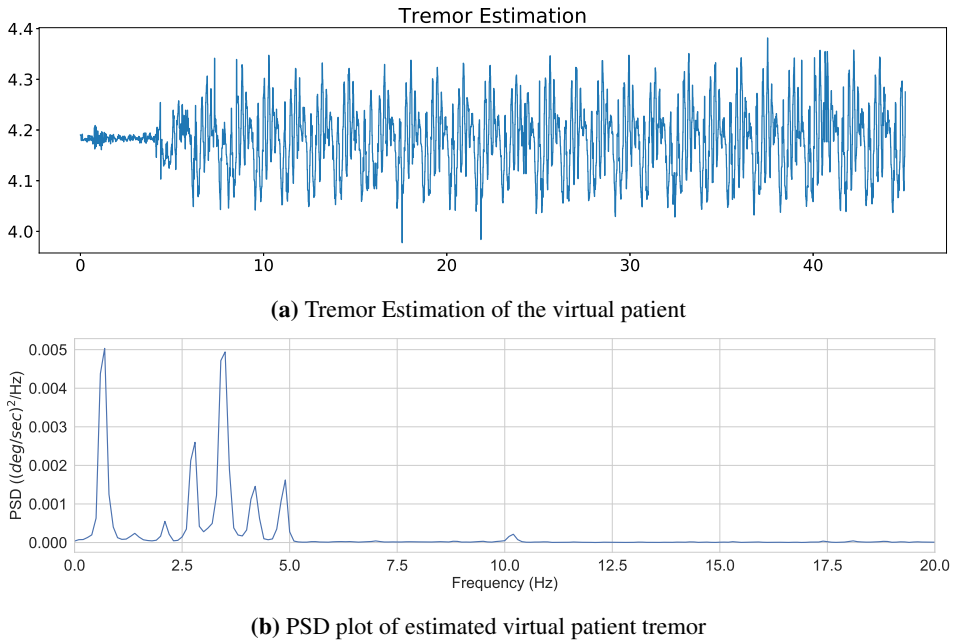
Figure 7.3: Tremor data of the virtual patient [Author]

Most of the tests ended with an unstable system, where the oscillations only increased in both amplitude and frequency. This was not surprising, and is elaborated further in chapter 7.4. For the heavily underdamped case, only a fixed frequency $f = 15$, was possible to record, the other frequencies, even a variable one, were violently unstable, trigging safety mechanisms instantaneously.

Yet, results from both the fixed frequency tests, and variable frequency are presented in the following sections. The rest of the test results can be found in appendix F.

Fixed Frequency Test

In this section, the best and worst cases for a fixed frequency are presented. This judgement is based on the perceived movement of the total system. In figure 7.4 the PSD plot and the movement plot of the system are presented. Here the manipulator is set to critical damping, and a desired frequency $f = 15$. Evidently, there are major changes in the PSD plot compared to the PSD plot of the reference. Only one peak remains, though this peak is now 20 times larger. In other words, energy persists in the tremor. This can be explained by the movement plot, which shows stable oscillations, with low amplitude.
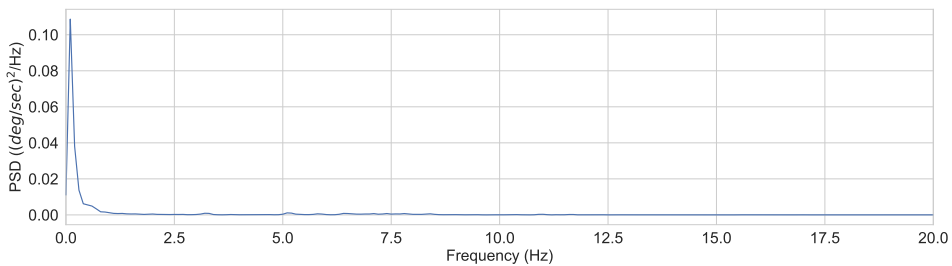
(a) PSD plot for critical damped system with fixed frequency, $f = 15$ [Author]
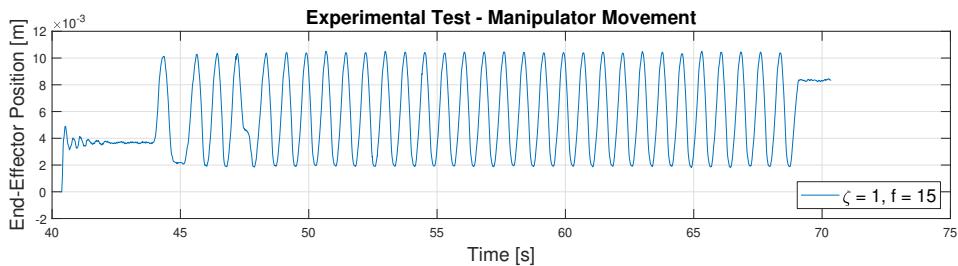
(b) Movement plot for critical damped system with fixed frequency, $f = 15$ [Author]

Figure 7.4: Plots of critical damped system with fixed frequency, $f = 15$ [Author]

The worst fixed frequency case is presented in figure 7.5. Here, the manipulator is set to heavily underdamped, and frequency $f = 15$. This was the only case were a heavily underdamped manipulator was recordable, and as seen in the movement plot in figure 7.5b, the system is shut down after 2 seconds by an internal safety mechanism. Several more plots are added to appendix F, however, most of them result in an unstable or oscillating behaviour, not providing new information to the discussion.

(a) PSD plot for heavily underdamped system with fixed frequency, $f = 15$ [Author]
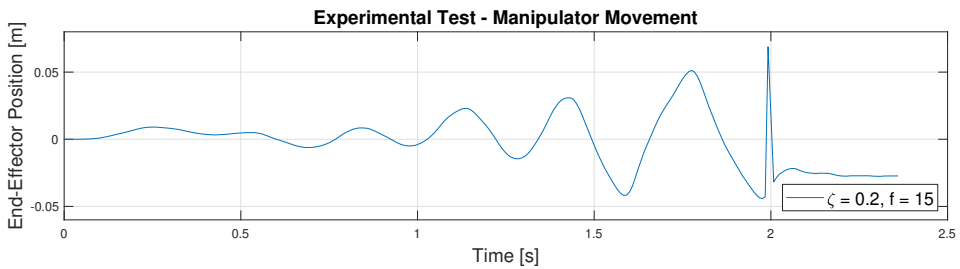
(b) Movement plot for heavily underdamped system with fixed frequency, $f = 15$ [Author]

Figure 7.5: Plots of heavily underdamped system with fixed frequency, $f = 15$ [Author]

Variable Frequency Test

The results of the variable frequency tests have the same tendencies as the fixed frequencies. In figure 7.6, the manipulator is critically damped with a variable frequency. Although it is seemingly able to suppress some frequencies, two frequencies, $f = 1.5$ and $f = 4.1$ are heavily boosted. Large, but stable oscillations are also found with this setup, as seen in figure 7.6b.
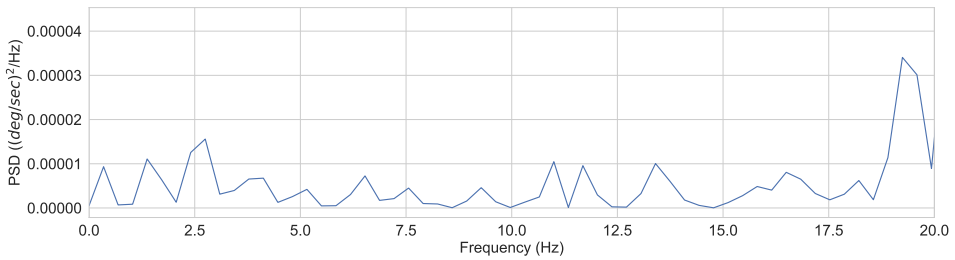

(a) PSD plot for critical damped system with variable frequency [Author]
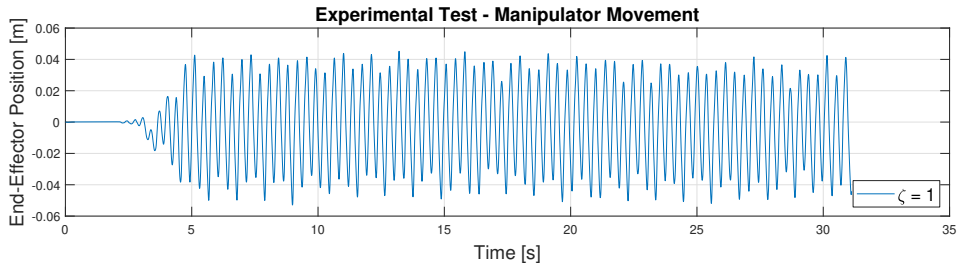
(b) Movement plot for critical damped system with variable frequency [Author]

Figure 7.6: Plots of critical damped system with variable frequency [Author]

The best results with a variable frequency came when the measured frequency were multiplied with a constant gain $= 4$. It is assumed that this is a natural consequence of a higher stiffness making it more difficult to move the manipulator in any case. The results of this implementation are highlighted in figure 7.7. Once again the results show that even with a critical damping the system has at best stable oscillations. The power certain frequencies are decreased, while others are increased. However, the power of the largest frequency $f = 7.5 : PSD \approx 0.003$ is lower than the power of the two largest reference frequencies, $f = 1 : PSD \approx 0.005$ and $f = 3.2 : PSD \approx 0.005$. Several more plots are added to appendix F, however, most of them result in an unstable or oscillating behaviour, not providing new information to the discussion.

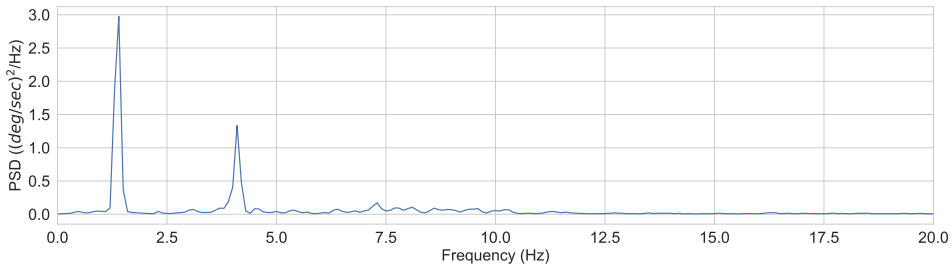**(a)** PSD plot for critical damped system with 4x variable frequency [Author]

(b) Movement plot for critical damped system with 4x variable frequency [Author]

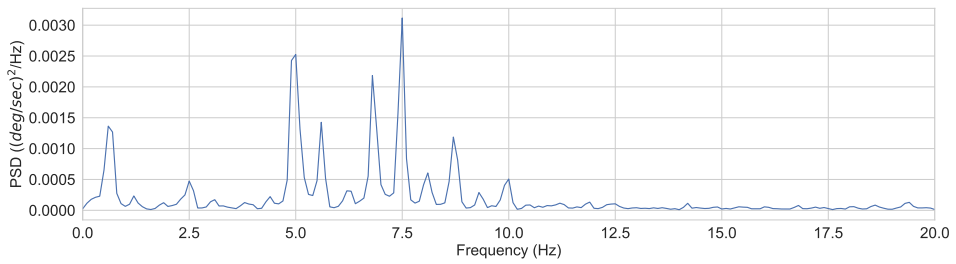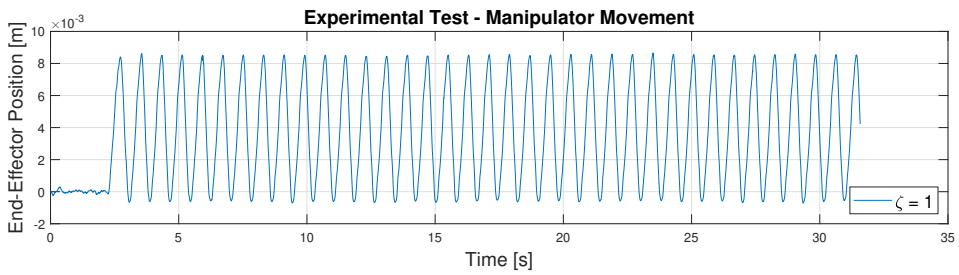**Figure 7.7:** Plots of critical damped system with 4x variable frequency [Author]

7.4 Discussion

Generally, the experiment yields unsatisfactory results. The only certainty that can be drawn from it, is that a higher desired manipulator frequency, which provides a higher spring stiffness, produces the least amount of movement. A critically damped manipulator also seems to keep the movement to a minimum, however as can be seen in figure F.11, a critically damped manipulator does not ensure stable movement. Given this behaviour, the PSD plots does not provide much insight to the system. Typically, the PSD plots show that the peaks in the reference signal is lowered. However, due to movement still persisting in the system, other peaks are increased, often to the point where the power of the frequency is higher than the power of the reference signal frequency peaks.

There are many reasons why this experiment did not yield satisfying results. The main reason, is due to initial phase problems with the experimental setup. The most substantial flaw being the hardware interface. Due to the design of the hardware interface, the total system does not become a DVA system with one mass-spring-damper system upon another. Instead, the total system becomes one mass-spring-damper system, that is driven by a force created by the movement in the drill. The total system is not representative of the system we desired to simulate.

Another point of failure was the choice of using velcro straps for fastening the virtual patient to the manipulator. This did not produce a rigid contact, and bouncing occurred between the F/T sensor and the pipe which may have increased the noise. Rigidly attaching the pipe by screwing it onto the F/T sensor was not possible either as the drill design required the pipe to be able to rotate to exhibit the desired tremors.

In addition, the angular velocity of the the drill is not the same for every test. That is, there are no guarantee that speed of the drill is the same from test to test, since even though a clamp is used to secure that the button is pressed down constantly throughout a test, there is no mechanism installed to ensure that the button is pressed the same amount every time. This was done purposely as a test on a human would not have been repeatable either. The battery of the drill also impacts this aspect, as the battery was not charged between tests.

Lastly, as explained in chapter 7.1 about experimental setup, the structure on which the manipulator is placed is not stable. Even though the virtual patient was secured to another table, the manipulator is still exposed to the instability. This may have had little impact on the outcome of the experiment, however the effects of the instability are not positive.

7.5   Conclusion

The experiments are inconclusive with regards to whether a semi-active system is better at damping tremors in the virtual patient than a simple mass-spring-damper system. The experimental setup and protocol is still seen as satisfying, hence the experiment should be repeated after a redesign of the hardware interface. Conclusively, it could be said that the virtual patient experiments suffered from initial phase problems. Certain hardware design decisions early on defined the task before the controller was implemented. The controller implementation proved to require a rigid connection between the virtual patient and the manipulator. An aspect which was not taken into consideration during the initial hardware design phase.

Chapter 8

Conclusion

This thesis has focused on emulating a semi-active tremor suppression device on a robotic manipulator. A literature study on tremor assessment has been conducted; in addition, research and development of a tremor suppression system has been performed. A system has been engineered by combining hardware and software components, for which communication has been established and a control system developed. Tests and validations have been performed for every implemented system.

The literature review of the tremor assessment showed that there are several tremor assessment scales, none of which are explicitly used to assess tremor suppression devices. What did become clear was that both an objective assessment, through tests reviewing the ability to perform certain tasks; and a subjective assessment, through e.g. a patient survey reviewing the patients own perception of the device should be combined for an overall assessment. The Fahn-Tolosa-Marin tremor assessment scale includes both assessments and seems promising. The tremor scale should be combined with an assessment of the tremor signal, through e.g. Power Spectral Density.

The complete system is a modular system, which allows modifications of components within each module. In addition, some modules may also be removed completely, which will be the case for a completed wearable prototype.

This is also the case for the designed control system. However, As the purpose of this thesis is to emulate the wearable using a manipulator, both the high- and low-level control system were necessary to investigate. The implementation of each element of the control systems are considered successful, with the exception of the filter that separates intended patient motion signal from the tremor signal, and distributes the signals to the compliance and admittance controller.. Both the force controller and the admittance controller behaviour were validated and tuned through experimental tests. The implementation of the semi-active spring stiffness yielded a system that was easy to displace while quickly returning to the equilibrium. The behaviour took the form of a nonlinear spring, which

should be further investigated.

The experiment verifying the whole system as a tremor suppressor lacks a satisfying hardware interface. Even though the hardware interface was adequate for the purpose of development and testing of each implemented element by themselves, it was clearly unsuitable for a complete system test. The experimental setup and protocol should be repeated with a new hardware interface, as they were not invalidated.

Overall, this thesis provides insight to the R&D of the concept, in terms of testing and assessment, the development process and implementation. The work done will significantly reduce future efforts in developing a system, and it is a right step towards an end product. More research and development is needed before an end product is ready, some of these are presented in chapter 9.

Chapter 9

Future Work

There is still a lot of work left to be done before a wearable semi-active tremor suppression device may be realised. The main objective should still be to continue the progress and the investigation of the concept choices made in the earlier theses and those made in this. Some suggestions regarding work to do related to this thesis are listed below.

- Design of a hardware interface for the robot manipulator that ensures accurate representation of the physics of the DVA.

- Implement a solution for a hybrid controller with compliance and admittance.

- After testing a complete system on the test-rig, a project application could be applied to REK for testing on patients, using the FTM assessment scale.

Sunde also suggest improvements of the BMWFLC filter, some of these are listed below together with some suggestion made by the author.

- Implement the BMWFLC filter on a better microcontroller (16-bit or 32-bit) to see how much the performance improves.

- Expand the algorithm to estimate frequencies for 3 DOF.

- Design and make a printed circuit board (PCB) of the arduino and sensor system, with an optimal BMWFLC algorithm implemented.

- Optimize the stiffness coefficient tuning.

There is also work remaining regarding the prototype when the technology is tested and validated. Some examples are listed.

- Perform an assessment on prototype components.

- Design and build a prototype.

- Test and validate the prototype in clinical trials.

Unlike most dissipative approaches where there is active damping, the semi-active element in this approach is a spring. Further work includes investigating whether this is able to dissipate energy in the system, and accurately modeling the behaviour for different frequency signals. One way to do this is by performing a force reference signal that sweeps over the frequency spectrum, allowing the creation of a bode plot of the nonlinear spring

Bibliography

[1] Mads Johan Laastad. *NTNU-master-thesis (Code)*. Accessed: 2018-10-18. URL: https://github.com/madlaa/NTNU-master-thesis.

[2] Thomas Timm Andersen. *ur_modern_driver*. Accessed: 2018-10-20. URL: https://github.com/ros-industrial/ur_modern_driver.

[3] Bjarte Sunde. *BMWFLC-filter*. Accessed: 2018-12-24. URL: https://github.com/Bjarten/BMWFLC-filter.

[4] MediLexicon. *"Tremor"*. Accessed: 2018-09-15. 2018. URL: https://www.medilexicon.com/dictionary/93510.

[5] Andreas Puschmann and Zbigniew K Wszolek. "Diagnosis and Treatment of Common Forms of Tremor". In: *Seminars in neurology* 31 (1 2011). Accessed: 2018-09-07, pp. 65–77. DOI: 10.1055/s-0031-1271312.

[6] Stanley Fahn, Joseph Jankovic, and Mark Hallet. In: *Principles and Practice of Movement Disorders*. Accessed: 2018-09-07. Edinburgh: Elsevier Saunders, 2011, p. 32. ISBN: 9781437723694.

[7] Norsk Elektronisk Helsehåndbok. *Parkinsons Sykdom*. Accessed: 2018-09-10. 2017. URL: https://legehandboka.no/handboken/kliniske-kapitler/nevrologi/tilstander-og-sykdommer/bevegelsesforstyrrelser/parkinsons-sykdom/.

[8] Rashe Abdullah, Indranil Basak, Ketan S. Patil, Guido Alves, Jan Petter Larsen, and Simon Geir Møller. "Parkinson's disease and age: The obvious but largely unexplored link". In: *Experimental Gerontology* 68 (2015). Accessed: 2018-09-15, pp. 33–38. DOI: https://doi.org/10.1016/j.exger.2014.09.014.

[9] Constance Hammond, Hagai Bergman, and Peter Brown. "Pathological synchronization in Parkinson's disease: networks, models and treatments". In: *Trends in Neurosciences* 30 (7 2007). Accessed: 2018-05-15, pp. 357–364. DOI: https://doi.org/10.1016/j.tins.2007.05.004.

[10]   Norsk Elektronisk Helsehåndbok. *Essensiell Tremor*. Accessed: 2018-09-10. 2016. URL: https://legehandboka.no/handboken/kliniske-kapitler/ nevrologi/tilstander-og-sykdommer/bevegelsesforstyrrelser/ essensiell-tremor/.

[11]   International Essential Tremor Foundation. "Exploring ET: Patient Survey Results". In: *Tremor Talk* (2017). Accessed: 2018-09-15, pp. 21–22. URL: https://www. essentialtremor . org / wp – content / uploads / 2018 / 08 / ET – Patient-Survey-2017.pdf.

[12]   Joan K Monin, Jesus Gutierrez, Sarah Kellner, Sarah Morgan, Kathleen Collins, Brittany Rohl, Fanny Migliore, Stephanie Cosentino, Edward Huey, and Elan D Louis. "Psychological Suffering in Essential Tremor: A Study of Patients and Those Who Are Close to Them". In: *Tremor and other hyperkinetic movements* 7 (2017). Accessed: 2018-15-09, p. 526. DOI: 10.7916/D8Q53WF0.

[13]   Duane A Lundervold, Patrick A Ament, and Peter Holt. "Social anxiety, tremor severity, and tremor disability: a search for clinically relevant measures". In: *Psychiatry journal* 2013 (2013). Accessed: 2018-09-15, p. 257459. DOI: 10.1155/ 2013/257459.

[14]   Günther Deuschl, Jan Raethjen, Helge Hellriegel, and Rodger Elble. "Treatment of patients with essential tremor". In: *The Lancet Neurology* 10 (2 2011). Accessed: 2018-05-15, pp. 148–161. DOI: https://doi.org/10.1016/S1474– 4422(10)70322-7.

[15]   Olivier Rascol, David J. Brooks, Amos D. Korczyn, Peter P. De Deyn, Carl E. Clarke, and Anthony E. Lang. "A Five-Year Study of the Incidence of Dyskinesia in Patients with Early Parkinson's Disease Who Were Treated with Ropinirole or Levodopa". In: *New England Journal of Medicine* 342 (20 2000). Accessed: 2018-09-15, pp. 1484–1491. DOI: 10.1056/NEJM200005183422004.

[16]   Angelo Antonini et al. "Wearing-Off Scales in Parkinson's Disease: Critique and Recommendations". In: *Movement Disorders* 26 (12 2011). Accessed: 2018-09-15. DOI: 10.1002/mds.23875.

[17]   V. V. Shah, S. Goyal, and H. J. Palanthandalam-Madapusi. "A Possible Explanation of How High-Frequency Deep Brain Stimulation Suppresses Low-Frequency Tremors in Parkinson's Disease". In: *IEEE Transactions on Neural Systems and Rehabilitation Engineering* 25 (12 2017). Accessed: 2018-09-10, pp. 2498–2508. DOI: 10.1109/TNSRE.2017.2746623.

[18]   Mathias Toft, Bård Lilleeng, Ramm-Pettersen Jon, Geir Ketil Røste, Lena Pedersen, Inger Marie Skogseid, and Espen Dietrichs. "Behandling av bevegelsesforstyrrelser med dyp hjernestimulering". In: *Tidsskriftet* 128 (11 2008). Accessed: 2018-09-15. URL: https://tidsskriftet.no/2008/09/tema-bevegelsesforstyrrelser/ behandling-av-bevegelsesforstyrrelser-med-dyp-hjernestimulering.

[19]   Günther Deuschl et al. "Deep brain stimulation: Postoperative issues". In: *Movement Disorders* 21 (14 2006). Accessed: 2018-05-15, pp. 219–237. DOI: doi : 10.1002/mds.20957.

[20] Donatus Cyron. "Mental Side Effects of Deep Brain Stimulation (DBS) for Movement Disorders: The Futility of Denial". In: *Frontiers in Integrative Neuroscience* 10 (2016). Accessed: 2018-09-15, p. 17. DOI: `10.3389/fnint.2016.00017`.

[21] Mads Johan Laastad. "Robotic rehabilitation of upper-limb after stroke". Accessed: 2018-11-13. MSc. Thesis. 2017.

[22] Ida Estenstad. "Design and Validation of a Wearable Device for Upper Limb Tremor Suppression". Accessed: 2018-09-15. MSc. Thesis. Department of Mechanical & Industrial Engineering, 2018.

[23] Bjarte Mehus Sunde. "Estimation of multiple frequencies in pathological hand tremor for a semi-active 2DOF dynamic vibration absorber designed for tremor supression". Accessed: 2018-09-15. MSc. Thesis. Department of Engineering Cybernetics, 2018.

[24] C. A. Vaz and N. V. Thakor. "Adaptive Fourier estimation of time-varying evoked potentials". In: *IEEE Transactions on Biomedical Engineering* 36 (4 1989). Accessed: 2018-09-15, pp. 448–455. DOI: `10.1109/10.18751`.

[25] C. N. Riviere, R. S. Rader, and N. V. Thakor. "Adaptive cancelling of physiological tremor for improved precision in microsurgery". In: *IEEE Transactions on Biomedical Engineering* 45 (7 1998). Accessed: 2018-09-15, pp. 839–846. DOI: `10.1109/10.686791`.

[26] K. C. Veluvolu, U. X. Tan, W. T. Latt, C. Y. Shee, and W. T. Ang. "Bandlimited Multiple Fourier Linear Combiner for Real-time Tremor Compensation". In: vol. 2847 - 2850. Accessed: 2018-09-15. 2007. DOI: `10.1109/IEMBS.2007.4352922`.

[27] S. F. Atashzar, M. Shahbazi, O. Samotus, M. Tavakoli, M. S. Jog, and R. V. Patel. "Characterization of Upper-Limb Pathological Tremors: Application to Design of an Augmented Haptic Rehabilitation System". In: *IEEE Journal of Selected Topics in Signal Processing* 10 (5 2016). Accessed: 2018-09-15, pp. 888–903. DOI: `10.1109/JSTSP.2016.2530632`.

[28] Sarah Gebai, Mohammad Hammoud, Ali Hallal, and Hassan Khachfe. "Tremor Reduction at the Palm of a Parkinson's Patient Using Dynamic Vibration Absorber". In: *Bioengineering* 3 (3 2016). Accessed: 2018-09-15, p. 18. DOI: `10.3390/bioengineering3030018`.

[29] Stephanie Keller and Leon S. Dure. "Tremor in Childhood". In: *Seminars in Pediatric Neurology* 16 (2 2009). Accessed: 2018-09-15, pp. 60–70. DOI: `10.1016/j.spen.2009.03.007`.

[30] R Bhidayasiri. "Differential diagnosis of common tremor syndromes". In: *Postgraduate Medical Journal* 81 (962 2005). Accessed: 2018-09-15, pp. 756–762. DOI: `10.1136/pgmj.2005.032979`.

[31] P. David Charles, Gregory J. Esper, Thomas L. Davis, Robert J. Maciunas, and David Robertson. "Classification of Tremor and Update on Treatment". In: *American Family Physician* 59 (6 1999). Accessed: 2018-09-15, pp. 1565–1572.

[32] Paul Crawford and Ethan E. Zimmerman. "Tremor: Sorting Through the Differential Diagnosis". In: *American Family Physician* 97 (3 2018). Accessed: 2018-09-15, pp. 180–186.

[33] Winona Tse et al. "Prevalence of movement disorders in an elderly nursing home population". In: *Archives of Gerontology and Geriatrics* 46 (3 2008). Accessed: 2018-09-15, pp. 359–366. DOI: `10.1016/j.archger.2007.05.008`.

[34] Rodger J. Elble. "Tremor in Ostensibly Normal Elderly People". In: *Movement Disorders* 13 (3 1998). Accessed: 2018-09-15, pp. 457–464. DOI: `10.1002/mds.870130314`.

[35] Joseph Jankovic and Eduardo Tolosa. "Essential Tremor and Other Tremors". In: *Parkinson's Disease and Movement Disorders*. Vol. Sixth edition. Accessed: 2018-09-22. Wolters Kluwer Health, 2015. ISBN: 1-4963-1763-7.

[36] Juan A Gallego, Eduardo Rocon, Javier O Roa, Juan C Moreno, and José L Pons. "Real-Time Estimation of Pathological Tremor Parameters from Gyroscope Data". In: *Sensors* 10 (3 2010). Accessed: 2018-09-15, pp. 2129–2149. DOI: `10.3390/s100302129`.

[37] J. H. McAuley and C. D. Marsden. "Physiological and pathological tremors and rhythmic central motor control". In: *BrainPhysiological and pathological tremors and rhythmic central motor control* 123 (8 2000). Accessed: 2018-09-15, pp. 1545–1567. DOI: `10.1093/brain/123.8.1545`.

[38] Abdul Qayyum Rana and Kelvin L. Chou. "Classification of Tremor". In: *Essential Tremor in Clinical Practice*. Accessed: 2018-09-22. Switzerland: Springer, Cham, 2015, pp. 2 & 33. ISBN: 978-3-319-14598-3. DOI: `10.1007/978-3-319-14598-3`.

[39] Bhomraj Thanvi, Nelson Lo, and Tom Robinson. "Essential tremor - the most common movement disorder in older people". In: *Age and Ageing* 35 (4 2006). Accessed: 2018-09-15, pp. 344–349. DOI: `10.1093/ageing/afj072`.

[40] Theresa A Zesiewicz, Abinaya Chari, Israt Jahan, Amber M Miller, and Kelly L Sullivan. "Overview of essential tremor". In: *Neuropsychiatric Disease and Treatment* 6 (2010). Accessed: 2018-09-15, pp. 401–408.

[41] C. D. Marsden. "Origins of normal and pathological tremor". In: *Movement Disorders: Tremor*. Ed. by Leslie J. Findley and Rudy Capildeo. Accessed: 2018-09-22. London: Palgrave Macmillan UK, 1984, pp. 37–84. ISBN: 978-1-349-06757-2. DOI: `10.1007/978-1-349-06757-2_4`.

[42] Elan D Louis. "Twelve clinical pearls to help distinguish essential tremor from other tremors". In: *Expert Review of Neurotherapeutics* 14 (9 2014). Accessed: 2018-09-15, pp. 1057–1065. DOI: `10.1586/14737175.2014.936389`.

[43] Julián Benito-León D., Félix Bermejo-Pareja D., and Elan Louis D. "Incidence of essential tremor in three elderly populations of central Spain". In: *Neurology* 64 (10 2005). Accessed: 2018-09-15, p. 1721. DOI: `10.1212/01.WNL.0000161852.70374.01`.

[44]   I. Rautakorpi, J. Takala, R. J. Marttila, K. Sievers, and U. K. Rinne. "Essential tremor in a Finnish population". In: *Acta Neurologica Scandinavica* 66 (1 1982). Accessed: 2018-09-15, pp. 58–67. DOI: 10.1111/j.1600-0404.1982.tb03129.x.

[45]   Theresa A. Zesiewicz and Robert A. Hauser. "Phenomenology and treatment of tremor disorders". In: *Neurologic Clinics* 19 (3 2001). Accessed: 2018-09-15, pp. 651–680. DOI: 10.1016/S0733-8619(05)70039-6.

[46]   Virgilio Gerald H. Evidente. "Understanding essential tremor". In: *Postgraduate Medicine* 108 (5 2000). Accessed: 2018-09-15, pp. 138–149. DOI: 10.3810/pgm.2000.10.1253.

[47]   Rodger J. Elble. "Essential tremor frequency decreases with time". In: *Neurology* 55 (10 2000). Accessed: 2018-09-15, pp. 1547–1551. DOI: 10.1212/WNL.55.10.1547.

[48]   John G. Nutt and G. Frederick Wooten. "Diagnosis and Initial Management of Parkinson's Disease". In: *New England Journal of Medicine* 353 (10 2005). Accessed: 2018-09-15, pp. 1021–1027. DOI: 10.1056/NEJMcp043908.

[49]   Lonneke ML de Lau and Monique MB Breteler. "Epidemiology of Parkinson's disease". In: *The Lancet Neurology* 5 (6 2006). Accessed: 2018-09-15, pp. 525–535. DOI: 10.1016/S1474-4422(06)70471-9.

[50]   de Lau LL, Schipper CA, Hofman A, Koudstaal PJ, and Breteler MB. "Prognosis of parkinson disease: Risk of dementia and mortality: the rotterdam study". In: *Archives of Neurology* 62 (8 2005). Accessed: 2018-09-15, pp. 1265–1269. DOI: 10.1001/archneur.62.8.1265.

[51]   Ole-Bjørn Tysnes and Anette Storstein. "Epidemiology of Parkinson's disease". In: *Journal of Neural Transmission* 124 (8 2017). Accessed: 2018-09-15, pp. 901–905. DOI: 10.1007/s00702-017-1686-y.

[52]   L.C. Triarhou. "Dopamine and Parkinson's Disease". In: *Madame Curie Bioscience Database [Internet]* (2000 - 2013). Accessed: 2018-09-15. URL: https://www.ncbi.nlm.nih.gov/books/NBK6271/.

[53]   C. E. Clarke. "Parkinson's disease". In: *British Medical Journal* 335 (7617 2007). Accessed: 2018-09-15, pp. 441–445. DOI: 10.1136/bmj.39289.437454.AD.

[54]   Mary Ann Thenganatt and Elan D Louis. "Distinguishing essential tremor from Parkinson's disease: bedside tests and laboratory evaluations". In: *Expert review of neurotherapeutics* 12 (6 2012). Accessed: 2018-09-15, pp. 687–696. DOI: 10.1586/ern.12.49.

[55]   Heidemarie Zach, Michiel Dirkx, Bastiaan R Bloem, and Rick C Helmich. "The Clinical Evaluation of Parkinson's Tremor". In: *Journal of Parkinson's Disease* 5 (3 2015). Accessed: 2018-09-15, pp. 471–474. DOI: 10.3233/JPD-150650.

[56]   Erwin Kreyszig. "Fourier Analysis". In: *Advanced Engineering Mathematics*. Ed. by Shannon Corliss. Accessed: 2018-09-22. United States of America: John Wiley & Sons, 2011, pp. 474–539. ISBN: 978-0-470-45836-5.

[57] Steven W. Smith. "Continuous Signal Processing". In: *The Scientist and Engineer's Guide to Digital Signal Processing*. Accessed: 2018-09-22. San Diego, USA: California Technical Publishing, 1997, pp. 243–260. ISBN: 0-9660176-3-3.

[58] Steven A Tretter. *Notes on Fourier Series*. https://ece.umd.edu/~tretter/enee322/FourierSeries.pdf. Accessed: 2018-09-15. 2013.

[59] Singiresu S. Rao. "Fundamentals of Vibration". In: *Mechanical Vibrations*. Accessed: 2018-09-22. United States of America: Addison-Wesley Publishing Company, 1990, pp. 1–50. ISBN: 0-201-50156-2.

[60] William T. Thomson and Marie Dillon Dahleh. "Theory of Vibration with applications". In: Accessed: 2018-09-22. United States of America: Prentice-Hall, 1998. ISBN: 9780136510680.

[61] Allan G. Piersol and Thomas L. Paez. "Basic Vibration Theory". In: *Harris' Shock and Vibration Handbook, Sixth Edition*. Accessed: 2018-09-22. McGraw Hill Professional, Access Engineering, 2010.

[62] Anders Hillestad Hauglid. "Nonlinear Mechanical Vibrations: The Effect of Gaps". Accessed: 2018-09-15. MSc. Thesis. Norwegian University of Science and Technology (NTNU), 2018.

[63] John Polking, Albert Boggess, and David Arnold. "Second-Order Equations and Systems". In: *Differential Equations with Boundry Value Problems*. Accessed: 2018-09-22. United Kingdom: Pearson Education, 2006. ISBN: 978-0-13-186236.

[64] André Preumont. "Vibration Alleviation". In: *Twelve Lectures on Structural Dynamics*. Accessed: 2018-09-22. Springer Netherlands, 2013, pp. 247–274. ISBN: 978-94-007-6383-8. DOI: 10.1007/978-94-007-6383-8_11.

[65] Nils Wagner and Reinhard Helfrich. "Dynamic Vibration Absorbers and its Applications". In: *NAFEMS World Congress* (2017). Accessed: 2018-09-15.

[66] James McNames. "Signal Processing". In: *Mechanisms and Emerging Therapies in Tremor Disorders*. Ed. by Mario Manto. Accessed: 2018-09-22. New York: Springer, 2013, pp. 371–389. ISBN: 978-1-4614-4027-7. DOI: 10.1007/978-1-4614-4027-7_20.

[67] Maurice S. Bartlett. "Periodogram analysis and continuous spectra". In: *Biometrika* 37 (1950). Accessed: 2018-09-10, pp. 1–16.

[68] Peter D. Welch. "The Use of Fast Fourier Transform for the Estimation of Power Spectra: A Method Based on Time Averaging Over Short, Modified Periodograms". In: *IEEE Transactions on Audio and Electroacoustics* 15 (1967). Accessed: 2018-09-10, pp. 70–73. DOI: 10.1109/TAU.1967.1161901.

[69] Allison S. Arnold, Michael J. Rosen, and Mindy L. Aisen. "Evaluation of a Controlled-energy-dissipation Orthosis for Tremor Suppression". In: *Journal of Electromyography and Kinesiology* 3 (3 1993). Accessed: 2018-09-15, pp. 131–148. DOI: https://doi.org/10.1016/S1050-6411(05)80001-X.

[70] Zulkifli Yusop, M. Z. Md. Zain, Mohamed Hussein, A.R. Musa, and Azizan As'arry. "Evaluation on an Assistive Device in Suppressing Hand Tremor during Writing". In: *International Journal of Automotive and Mechanical Engineering* 8 (1 2013). Accessed: 2018-09-15, pp. 1187–1196. DOI: `10.15282/ijame.8.2013.9.0097`.

[71] P. G. Bain, L. J. Findley, P. Atchison, M. Behari, M. Vidailhet, M. Gresty, J. C. Rothwell, P. D. Thompson, and C. D. Marsden. "Assessing tremor severity". In: *Journal of Neurology, Neurosurgery, and Psychiatry* 56 (8 1993). Accessed: 2018-09-15, pp. 868–873.

[72] Stanley Fahn, Eduardo Tolosa, and Concepcion Marin. "Clinical Rating Scale for Tremor". In: *Parkinson's disease and movement disorders*. Accessed: 2018-09-22. Munich: Urban and Schwarzenberg, 1988, pp. 225–234.

[73] Richard D. Sweet, Jqel Blumberg, John E. Lee, and Fletcher H. McDowell. "Propranolol treatment of essential tremor". In: *Neurology* 24 (1 1974). Accessed: 2018-09-15, pp. 64–67. DOI: `10.1212/WNL.24.1.64`.

[74] Rodger J. Elble. "The Essential Tremor Rating Assessment Scale". In: *Journal of Neurology & Neuromedicine* 1 (4 2016). Accessed: 2018-09-15, pp. 34–38.

[75] Mark A. Stacy, Rodger J. Elble, William G. Ondo, Shu-Chen Wu, and Joseph Hulihan. "Assessment of interrater and intrarater reliability of the Fahn-Tolosa-Marin Tremor Rating Scale in essential tremor". In: *Movement Disorders* 22 (6 2007). Accessed: 2018-09-15, pp. 833–838. DOI: `https://doi.org/10.1002/mds.21412`.

[76] Rodger Elble et al. "Task force report: Scales for screening and evaluating tremor: Critique and recommendations". In: *Movement Disorders* 28 (13 2013). Accessed: 2018-09-15, pp. 1793–1800. DOI: `10.1002/mds.25648`.

[77] Anupam Pathak, John A Redmond, Michael Allen, and Kelvin L Chou. "A Non-Invasive Handheld Assistive Device to Accommodate Essential Tremor: A Pilot Study". In: *Movement disorders* 29 (6 2013). Accessed: 2018-09-15, pp. 838–842. DOI: `10.1002/mds.25796`.

[78] *Service manual for UR5 with CB2, version 1.6 US*. Accessed: 2018-11-15. URL: `https://s3-eu-west-1.amazonaws.com/ur-support-site/17958/manual_en_UR5_CB2_1.6_US.pdf`.

[79] Zacobria. *UR 5 (CB3) specification*. Picture accessed: 2018-11-12. URL: `http://www.zacobria.com/images/robot_complete.jpg`.

[80] ATI Industrial Automation. *F/T Sensor: Gamma*. Accessed: 2018-16-11. URL: `https://www.ati-ia.com/products/ft/ft_models.aspx?id=Gamma`.

[81] Jean Jacques Fuchs and Bernard Delyon. "The Sampling Theorem and Time Delay Estimation". In: *IFAC Proceedings Volumes* 30 (11 1997). Accessed: 2018-09-15. DOI: `https://doi.org/10.1016/S1474-6670(17)42893-X`.

[82] John Catsoulis. "Analog". In: *Designing embedded hardware*. Accessed: 2018-09-22. United States: O'Reilly, 2001. ISBN: 9780596520939.

[83] Neville Hogan and Stephen P. Buerger. "Impedance and Interaction Contol". In: *Robotics and Automation Handbook*. Ed. by T.R. Kurfess. Accessed: 2018-04-22. CRC Press, 2004. Chap. 19, pp. 1–24. ISBN: 9781420039733.

[84] Rolf Johansson, Klas Nilsson, and Anders Robertsson. "Force Control". In: *Handbook of Manufacturing Engineering and Technology*. Ed. by Andrew Y. C. Nee. Accessed: 2018-09-22. London: Springer London, 2015, pp. 1933–1965. ISBN: 978-1-4471-4670-4. DOI: `10.1007/978-1-4471-4670-4_108`.

[85] Dawid Urbanski. *cArduino*. Accessed: 2018-12-23. URL: `https://github.com/ranma1988/cArduino`.

[86] Universal Robotics. *Parameters for calculations of kinematics and dynamics*. Accessed: 2018-10-20. URL: `https://www.universal-robots.com/how-tos-and-faqs/faq/ur-faq/parameters-for-calculations-of-kinematics-and-dynamics-45257/`.

[87] Thomas Timm Andersen. *Optimizing the Universal Robots ROS driver*. Tech. rep. Accessed: 2018-01-15. Technical University of Denmark, Department of Electrical Engineering, 2015.

Appendix

A   BMWFLC Algorithms and Equations

The following sections are parts of chapter 5 in [23], some modifications for the sake of readability and relevance have been done by the Author

Core Equations

Each n-WFLC in the BMWFLC has its own frequency and learning rate, enabling each WFLC to adapt to the signal individually with its own speed. The learning rates are

$$\mu_{\mathbf{k}} = \begin{bmatrix} \mu_{1_k} & \mu_{2_k} & \cdots & \mu_{n_k} \end{bmatrix} \tag{9.1}$$

and the angular frequencies for the WFLC in the filter are

$$\omega_{\mathbf{k}} = \begin{bmatrix} \omega 1_k & \omega 2_k & \cdots & \omega_{n_k} \end{bmatrix} \tag{9.2}$$

where k is the sampling instance. When $k = 0$ we get the size frequency window, where the frequencies have the distance $\Delta\omega$ between them

$$\begin{bmatrix} \omega_{1_0}, \omega_{n_0} \end{bmatrix} \tag{9.3}$$

The frequency window is divided into a number of divisions

$$\eta = \frac{\omega_{n_0} - \omega_{1_0}}{\Delta\omega} \tag{9.4}$$

and n is then the number of harmonics in for the Fourier combiner model of y_k.

$$y_k = \sum_{r=1}^{n} a_{r_k} \sin(\omega_{r_k} k) + b_{r_k} \cos(\omega_{r_k} k) \tag{9.5}$$

y_k will not be used as an output for this filter, since it will not be tuned to have an accurate estimate of the amplitude, only the frequencies (9.3) are of interest. Then $\mathbf{x_k}$ and $\mathbf{w_k}$ are defined

$$\mathbf{x_k} = \begin{bmatrix} \begin{bmatrix} \sin(\omega_{1_k} k) & \sin(\omega_{2_k} k) & \cdots & \sin(\omega_{n_k} k) \end{bmatrix}^{\mathsf{T}} \\ \begin{bmatrix} \cos(\omega_{1_k} k) & \cos(\omega_{2_k} k) & \cdots & \cos(\omega_{n_k} k) \end{bmatrix}^{\mathsf{T}} \end{bmatrix} \tag{9.6}$$

$$\mathbf{w_k} = \begin{bmatrix} \begin{bmatrix} a_{1_k} & a_{2_k} & \cdots & a_{n_k} \end{bmatrix}^{\mathsf{T}} \\ \begin{bmatrix} b_{1_k} & b_{2_k} & \cdots & b_{n_k} \end{bmatrix}^{\mathsf{T}} \end{bmatrix} \tag{9.7}$$

Using 9.6 and 9.7 the linear combiner can be written as

$$y_k = \mathbf{w_k}^\mathsf{T}\mathbf{x_k} \tag{9.8}$$

and the error between the signal of the complete motion of the hand and the estimated signal y_k is

$$\epsilon_k = s_k - y_k \tag{9.9}$$

The recursive LMS algorithm used to update the weights of $\mathbf{w_k}$

$$\mathbf{w_{k+1}} = \rho\mathbf{w_k} + 2\mu_k\mathbf{x_k}\epsilon_k \tag{9.10}$$

$$\rho = \sqrt[\delta]{\alpha} \tag{9.11}$$

$$\delta = \frac{1}{\Delta T}T_p \tag{9.12}$$

This is the memory manipulation from the E-BMFLC algorithm. It makes the filter forget past information, making it adapt faster when sudden changes occur in the signal s_k, E.g., a sudden change of frequency. Decreasing ρ increases the rate of forgetting past information. ΔT is the sampling time (in seconds), T_p is the width of the considered memory window (in seconds), and α is the minimum amplification gain considered within the window.

The fundamental angular frequencies mu_k, are updated using multiple modified LSM algorithms, one for each WFLC, each with its own adaptive gain $\omega_\mathbf{k}$

$$\omega_{r_{k+1}} = \omega_{r_k} + 2\epsilon_k\mu_{r_k}\left[a_{r_k}cos(r\omega_{r_k}k) - b_{r_k}sin(\omega_{r_k}k)\right], \qquad r = 1, 2, ..., n \tag{9.13}$$

Equation (9.13) uses the LMS algorithm to descend the performance surface to minimize the Minimum-Square-Error. If the learning rates $\mathbf{mu_k}$, are too large all the frequencies will try to reach the frequencies with the largest magnitude in the magnitude spectrum, the global minimum on the performance surface. This is because the error ϵ_k looks at the error between the input signal s_k and the estimate of the entire signal y_k, so each WFLC in the BMWFLC wants to go for the dominant frequency in the signal. If the learning rate $\mathbf{mu_k}$, is set small enough, each WFLC will get stuck in its local minimum, this is what we want, enabling each WFLC only converge towards the real frequency closest to it. When tracking multiple frequencies, the learning rate needs to be small, resulting in slow convergence, if only the frequency with the largest magnitude is being tracked, the learning rate can be set much higher since only the global minimum is of interest, resulting in faster convergence.

Adaptive Learning Rate

One of the drawbacks with the FLC, WFLC and BMFLC algorithms is that the learning rate parameters μ and μ_0 need fine tuning, and are sensitive to change in the amplitude of the input signal. The two parameters also need to be tuned separately. When the tremor is suppressed the amplitude of the signal will be decreased, and the sensitivity of the

estimation will decrease. To solve this problem, we can use the amplitude of the input signal to adapt the learning rate. We will use a queue data structure Q, which uses the first-in, first-out, or FIFO, policy. The queue will have a fixed length L, a good value for its length is to set it equal to the sampling rate of the signal, f_s.

Algorithm 1: Max Amplitude Window

   Input : The measured signal y_k
   Input : Max length of queue; L
   Output: The peak amplitude from the time slice; A_{peak}
   Q.enqueue($abs(y_k)$);
   if $Q.length > L$ **then**
      | Q.dequeue();
   end
   $A_{peak} = \max Q$

Algorithm 1 checks the L last samples from the tremor signal, and return the peak amplitude. This value can now be used to adapt the learning rates. If the length L is set to 100 and our sample rate of the signal is 100 Hz, the window will contain the tremor values for the past 1 second so that the learning rates can adapt relatively fast to any changes in the amplitude of the tremor. The following equations adapt the learning rates.

$$\mu_k = \frac{\kappa}{A_{peak}} \tag{9.14}$$

The value for the scaling parameter κ can be found by tuning. The equation makes μ_{rk} adaptive is

$$\mu_{rk} = \mu_k h + \mu_{rk} \beta e^{-\lambda t}, \qquad r = 1, 2, ..., n \tag{9.15}$$

Magnitude spectrum - extracting frequencies

To find the frequencies in the input signal, we will look at the magnitudes of the Fourier components in the BMFLC, the magnitude of each FLC; the FLC with the highest magnitude should contain the dominant frequency in the estimated signal, which then is the estimate of the dominant frequency for the real signal

$$M_{rk} = \sqrt{a_{rk}^2 + b_{rk}^2}, \qquad r = 1, 2, ..., n \tag{9.16}$$

$$\mathbf{M} = \begin{bmatrix} M_{1k} & M_{2k} & \cdots & M_{nk} \end{bmatrix} \tag{9.17}$$

With this method we can estimate multiple frequencies in the signal. To accomplish this, we look for the magnitudes that are peaks in the magnitude spectrum. That is, the magnitude of interest should be larger than the magnitude to its immediate left and right in the magnitude spectrum, $M_{r-1} < Mr > M_{r+1}$. We want to be able to tell our algorithm how many peaks it should track in the spectrum, each peak it tracks is an estimate of a frequency, so we define a variable called ftt (frequencies to track). Instead of making all

the FLC in the truncated Fourier series into WFLC, we can say that the ftt number of FLC with the largest magnitude of Fourier coefficients are allowed to become WFLC. When the learning rate is set to zero, $\mu_{rk} = 0$, it becomes an FLC, and its respective frequency ω_{rk} lose its capability to adapt to the signal. When the BWMFLC starts to adapt to the signal, all the magnitudes of the FLC are tracked, and the fft number of FLC with the largest peak magnitudes in the magnitude spectrum become WFLC, by setting $\mu_{rk} > 0$. We define an array to store the peak magnitudes and their position in the spectrum. M_{peak_1} is the largest peak, M_{peak_2} the second largest peak; and Pos_{p1} and Pos_{p2} are their position in the spectrum respectively.

$$\mathbf{M}_{peak} = \begin{bmatrix} [M_{p1}, Pos_{p1}] & [M_{p2}, Pos_{p2}] & \cdots & [M_{pr}, Pos_{pr}] \end{bmatrix} \quad (9.18)$$

Algorithm 2 shows how we can find the magnitude peaks, and return an array with all the peaks, it should be sorted the same way as (9.18). It is now easy to get the estimate for the

---

Algorithm 2: Find peak magnitudes

Input : Magnitude spectrum; $\mathbf{M}$
Output: Peak magnitudes; $\mathbf{M_{peak}}$
for $i = 0; i < M.length; i = i + 1$ **do**
  if $i == 0$ **then**
    if $M[i] > M[i + 1]$ **then**
    | $M_{peak}.append([M[i], i])$
    end
  else if $i < M.length$ **then**
    if $M[i] > M[i - 1] \ and \ M[i] > M[i + 1]$ **then**
    | $M_{peak}.append([M[i], i])$
    end
  else if $i == M.length$ **then**
    if $M[i] > M[i - 1]$ **then**
    | $M_{peak}.append([M[i], i])$
    end
  end
end
$M_{peak}.sort()$

---

frequencies; we use the positions from (9.18), and the estimates will be the frequencies in (9.3) that correspond to them. E.g if $Pos_{p1} = 8$, the estimate for the frequency with the most power in the input signal will be ω_{8_k}.

Since the frequencies in ω_k will change over time, there should be a mechanism to reset the frequencies to their original values ω_0, if they no longer are present in the signal. An easy way to do this is to make a threshold variable, η, and if any of the magnitudes in $\mathbf{M}_k$ get under this threshold, their respective frequency in ω_k should reset to their original value ω_0.

Algorithm 3: Adapt and return ω_k, the estimated frequencies

Input : Peak magnitudes sorted; $\mathbf{M_{peak}}$
Input : Number of frequencies to track; ftt
Input : Angular frequencies; ω_k
Input : Learning rates; μ_k
Output: Estimated frequencies; ef
ef = []
for $i = 0; i < ftt; i = i + 1$ **do**
   positionOfPeak = $M_{peak}[i][1]$
   adaptLearningRate($\mu_k[positionOfPeak]$)
   adaptAngularFrequency($\omega_k[positionOfPeak]$)
   ef.append($\omega_k[positionOfPeak]$)
end

$$\omega_{r_k} = \begin{cases} \omega_{r0} & \text{if } M_{rk} < \eta \\ \omega_{r_k} & \text{otherwise} \end{cases} \qquad r = 1, 2, ..., n \qquad\qquad (9.19)$$

B BMWFLC Flowchart
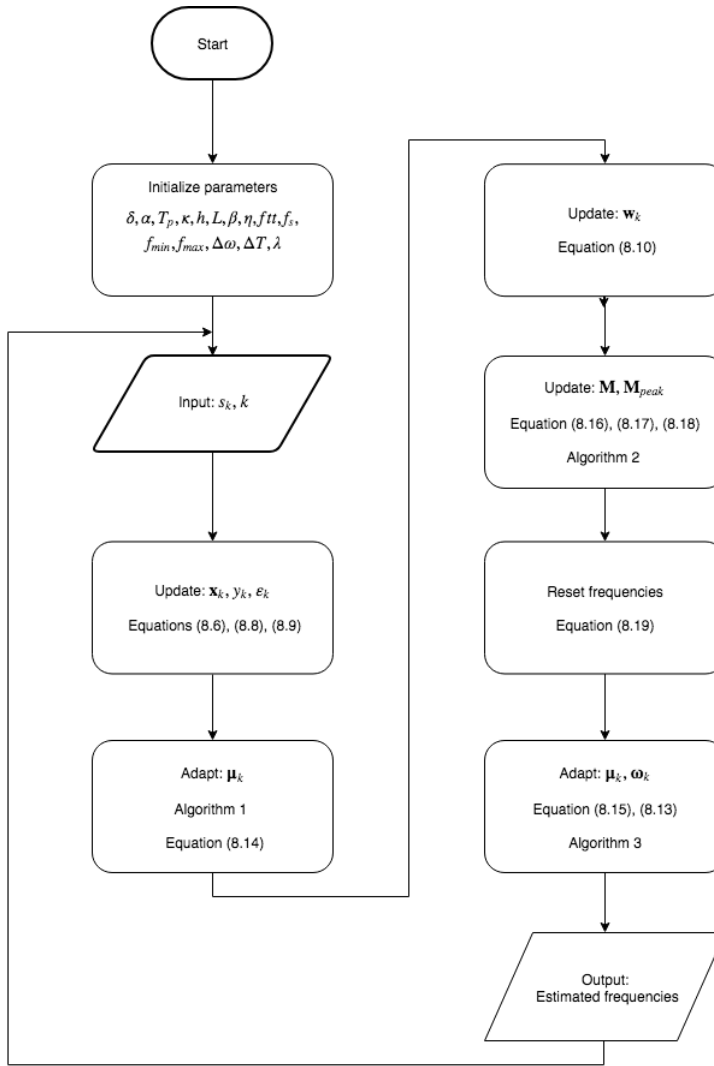
Figure B.1: Flowchart of the BMWFLC [Author], inspired by [23]

C Design Proposals

(a) Design proposal 1
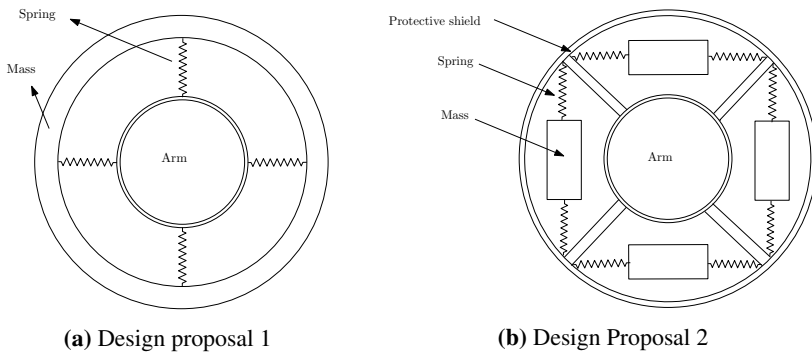
(b) Design Proposal 2

Figure C.1: Cross-sectional view of arm with DVA[22]
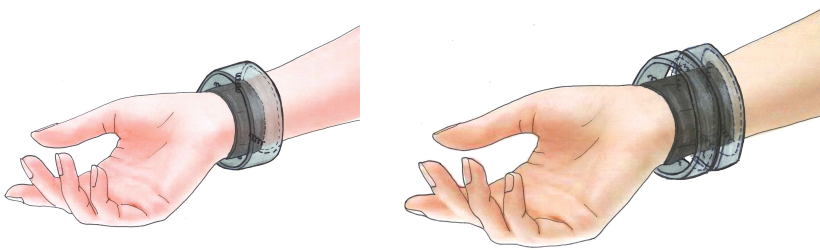
(a) Design proposal for a single DVA system **(b)** Design Proposal for a dual DVA system

Figure C.2: Sketch of design proposals of the implementation of DVA systems [22]
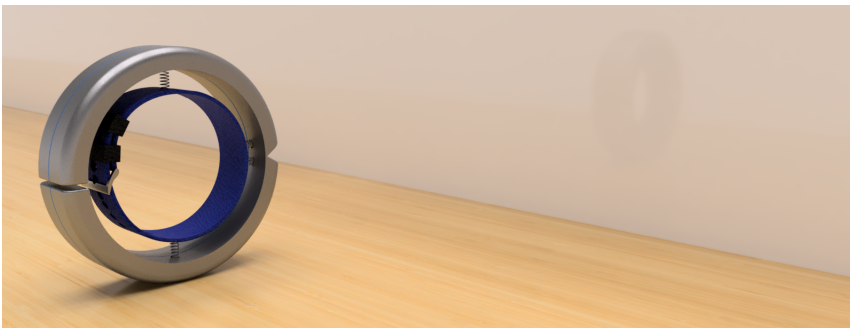
Figure C.3: Render of how the above design might be implemented [22]

D UR5 Denavit Hartenberg

Reference frames for Denavit-Hartenberg parameters of the UR5 manipulator
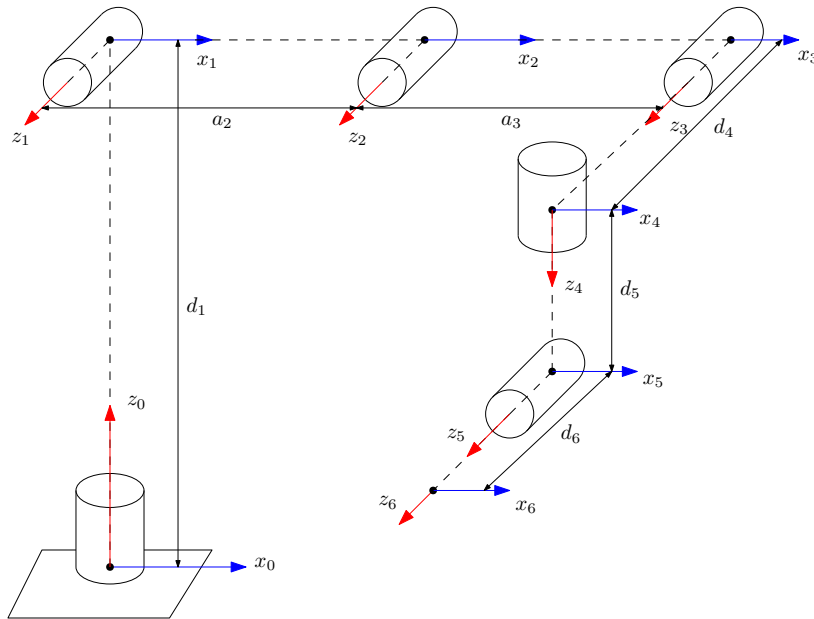
Figure D.1: Reference Frames for the UR5 manipulator based on its DH-parameters [Author]

Denavit-Hartenberg parameters

Link	θ_i[rad]	d_i[mm]	a_i[mm]	α_i[rad]
1	q_1	89.459	0	$\pi/2$
2	q_2	0	-425	0
3	q_3	0	-392.25	0
4	q_4	109.15	0	$\pi/2$
5	q_5	94.65	0	$-\pi/2$
6	q_6	82.3	0	0

Table D.1: DH parameters for UR5, values taken from [86]

E Code

This appendix briefly describes the source code and implementation files. It assumes fundamental of understanding of Linux OS and code compilation. The source code may be obtained by contacting ITK.

Directory Structure

```
UR5−Master/                    − Main Directory
    BMWFLC−filter/             − BMWFLC filter code and figure
    cArduino/                  − C++ and Arduino communication
        cArduino.cpp
        cArduino.h
    data/                      − Raw log files
        log_library/
        logs/
    force/                     − External Controller
        force.cpp
        force.h
        ujac_c.c
        ufwdkin.c
    MATLAB_data_analysis/      − Matlab code and figures
    TremSup/                   − Main file directory
        Makefile
        TremSup.cpp
        TremSup.h
        start.exe
    ur_moder_driver−master/ − Driver for UR Robots
```

File Description

- **Makefile** & **start.exe**: These files contain the makefile and executable file for the tremor suppression system developed during this master thesis.

- **TremSup.cpp** & **TremSup.h**: These files contain the main file, various robot motions and user interface for the tremor suppression system developed during this master thesis. Parts of the framework seeks to re-use code developed by [21].

- **force.cpp** & **force.h**: These files contain the external controller and safety mechanisms developed and implemented during this master thesis. Parts of the code is developed by [21].

- **ujac_u.c** & **ufwdkin.c**: These files are the C implementation of the kinematics and the Jacobian for the UR5. The DH parameters can be changed in order to fit the Jacobian for the UR3 or UR10. This is re-used code from [21].

- **ur modern driver-master/**: Drivers for the UR3, UR5 and UR10 from Universal Robot developed by [2]. The driver documentation is developed by the same author [87].

- **cArduino.cpp** & **cArduino.h**: These files are the implementation of the communication between Linux C++ and Arduino developed and implemented during this master thesis. Code based on [85].

- **BMWFLC-filter/**: This folder contains code for the BMWFLC filter. Both for the Arduino implementation and for plotting in python. Code is developed by [23].

Running the code

The tremor suppression system needs a non-standard Linux library before it can be utilised. The GNU Scientific Library is utilized to calculate the inverse Jacobian. Follow the installation instructions and update the library before proceeding. Other essential preparations require recreating parts of the laboratory setup utilised in this master thesis.

- Mount the F/T sensor Gamma transducer with the sensor frame identical to the tool frame. Utilise the F/T Net Box web interface to configure the Gamma F/T sensor with a 250Hz sampling frequency, low-pass filtration with a cut-off frequency of 5Hz.

- Contact the Department of Engineering Cybernetics at NTNU to obtain a copy of the source code.

- The IP addresses of the UR5 and F/T sensor are defined in TremSup.cpp and force.cpp respectively. Make sure to change them appropriately to fit your laboratory setup.

- Recompile the code, remember to do this every time the the code is changed. Enter the directory NTNU-master-thesis/TremSup and run the terminal command "make clean && make".

  username@ubuntu:∼/NTNU-master-theis/rrulas$ make clean && make

- Be aware and make the workspace available for the predetermined initial pose the manipulator moves to when the system is executed. The external controller is not active during this initial movement.

- The robotic rehabilitation system can now be executed with the newly compiled executable start.exe file with the terminal command "./start".

  username@ubuntu:∼/NTNU-master-theis/rrulas$ ./start

- Always keep the teach pendent with the emergency button available while running the tremor suppression system and respect the power of the UR5 manipulator.

F Additional Results

This appendix contains additional results of the experimental tests performed in this thesis.
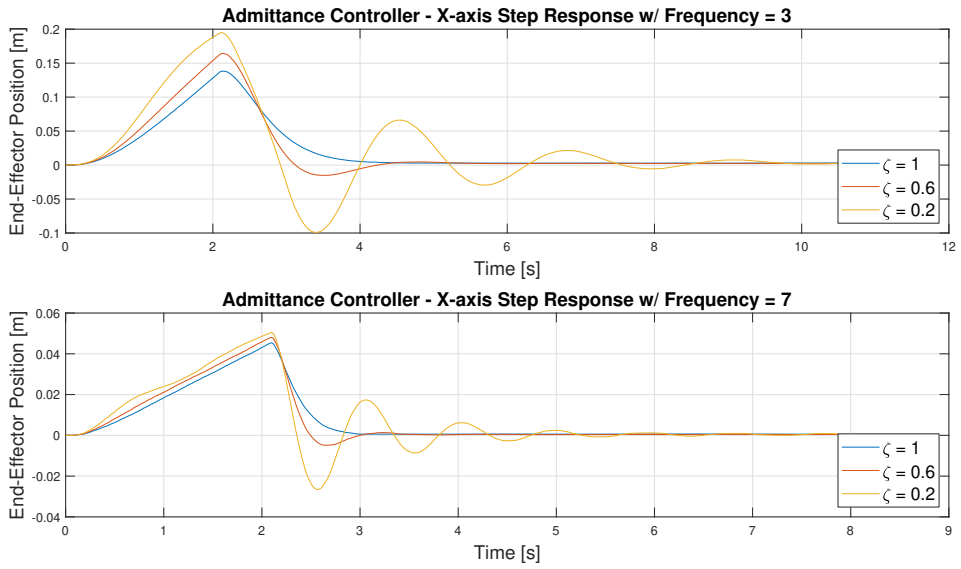
F.1 Step Response Results

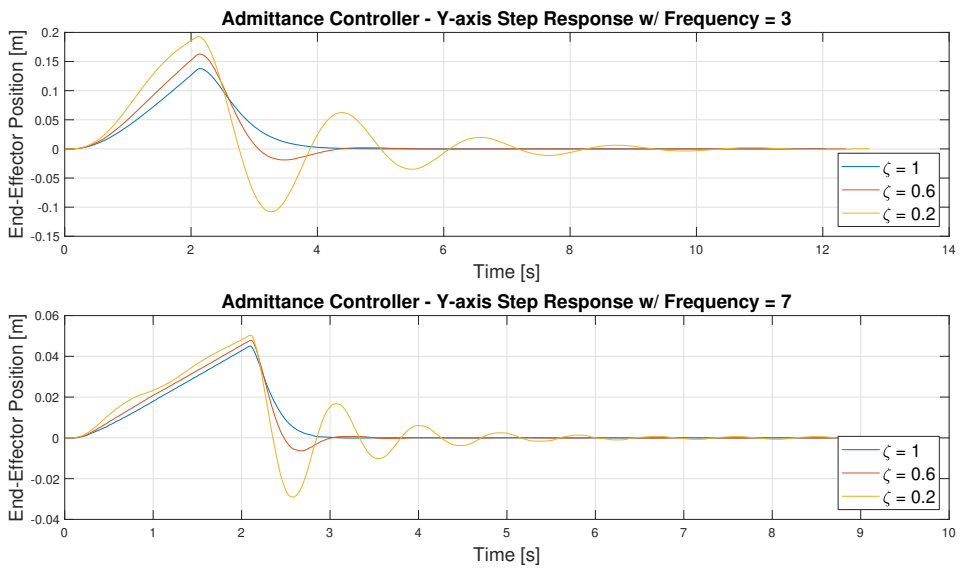**Figure F.1:** Step response for X-axis with fixed frequencies [Author]

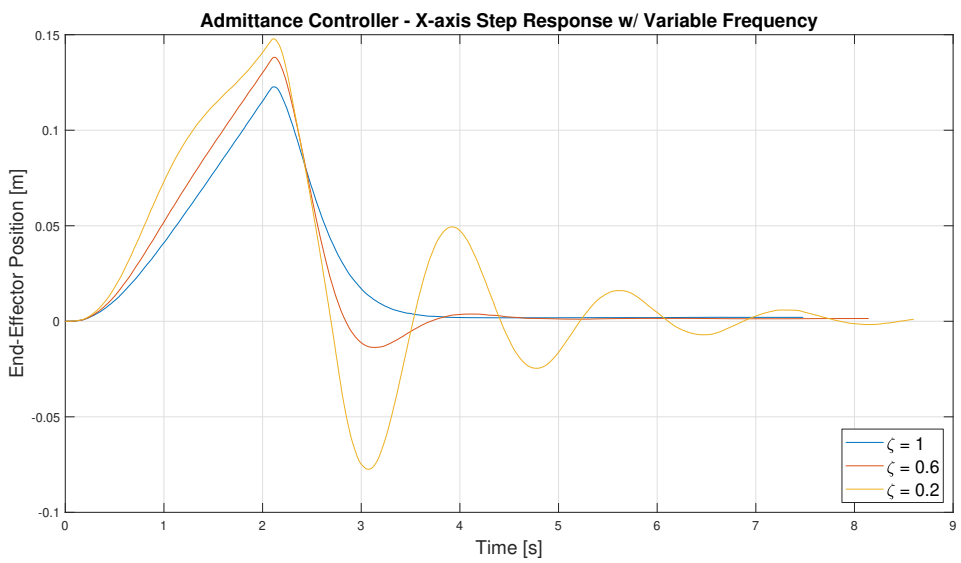**Figure F.2:** Step response for Y-axis with fixed frequencies [Author]

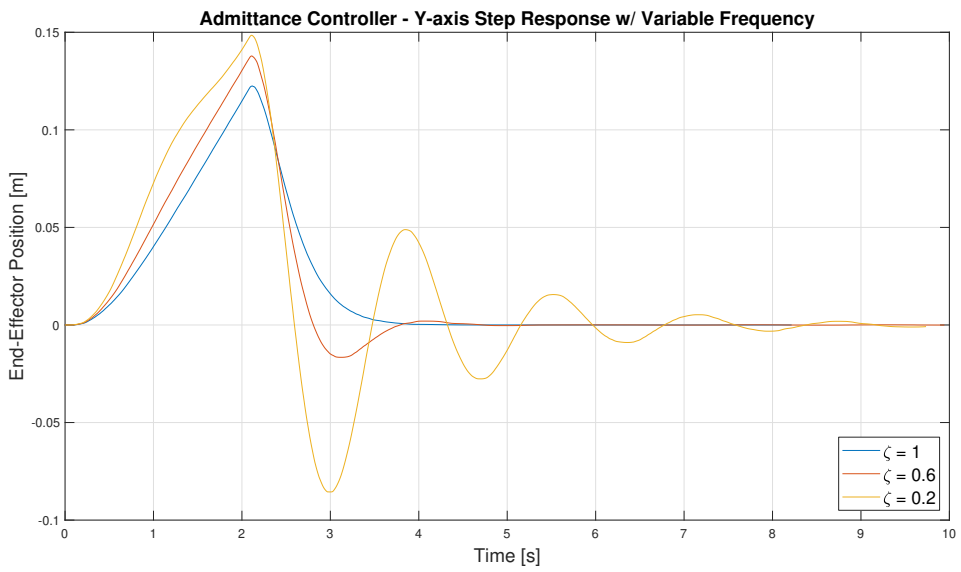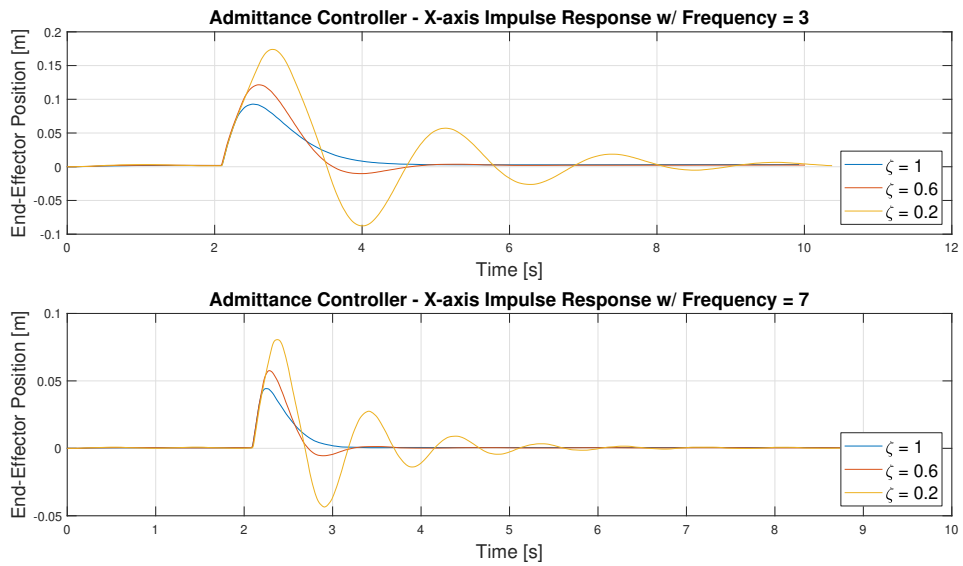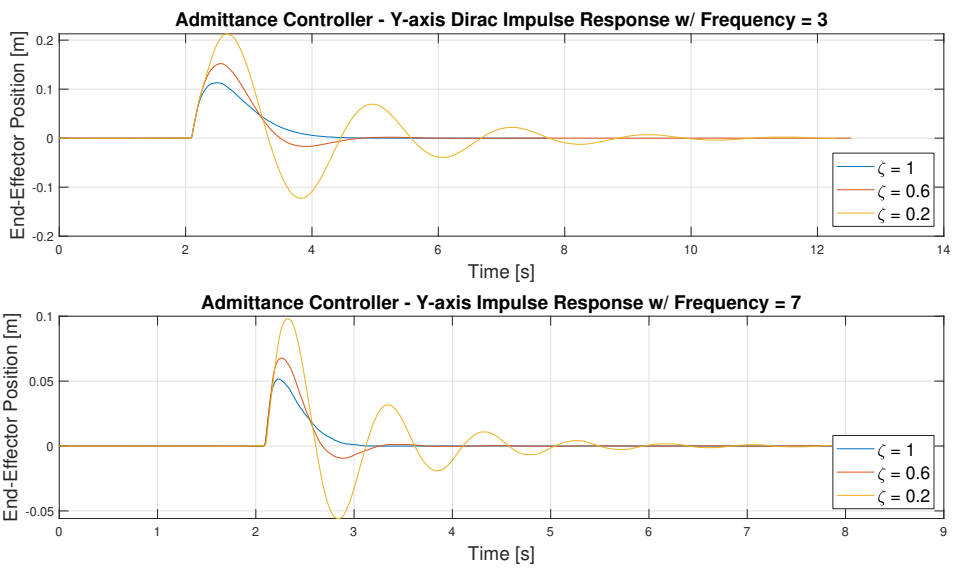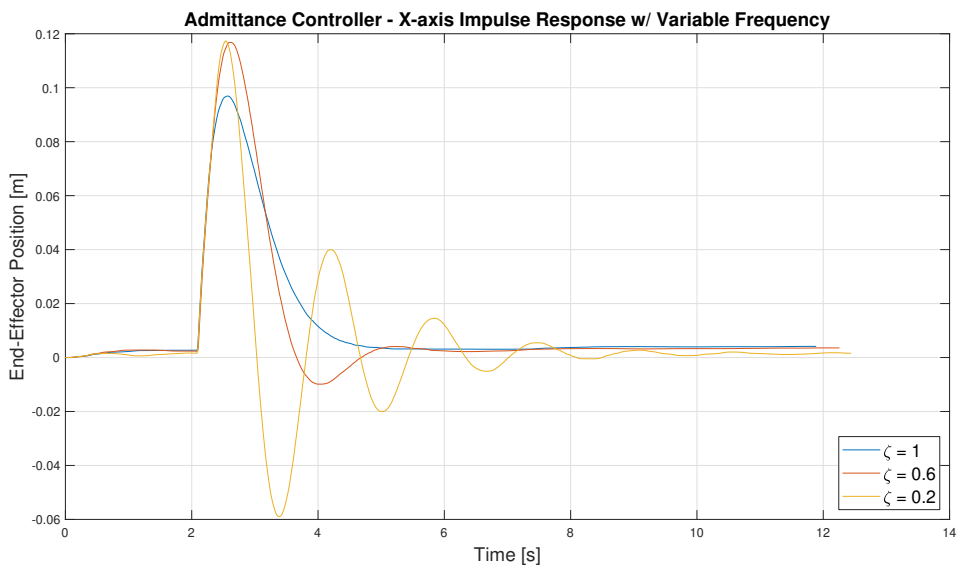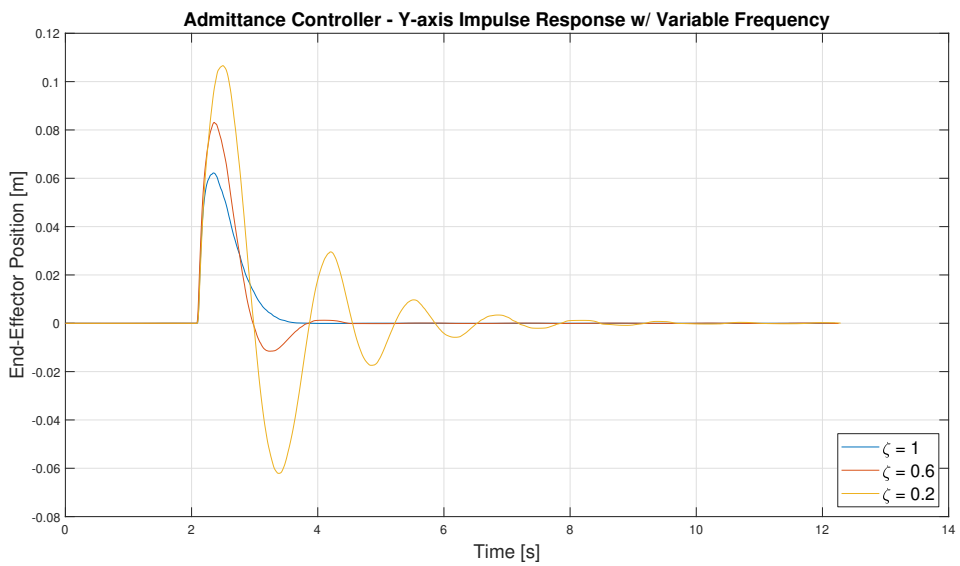**Figure F.3:** Step response for X-axis with variable frequency [Author]

Figure F.4: Step response for Y-axis with variable frequency [Author]

F.2 Impulse Response Results

**Figure F.5:** Impulse response for the X-axis with fixed frequencies [Author]

Figure F.6: Impulse response for the Y-axis with fixed frequencies [Author]

Figure F.7: Impulse response for the X-axis with variable frequency [Author]

Figure F.8: Impulse response for the Y-axis with variable frequency [Author]

F.3 Experimental Results

Fixed Frequency
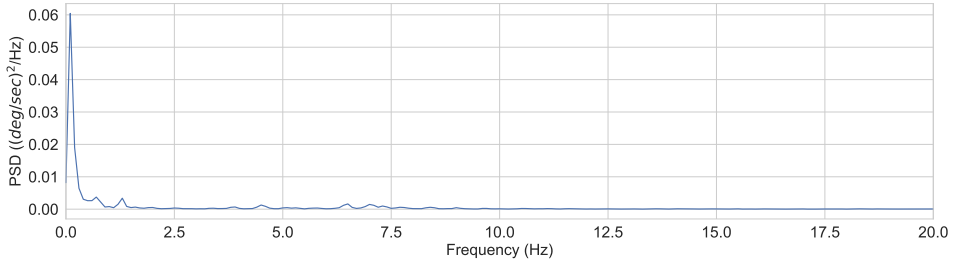
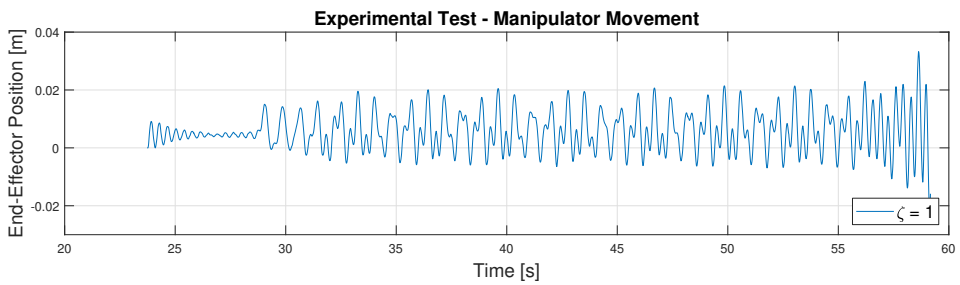**(a)** PSD plot for critical damped system with fixed frequency, $f = 10$ [Author]
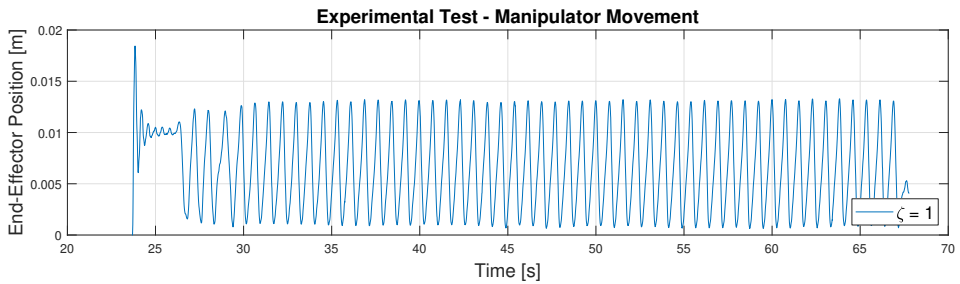
(b) Movement plot for critical damped system with fixed frequency, $f = 10$ [Author]

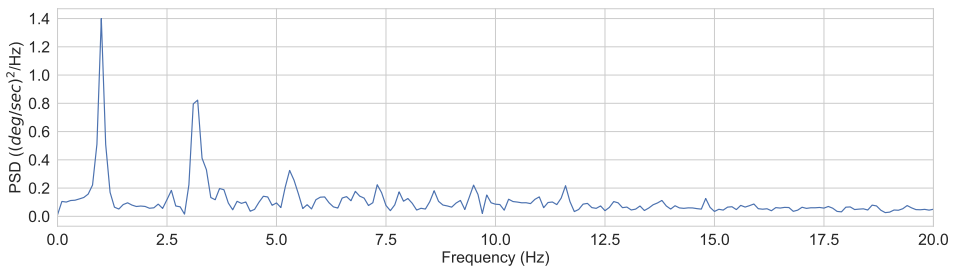**Figure F.9:** Plots of critical damped system with fixed frequency, $f = 10$ [Author]
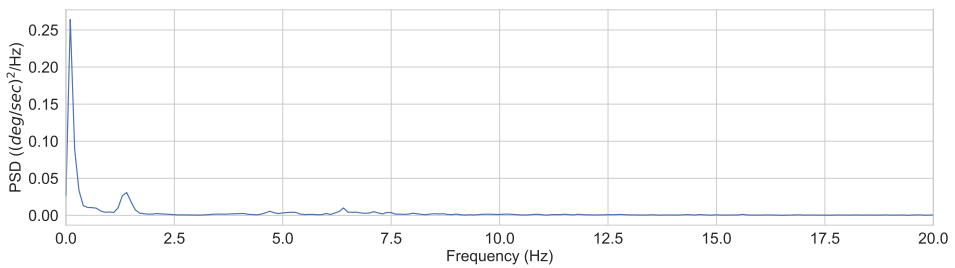
(a) PSD plot for critical damped system with fixed frequency, $f = 6$ [Author]
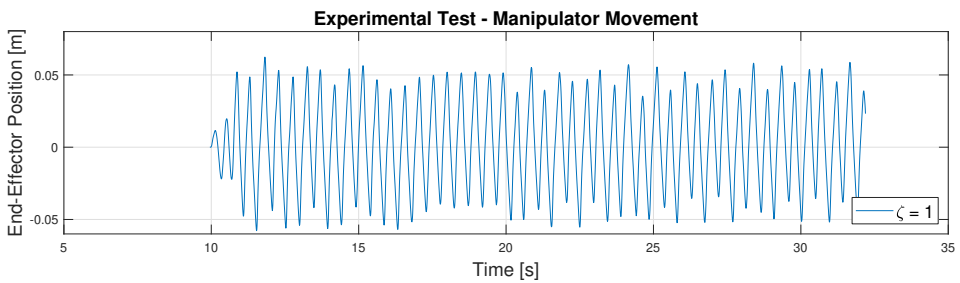

(b) Movement plot for critical damped system with fixed frequency, $f = 6$ [Author]

Figure F.10: Plots of critical damped system with fixed frequency, $f = 6$ [Author]
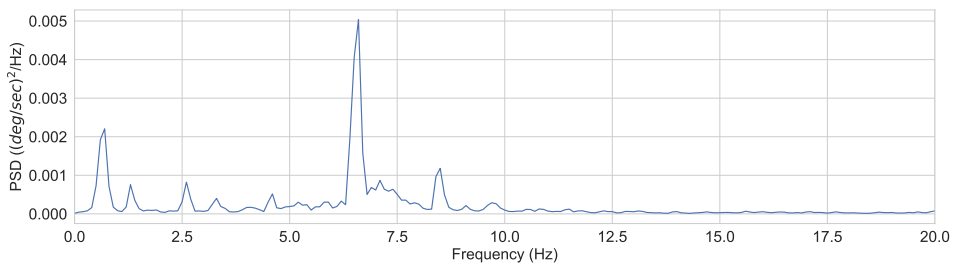
(a) PSD plot for critical damped system with fixed frequency, $f = 3$ [Author]
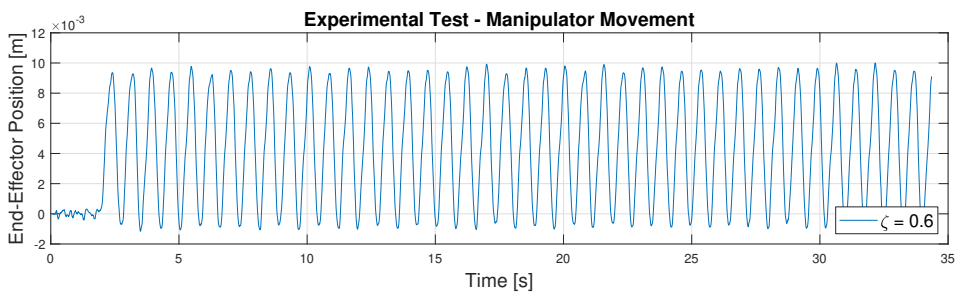

(b) Movement plot for critical damped system with fixed frequency, $f = 3$ [Author]

Figure F.11: Plots of critical damped system with fixed frequency, $f = 3$ [Author]

(a) PSD plot for mildly underdamped system with fixed frequency, $f = 15$ [Author]

(b) Movement plot for mildly underdamped system with fixed frequency, $f = 15$ [Author]

Figure F.12: Plots of mildly underdamped system with fixed frequency, $f = 15$ [Author]
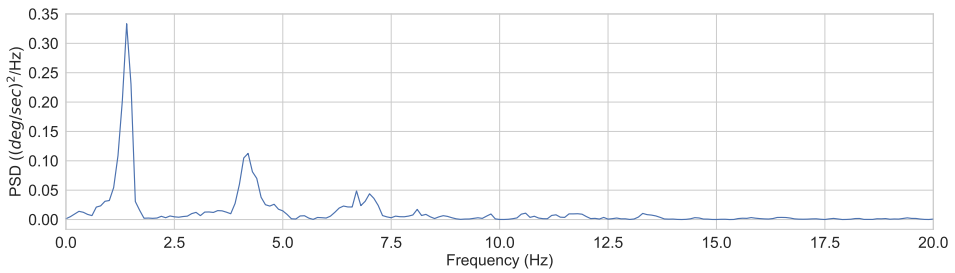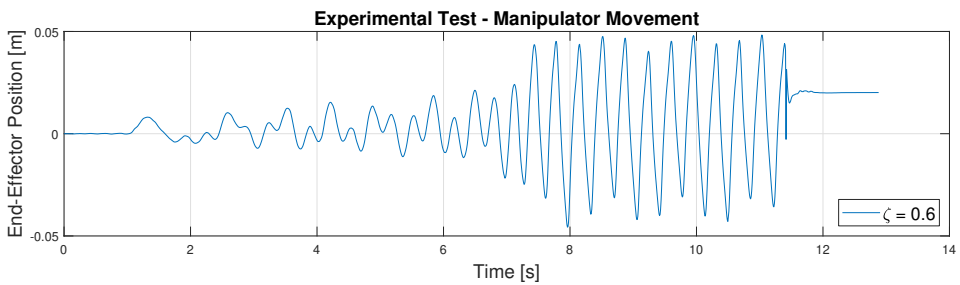
(a) PSD plot for mildly underdamped system with fixed frequency, $f = 10$ [Author]

(b) Movement plot for mildly underdamped system with fixed frequency, $f = 10$ [Author]

Figure F.13: Plots of mildly underdamped system with fixed frequency, $f = 10$ [Author]
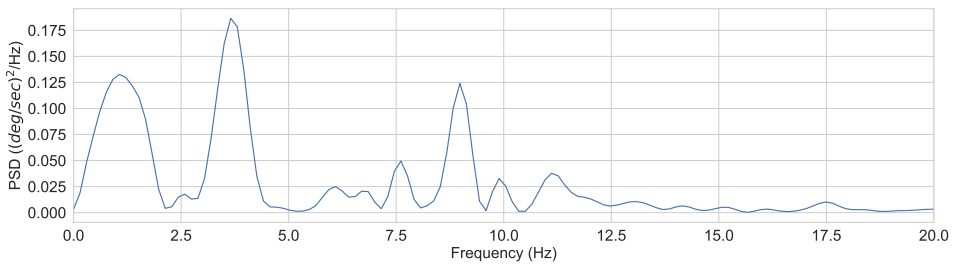
(a) PSD plot for mildly underdamped system with fixed frequency, $f = 6$ [Author]
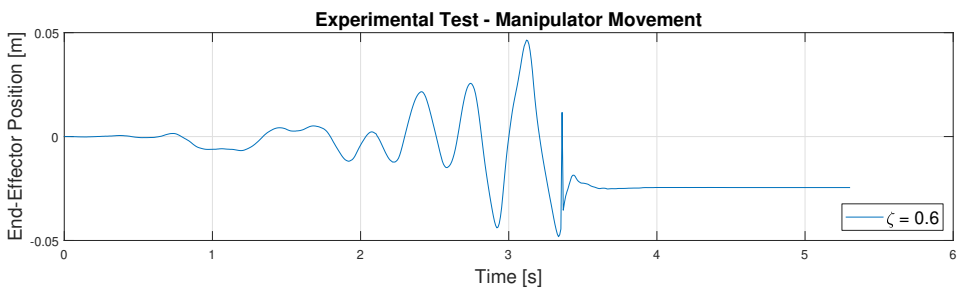

(b) Movement plot for mildly underdamped system with fixed frequency, $f = 6$ [Author]

Figure F.14: Plots of mildly underdamped system with fixed frequency, $f = 6$ [Author]

Variable Frequency

(a) PSD plot for critical damped system with 2x variable frequency [Author]

(b) Movement plot for critical damped system with 2x variable frequency [Author]

Figure F.15: Plots of critical damped system with 2x variable frequency [Author]
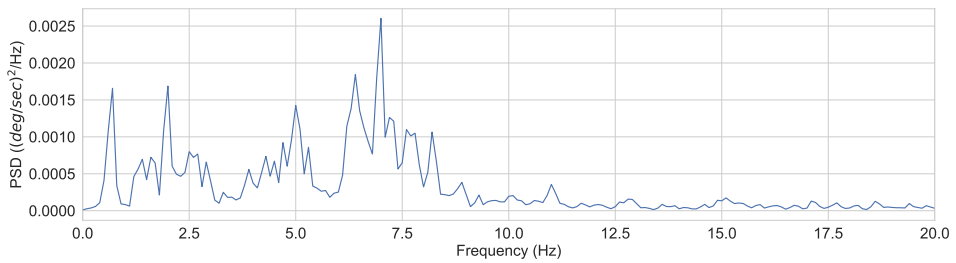
(a) PSD plot for mildly underdamped system with 4x variable frequency [Author]
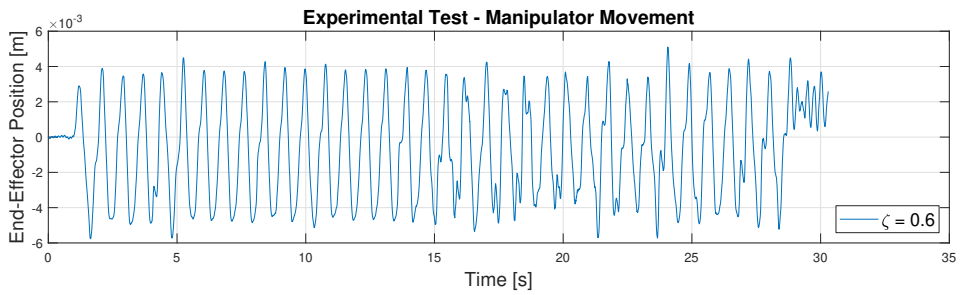
(b) Movement plot for mildly underdamped system with 4x variable frequency [Author]

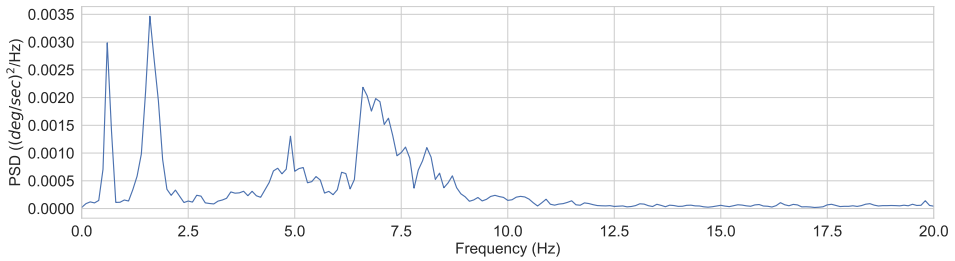**Figure F.16:** Plots of mildly underdamped system with 4x variable frequency [Author]

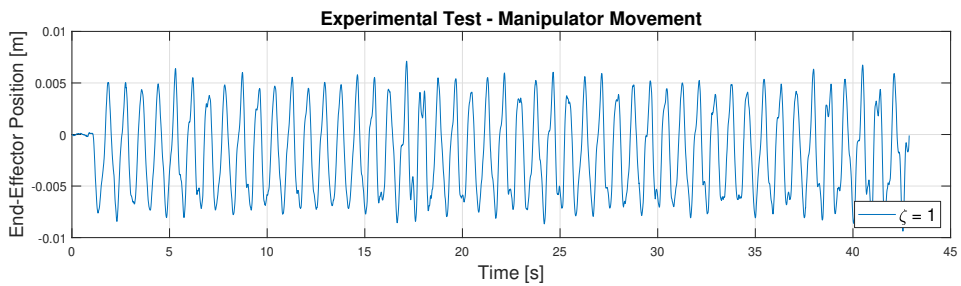**(a)** PSD plot for mildly underdamped system with 2x variable frequency [Author]

(b) Movement plot for mildly underdamped system with 2x variable frequency [Author]

Figure F.17: Plots of mildly underdamped system with 2x variable frequency [Author]

G   Lab Risk Assessment
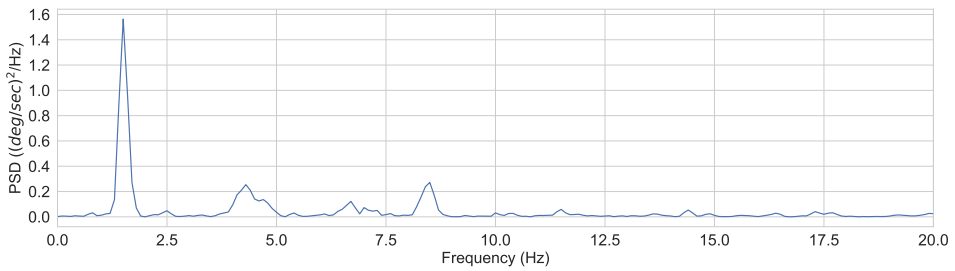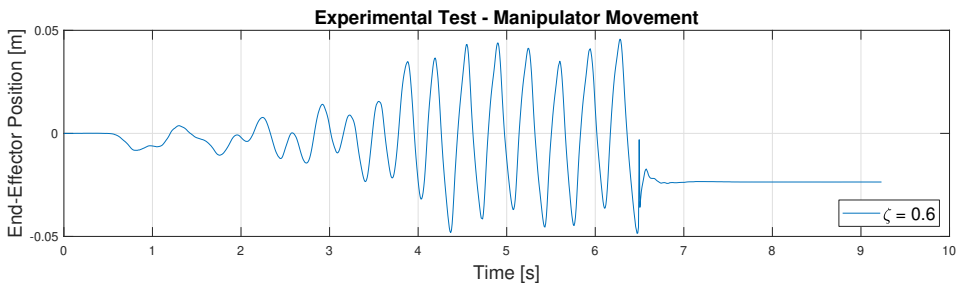
This appendix contains safety documentation relevant for the use of the UR5 manipulator in this thesis. The risk assessment follows the template developed by [21], and is presented in its entirety.

NTNU

Faculty of Information Technology and Electrical Engineering
Department of Engineering Cybernetics

20.11.2018

Report

Risk assessments of the UR5 robot for use in master thesis

Summary

This report gives an overview of the persons and equipment associated with the use of a UR5 robot in a master thesis during the fall of 2018. The report includes an overview of the risks and security measures connected to the use of a UR5 robot. The safety instructions and risk assessments developed by Universal Robots for the relevant firmware version of the UR5 in the department's laboratory is available here.

This report is the 2nd iteration of a risk assessment first done by Mads Johan Laastad in the spring of 2017.

Inspection - risk assessment of the UR5

Date:	20.11.2018
Present:	Shahrukh Khan, 5th year master student

Report

Date:	20.11.2018
Author:	Shahrukh Khan, 5th year master student

Original Report by

Date:	31.03.2017
Author:	Mads Johan Laastad, 5th year master student

Content

1   Introduction

Department of Engineering Cybernetics owns a UR5 robot produced by Universal Robots AS. The applications are demonstrations of robotics for students, research and development of 6DOF robotics, etc. This report summaries the safety measures that have been implemented in order to ensure safety during use, operation and code development on the UR5 robot associated with a master thesis developed during the fall of 2018.

2   Personnel

2.1   Involved persons

Person	Role
Jan Tommy Gravdahl	Professor and main supervisor.
Shahrukh Khan	5th year master student. Writing master thesis and using the UR5 robot for testing and developing for experimental applications.
Audience	Simple interactions during supervision of approved operator.

3   Description of the UR5 system

The UR5 system consist of:
- A 6 DOF industrial robot manipulator, consisting of six revolute joints.
- Controller cabinet containing essential firmware for control of the UR5 robot. The cabinet can be locked with a special key.
- Tablet with a GUI interface for controlling the UR5 robot. The tablet is connected to the controller cabinet through a cord, and contains a physical emergency stop button.

3.1   Human - robot interface

A hardware interface has been developed by the technical staff at the mechanical workshop at the department. The interface consist of a round metal plate connected to the force sensor to provide equal force distribution in addition to a velcro strap to attach the hand.

3.2   Safety equipment

1. Physical emergency stop button
2. Several firmware safety mechanisms
3. Several new software safety mechanisms

Proper use of the UR5 robot always includes having the emergency stop button within an easy reach. There are no requirements for the UR5 robot to operate within a physical cage, but it is encouraged to keep the working space free from any unnecessary exposure to persons or obstacles.

4   Risk assessment of the UR5 robot

4.1   Risk matrix

This chapter summarize the risks associated with the operation and use of the UR5 robot. The following risk matrix describes the operation risks prior to implementing preventive security measurements.

Risk matrix

C O N S E Q U E N C E		Very small 1	Small 2	Moderate 3	Large 4	Very large 5
	Very serious E					
	Serious D	3	6			
	Moderate C					5,7
	Small B					
	Very small A				2	1,4
		Very small 1	Small 2	Moderate 3	Large 4	Very large 5
		PROBABILITY				

Risks - summary

Nr.	Risks
1.	Unauthorized personnel gets access to the UR5 robot
2.	Unauthorized startup of the UR5 robot system
3.	Unwanted behaviour by the UR5 robot firmware
4.	Collision between the UR5 robot and objects
5.	Collision between the UR5 robot and persons
6.	Hacking or cracking of the UR5 robot
7.	Unwanted behaviour by the experimental and newly developed UR5 robot software.

Explanation of the colors which are used in the risk matrix

Color		Description
Red		High risk. Efforts must be made to reduce the risk.
Yellow		Assessment area. Efforts should be considered based on a cost-/benefit assessment.
Green		Acceptable or negligible risk. Effort are not necessary, but can be assessed based on other considerations.

Guidelines for quantification of probability and consequences

Probability is assessed based on the following criterias:

Very small 1	Small 2	Moderate 3	Large 4	Very large 5
1 incident every 50 years or less	1 incident every 10 years or less	1 incident every year or less	1 incident every month or more	Happens weekly

Consequences is assessed based on the following criterias:

Grading	Human	Environment, water, earth and air	Economy/material	Reputation
E Very serious	Death	Very long term and irreversible damage.	Operations/activities stopped >1 year.	Credibility and respect substantially and lastingly weakened.
D Serious	Serious injury. Risk of permanent disability.	Long term damage. Long recovery time.	Operations stopped > ½ year. Activities stopped for up to 1 year.	Credibility and respect considerably weakened.
C Moderate	Serious injury.	Minor damage and long recovery time.	Operations/activities stopped <1 month.	Credibility and respect weakened.
B Small	Injury that requires medical treatment.	Minor damage and short recovery time.	Operations/activities stopped <1 week.	Negative effect on credibility and respect.
A Very small	Injury that requires first aid.	Insignificant damage and short recovery time.	Operations/activities stopped <1 day.	Small effect on credibility and respect.

Risk value = Probability x Consequences
Calculate risk value for humans. Independently assess if risk value calculations based on environment, economy/materials and reputation are necessary.

4.2   Security measures
This chapter describes the security measures that has been implemented associated with each risk factor described in the risk matrix.

	Risks	Security measures	Status	Risk		
				Probability	Consequence	Value
1.	Unauthorized personnel gets access to the UR5 robot	• Access to laboratory limited to authorized personnel • Visual inspection of hardware damage	Preventive measures taken.	5	A	5A
2.	Unauthorized startup of the UR5 robot system	• Access to laboratory limited to authorized personnel • Making significant firmware changes requires a password	Preventive measures taken. Password access limited, but has not been changed for some time.	4	A	4A
3.	Unwanted behavior by the UR5 robot firmware	• Never assuming that the UR5 firmware is completely safe • Emergency stop button	Mental preventive measures taken.	1	D	1D
4.	Collision between the UR5 robot and objects	• Limiting objects inside the workspace • Firmware safety mechanisms • Software safety mechanisms • Emergency stop button	Preventive measures taken. Only object inside the workspace should be a small table. All other object removed.	5	A	5A
5.	Collision between the UR5 robot and persons	• Limiting persons inside the workspace • Firmware safety mechanisms • Software safety mechanisms. Including position, velocity and acceleration limitations. • Emergency stop button	Preventive measures taken. Workspace limited to minimize clamping hazards, velocity and acceleration limited by software. Always keeping the emergency button available.	5	C	5C
6.	Hacking or cracking of the UR5 robot	• Limited physical access • Wireless internet connection on stationary PC which require username and password upon	Preventive measures taken. No permanent ethernet connection to robot system or stationary PC on the same local	2	D	2D

		each new session	network.			
7.	**Unwanted behavior by the experimental and newly developed UR5 robot software.**	• Changes in experimental code require safety checks* before further use. • Always operating with the physical emergency stop button in the other hand.	Preventive measures taken. Safety checklist developed and implemented.	5	C	5C

*Safety checks: This procedure include five mandatory safety steps that must be performed after any significant code change. Any unwanted behavior or deviations from expected behavior require a review of the changes in the code and a re-initialization of the safety checklist.

1. Run new code while only observing the robot
2. Run new code and provide a simple impulse interaction with the system.
3. Run new code and move the end-effector by grasping the hardware interface lightly with two fingers
4. Run new code and move the end-effector by grasping the hardware interface firmly
5. Run new code and move the end-effector by using the hardware interface as intended, but without attaching the wristband.

Safety instruction for users of the UR5 robot

Generel

1. Use of the UR5 robot should always be authorized by key personnel inside the department of engineering cybernetics.
2. First time users should get a brief introduction by a key personnel.
3. The working space should contain a minimum number of obstacles and persons.
4. All use should be performed with the emergency stop button readily available.

Before starting the UR5 system

5. Minimize the number of objects and persons inside the workspace.
6. Perform a visual inspection of the hardware for any tampering or damages.

During use

7. Perform safety check if there has been made any changes to the software code regardless of the type of change that was made.
8. Always keep the emergency stop button readily available.
9. Be observant of persons entering the workspace.

Before the system is vacated

10. Make sure the robot is completely turned off before leaving the laboratory.
11. Turn off the stationary computer connected to the UR5 robots local network. Make sure the UR5 robot is not connected to the internet.
12. Enable the emergency stop button for an extra level of security.

Approval of operator:
The following is an approval for use of the UR5 robot in experimental applications as part of a master thesis during the fall of 2018. The operator should be aware of the potential dangers and comply with the safety measurements described in this risk assessment document.

Signature

Operator – Shahrukh Khan

Signature

Main supervisor – Jan Tommy Gravdahl

Shahrukh Khan

Control and Development of a Wearable Semi-Active Tremor Suppression Device

NTNU
Norwegian University of
Science and Technology